

1 **Ultradian rhythms in shell composition of photosymbiotic and non-photosymbiotic**
2 **mollusks**

3 Niels J. de Winter^{1,2}, Daniel Killam³, Lukas Fröhlich⁴, Lennart de Nooijer⁵, Wim Boer⁵, Bernd R.
4 Schöne⁴, Julien Thébault⁶, Gert-Jan Reichart^{2,5,7}

5

6 *Affiliations*

7 ¹~~Analytical, Environmental and Geochemistry group (AMGC), Vrije Universiteit Brussel, Brussels,~~
8 ~~Belgium~~

9 ²~~Dept~~¹Dept. of Earth Sciences, ~~Utrecht University~~Vrije Universiteit Amsterdam,
10 ~~Utrecht~~Amsterdam, the Netherlands

11 ²Analytical, Environmental and Geochemistry group (AMGC), Vrije Universiteit Brussel, Brussels,
12 Belgium

13 ³ San Francisco Estuary Institute, Richmond, CA, USA

14 ⁴ ~~Department of Paleontology,~~ Institute of Geosciences, ~~Johannes Gutenberg~~
15 ~~Universität~~University of Mainz, Germany

16 ⁵ Dept. of Ocean Systems, Royal Netherlands Institute for Sea Research (NIOZ), Texel, the
17 Netherlands

18 ⁶Univ Brest, CNRS, IRD, Ifremer, LEMAR, 29280 Plouzané, France, (ORCID: 0000-0002-3111-
19 4428)

20 ⁷Dept. of Earth Sciences, Utrecht University, Utrecht, the Netherlands

21

22 Corresponding author: N.J. de Winter, niels.de.winter@vub.be, ben.j.de.winter@vu.nl

24 **Abstract**

25 The chemical composition of mollusk shells is a useful tool in (paleo)climatology since it captures
26 inter- and intra-annual variability in environmental conditions. Trace element and stable isotope
27 ~~analyses~~ analysis with improved sampling resolution now allows *in-situ* determination of the
28 composition of mollusk shell volumes precipitated at daily to sub-daily time intervals~~now enable~~
29 ~~the use of mollusk shells for paleoenvironmental reconstructions at a daily to sub-daily resolution.~~

30 Here, we discuss hourly resolved Mg/Ca, Mn/Ca, Sr/Ca and Ba/Ca profiles measured by laser
31 ablation ICP-MS through shells of photosymbiotic giant clams (*Tridacna maxima*, ~~*Tridacna*~~ *T.*
32 *squamosa* and ~~*Tridacna*~~ *T. squamosina*) and the non-photosymbiotic scallop *Pecten maximus*.
33 Precise sclerochronological age models and spectral analysis allowed us to extract daily and tidal
34 rhythms in the trace element composition of these shells. We find weak but statistically significant
35 expression of these periods and conclude~~We find significant expression of these periodicities but~~
36 ~~conclude~~ that this cyclicity explains less than 10% of the sub-annual variance in trace element
37 profiles. Tidal and diurnal rhythms explain variability of at most 0.2 mmol/mol (~10% of mean
38 value) in Mg/Ca and Sr/Ca, while ultradian Mn/Ca and Ba/Ca cyclicity has a median amplitude of
39 less than 2 $\mu\text{mol/mol}$ (~40% and 80% of the mean of Mn/Ca and Ba/Ca, respectively). Daily
40 periodicity in Sr/Ca and Ba/Ca is stronger in *Tridacna* than in *Pecten*, with *Pecten* showing
41 stronger tidal periodicity. One *T. squamosa* specimen which grew under a sunshade exhibits
42 ~~some of~~ among the strongest diurnal cyclicity. Daily cycles in trace element composition of giant
43 clams are therefore unlikely to be driven by variations in direct insolation ~~itself~~, but rather reflect
44 an inherent biological rhythmic process affecting element incorporation. Finally, the large amount
45 of short-term trace element variability unexplained by ~~periodic variability~~ tidal and daily rhythms
46 highlights the dominance of aperiodic processes in mollusk physiology and/or environmental
47 conditions on shell composition at the sub-daily scale. Future studies should aim to investigate

48 whether ~~part of~~ this ~~aperiodic-remaining~~ variability in shell chemistry reliably records weather
49 patterns or circulation changes in the paleoenvironment.

50

51 **1. Introduction**

52 Patterns in growth increments, microstructure, and chemical composition of accretionary
53 carbonate bioarchives yield detailed information about the environmental conditions and
54 biological rhythm of carbonate producing animals ((Dunbar and Wellington, 1981; Jones, 1983;
55 Witbaard et al., 1994; Klein et al., 1996; Surge et al., 2001; Schöne et al., 2005a; Ivany, 2012;
56 Schöne and Gillikin, 2013; DeCarlo and Cohen, 2017; Killam and Clapham, 2018a)~~Dunbar and
57 Wellington, 1981; Jones, 1983; Witbaard et al., 1994; Klein et al., 1996; Surge et al., 2001; Schöne
58 et al., 2005a; Ivany, 2012; Schöne and Gillikin, 2013; DeCarlo and Cohen, 2017; Killam and
59 Clapham, 2018)~~. These characteristics have spurred the development of a multitude of
60 techniques for extracting information about life history (Jones and Quitmyer, 1996; Schöne et al.,
61 2005b; Eggins et al., 2003; Anand and Elderfield, 2005; Goodwin et al., 2009; Mahé et al., 2010;
62 Comboul et al., 2014; DeCarlo and Cohen, 2017; Judd et al., 2018; Winter et al., 2022)~~(Jones
63 and Quitmyer, 1996; Schöne et al., 2005b; Goodwin et al., 2009; Mahé et al., 2010; Comboul et
64 al., 2014; DeCarlo and Cohen, 2017; Judd et al., 2018; de Winter, 2022)~~, carbonate chemistry
65 (Sinclair et al., 1998; Lazareth et al., 2003; Schöne et al., 2010; de Winter and Claeys, 2017;
66 Warter and Müller, 2017; Huyghe et al., 2021; de Winter et al., 2021b) ~~(Sinclair et al., 1996;
67 Lazareth et al., 2003; Schöne et al., 2010; de Winter and Claeys, 2017; Warter and Müller, 2017;
68 Huyghe et al., 2021; de Winter et al., 2021a)~~ and microstructure (Lazier et al., 1999; Checa et al.,
69 2007; Popov, 2014; Gilbert et al., 2017; Crippa et al., 2020; Höche et al., 2020, 2021; Wichern et
70 al., 2022)~~(Lazier et al., 1999; Checa et al., 2007; Popov, 2014; Gilbert et al., 2017; Crippa et al.,
71 2020; Höche et al., 2020; 2021; Wichern et al., 2022)~~ from carbonate shells and skeletons. As a
72 result, (fossil) carbonate skeletons have gained much attention as archives of past environmental

73 and climate change_(Lough, 2010; Schöne and Gillikin, 2013; Ivany and Judd, 2022) ~~(e.g., Lough,~~
74 ~~2010; Schöne and Gillikin, 2013; Ivany and Judd, 2022~~ and references therein).

75 Three characteristics make the shells of marine mollusks especially valuable as climate archives:

76 (1) Nearly all marine mollusks precipitate their shells in ~~isotopic~~ equilibrium with the oxygen
77 isotope value of ambient sea water, except for juvenile oysters ~~and~~, some mollusks growing near
78 hydrothermal vents and some deep-burrowing species (Schöne et al., 2004; Hallmann et al.,
79 2008; Wisshak et al., 2009; Huyghe et al., 2021; de Winter et al., 2022) ~~(Schöne et al., 2004;~~
80 ~~Wisshak et al., 2009; Huyghe et al., 2021; de Winter et al., 2022)~~, (2) mollusk shells have a high
81 fossilization potential and long geological history, dating back to the beginning of the Phanerozoic
82 (Al-Aasm and Veizer, 1986a, b; Jablonski et al., 2003; Cochran et al., 2010; Jablonski et al., 2017;
83 de Winter et al., 2017, 2018; Coimbra et al., 2020) ~~(Al-Aasm and Veizer, 1986a; b; Jablonski et~~
84 ~~al., 2003; Cochran et al., 2010; Jablonski et al., 2017; de Winter et al., 2017; 2018; Coimbra et~~
85 ~~al., 2020)~~, (3) the incremental growth of mollusk shells allows for internal dating within the shell,
86 yielding chronologies of shell growth with sub-annual precision_(Richardson et al., 1980; Jones,
87 1983; Schöne et al., 2005b; Goodwin et al., 2009; Huyghe et al., 2019) ~~(Richardson et al., 1980;~~
88 ~~Jones, 1983; Schöne et al., 2005c; Goodwin et al., 2009; Huyghe et al., 2019)~~. These advantages
89 enable mollusk shells to record important information about climate and ambient water chemistry
90 on the seasonal scale. Thereby, reconstructions from mollusk shells are highly complementary to
91 other, less highly resolved but longer-term, climate and environmental reconstructions like
92 sedimentary records, tree rings and ice cores_(Black, 2009; Bougeois et al., 2014; Petersen et al.,
93 2016; Tierney et al., 2020; de Winter et al., 2021a) ~~(Black, 2009; Bougeois et al., 2014; Petersen~~
94 ~~et al., 2016; Tierney et al., 2020; de Winter et al., 2021b)~~.

95 The resolution of the mollusk shell archive is not limited to seasonal variability. Studies monitoring
96 the behavior of mollusks during growth experiments show that their activity varies as a function
97 of environmental conditions (e.g., temperature and food availability) and follows ultradian rhythms

98 which may contain daily to hourly periodicities, probably linked to diurnal and tidal cycles, or lack
99 periodic behavior altogether (Rodland et al., 2006; García-March et al., 2008; Tran et al., 2011;
100 Ballesta-Artero et al., 2017; Xing et al., 2019; Tran et al., 2020) (~~Rodland et al., 2006; García-~~
101 ~~March et al., 2008; Tran et al., 2011; Ballesta-Artero et al., 2017; Xing et al., 2019; Tran et al.,~~
102 ~~2020~~). Analyses of growth patterns and, more recently, composition of shell carbonate deposited
103 at these short time intervals show that these rhythms can be recorded in mollusk shells (Pannella,
104 1976; Richardson et al., 1980; Sano et al., 2012; Warter et al., 2018; de Winter et al., 2020)
105 (~~Pannella, 1976; Richardson et al., 1980; Sano et al., 2012; Warter et al., 2018; de Winter et al.,~~
106 ~~2020~~). This raises the question whether mollusk shells reliably record behavioral changes, high
107 frequency (paleo-)weather or circulation patterns (e.g. (Komagoe et al., 2018; Yan et al., 2020;
108 Poitevin et al., 2020) (~~e.g., Komagoe et al., 2018; Yan et al., 2020; Poitevin et al., 2020~~).
109 Alternatively, the presence of daily cyclicity in shell chemistry may yield information about the
110 paleobiology of extinct mollusks, such as the ~~presence~~ use of photosymbiosis (e.g. (Sano et al.,
111 2012; Warter et al., 2018; de Winter et al., 2020) (~~e.g., Sano et al., 2012; Warter et al., 2018; de~~
112 ~~Winter et al., 2020~~). The latter seems plausible given the effect of photosymbiosis on shell
113 mineralization in modern tridacnids (Ip and Chew, 2021) (~~Ip and Chew, 2021~~) and on the trace
114 element composition of aragonite in modern photosymbiotic scleractinian corals (Cohen et al.,
115 2002; Meibom et al., 2003; Inoue et al., 2018) (~~Cohen et al., 2002; Meibom et al., 2003; Inoue et~~
116 ~~al., 2018~~). If proven true, daily variability in bivalve shells may serve as a proxy for photosymbiosis
117 in the fossil record (e.g. (de Winter et al., 2020) (~~e.g., de Winter et al., 2020~~). This is of interest
118 because photosymbiosis is a derived adaptation of some tropical bivalve species (e.g., tridacnids)
119 and its prevalence in the fossil record has important implications for the ecological niche of fossil
120 mollusks (e.g., (Vermeij, 2013) (~~Vermeij, 2013~~). In addition, photosymbiosis can affect mollusk
121 shell composition, and understanding it is therefore critical for the interpretation of chemical
122 proxies in mollusk shells for environmental reconstructions (Killam et al., 2020) (~~Killam et al.,~~
123 ~~2020~~). Finally, improving our understanding of photosymbiosis in tropical ecosystems sheds light

124 on the resilience of photosymbiotic organisms to environmental change, now and in the geological
125 past. The latter is of special interest in light of the ongoing climate and biodiversity crises, which
126 are profoundly affecting these sensitive ecosystems_(Pandolfi and Kiessling, 2014)~~(Pandolfi and~~
127 ~~Kiessling, 2014).~~

128 In this study, we investigate shell growth patterns and shell chemistry of the photosymbiotic
129 bivalves *Tridacna maxima*, *T. squamosa* and *T. squamosina* as well as the non-photosymbiotic
130 scallop *Pecten maximus*. *P. maximus* was chosen as a non-photosymbiotic counterpart in
131 comparison with the tridacnids because of its comparatively high growth rate and the presence of
132 daily striae visible on the ~~outside-outer surface~~ of its shell, which make it possible to construct
133 accurate shell chronologies_(Chauvaud et al., 2005)~~(Chauvaud et al., 2005)~~. We combine ultra-
134 high-resolution (hourly resolved) Mg/Ca, Sr/Ca, Mn/Ca and Ba/Ca measurements in the shells
135 with detailed sclerochronology to investigate the variability in these trace elements over time in
136 all four species. The aim of this study is to investigate (1) whether the shells record high-frequency
137 variability in shell chemistry that can be linked to environmental and/or circadian rhythms and (2)
138 whether the presence of photosymbiosis influences the expression of this variability in the shells'
139 composition.

140

141 2. Materials and methods

142 2.1 Preparation of *P. maximus* specimens

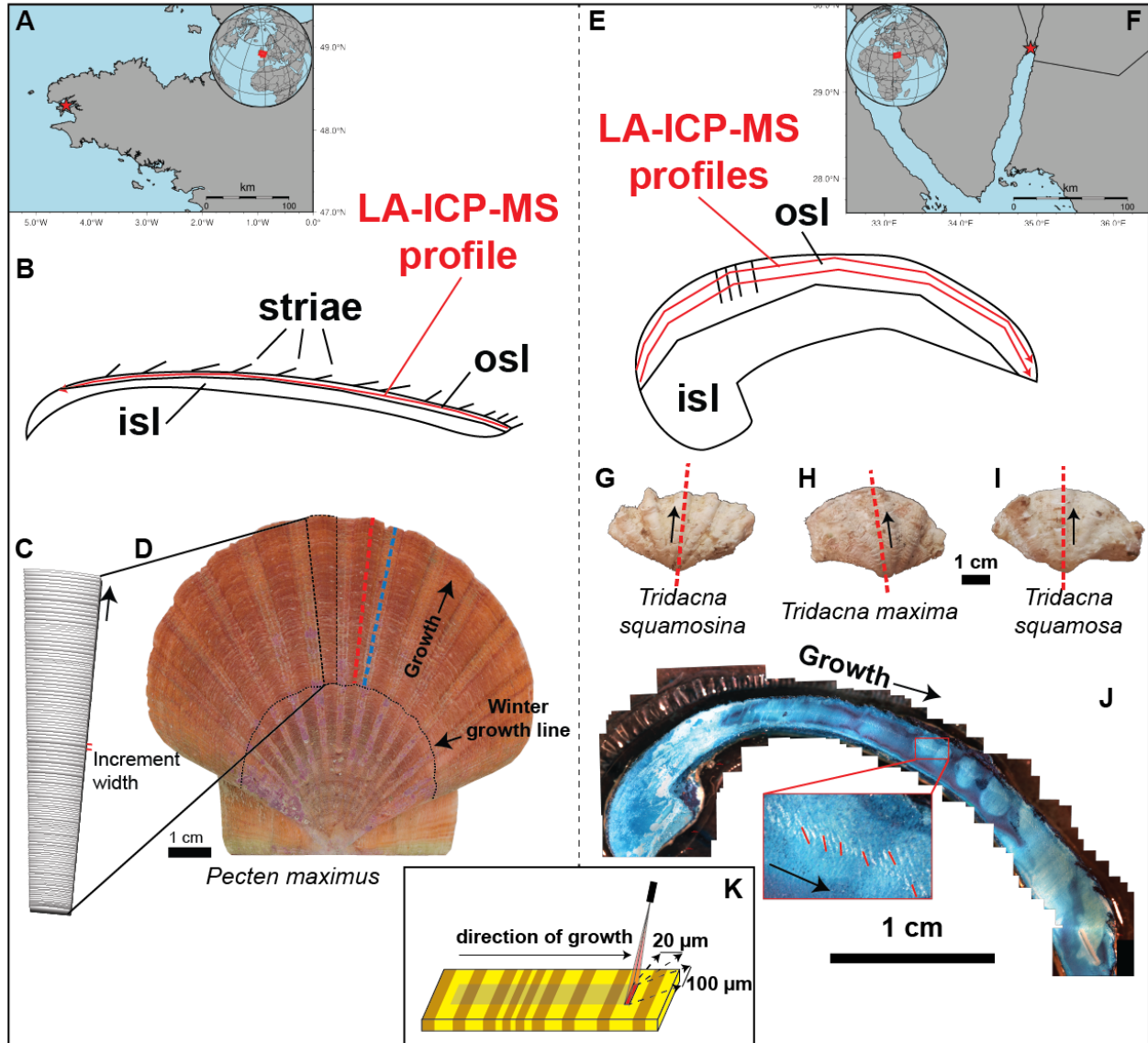
143 Three specimens of the King scallop *P. maximus* (labeled “PM2”, “PM3” and “PM4”) were
144 collected alive on 15/11/2019 on the southern coast of the Bay of Brest near Lanvéoc, France
145 (48°17'N 4°30'W) by SCUBA divers at a depth of approximately 8 m (see ~~(Fröhlich et al., 2022)~~
146 ~~Fröhlich et al., 2022; Figure 1~~). Note that water depth in the Bay of Brest varies significantly due
147 to the macrotidal regime with a mean tidal range of 2.8 – 5.9 m with extreme ranges up to 7.2 m
148 (Guillaume Olivier et al., 2021; Service Hydrographique et Océanographique de la Marine -
149 Géoportail, 2022) ~~(Guillaume Olivier et al., 2021; Service Hydrographique et Océanographique~~
150 ~~de la Marine; 2022)~~. Collected specimens contained at least one full year of growth based on the
151 visibility of one winter growth line on the outside of the shell (age class 1; see (Thébault et al.,
152 2022) ~~Thébault et al., 2022; Fig 1F and S1~~). Specimens were frozen at -20°C immediately after
153 collection. Soft body parts and epibionts were removed from the shells before further treatment.
154 Shells were superficially cleaned using a plastic brush and adhering sediment was removed by
155 ultrasonication in deionized water. The flat, left valves were used for elemental and
156 sclerochronological analysis following previous studies on *P. maximus* ~~(Thébault et al., 2022;~~
157 ~~Fröhlich et al., 2022) (Thébault et al., 2022; Fröhlich et al., 2022)~~.

158 High-resolution color photos were made of the outside of the left valve of the shell using a mirror-
159 reflex camera (Canon EOS 600 DSLR camera connected to a Wild Heerbrugg binocular
160 microscope equipped with a Schott VisiLED MC 1000 sectoral dark-field light source) aimed
161 downward perpendicular to the working surface. Overlapping images of the shells were stitched
162 together using Image Composite Editor v2.0.3.0 (Microsoft Research Computational Photography
163 Group, Redmond, WA, USA). The stitched images were used to count and measure daily striae
164 on the shell surface (see **Fig. 1** and **S1**). To obtain a fully focused composite of the complete
165 shell, dynamic focusing was applied to allow all parts of the slightly curved surface of the shell to

166 come into focus. Dynamic focus images were later stitched together using focus stacking in
167 Helicon Focus (Helicon Focus 7.7.5; HeliconSoft, Kharkiv, Ukraine; see **S1**).

168 Cross sections were cut through all three *P. maximus* shells perpendicular to the daily growth
169 lines (striae) from the ventral margin of the shell to the shell hinge (see **Fig. 1B**, ~~**Fig. 1E-FD**~~ and
170 **S1**) along the axis of maximal growth. Shells were fortified with a protective layer of metal epoxy
171 (Gluetec Wiko Epofix 05) before sectioning using a Buehler Isomet 1000 low-speed precision saw
172 (Buehler Inc, Lake Bluff, IL, USA) equipped with a diamond-coated wafering thin blade (0.4 mm
173 thickness; number 15LC 11–4255) at 200 rpm. Parallel cuts were made to allow shell sections to
174 be glued to glass plates for ~~grinding high-grade polishing~~ (down to F1200 grit SiC powder) and
175 high-grade polishing and (1 μm Al₂O₃ suspension on Buhler polishing cloth, MasterTex). Two
176 cross sections were made through specimens **PM2** and **PM3**: One through a “rib” of the shell (i.e.,
177 radial segment that protrudes away from the interior, named **PM2_1** and **PM3_1**) and one through
178 a “valley” (i.e., radial segment between two “ribs” that lies deeper towards the interior, named
179 **PM2_2** and **PM3_2**; see **Fig. 1** and **S1**). The dual sections were cut to compare shell chemistry
180 between the “ribs” and “valleys” of the shell-. Specimen **PM4** was only sectioned once, through a
181 “valley” in the shell, making a total of five cross sections through the *P. maximus* specimens.

182



183

184 **Figure 1: Overview of sample locations and preparation steps.** **A)** Location of the Bay of
 185 Brest, with the red star indicating the sampling location. **B)** Schematic cross section through *P.*
 186 *maximus* showing how the LA-ICP-MS line_scan (red line) was positioned within the outer shell
 187 layer (OSL). **C)** Schematic representation of a segment through the shell of *P. maximus* showing
 188 the striae which are deposited daily and which were counted to establish age models (see also
 189 **B).** **D)** Left valve of *P. maximus* (PM2) used in this study, with dashed lines showing the position
 190 of cross sections through ribs (red) and valleys (blue) in the shell. Black arrow indicates growth
 191 direction away from the shell hinge. The black dotted line highlights a winter growth stop. **E)**

192 Schematic cross section through a tridacnid, illustrating the positions of ~~parrallel~~parallel LA-ICP-
193 MS line scans (red lines) through these shells within the OSL. ~~DF~~ **DF**) Position of the Gulf of Aqaba,
194 with the red star indicating the sample location for tridacnids. ~~E~~ **E**) ~~Schematic representation of a~~
195 ~~segment through the shell of *P. maximus* showing the striae which are deposited daily and which~~
196 ~~were counted to establish age models (see also B).~~ **F**) ~~Left valve of *P. maximus* (PM2) used in~~
197 ~~this study, with dashed lines showing the position of cross sections through ribs (red) and valleys~~
198 ~~(blue) in the shell. Black arrow indicates growth direction away from the shell hinge. The black~~
199 ~~dotted line highlights a winter growth stop.~~ **G-I**) Pictures of (from left to right) *T. squamosa*
200 (specimen **TSFRS1**), *T. maxima* (specimen **TM29**) and *T. squamosina* (specimen **SQSA1**) with
201 dashed red lines indicating the positions of the cross sections used for LA-ICP-MS analysis (see
202 **C**) and black arrows indicating the direction of growth. ~~KJ~~ **KJ**) Example of Mutvei-stained cross
203 section through a *T. maxima* specimen used to visualize and count growth lines, with the insert
204 showing part of the OSL where growth lines were counted (red lines) to establish age models for
205 the tridacnids. Black arrows indicate the direction of growth. ~~JK~~ **JK**) Schematic representation of the
206 LA-ICP-MS line scanning setup with the rectangular spot size (100 * 20 µm; see **S11**) that was
207 positioned parallel to the growth layers in the shell. ~~K~~ **K**) ~~Example of Mutvei-stained cross section~~
208 ~~through a *T. maxima* specimen used to visualize and count growth lines, with the insert showing~~
209 ~~part of the OSL where growth lines were counted (red lines) to establish age models for the~~
210 ~~tridacnids. Black arrows indicate the direction of growth.~~

211

212 2.2 Preparation of *Tridacna* specimens

213 A total of 5 tridacnid specimens, two *T. maxima* (named **TM29** and **TM84**), two *T. squamosa*
214 (named **TS85** and **TSFRS1**) and one *T. squamosina* (**SQSA1**) specimen, were collected in the
215 summer of 2016 from beach death assemblages on the coast of the Gulf of Aqaba with permit
216 from the Israeli National Parks Authority (**Figure 1**; see details in ~~(Killam et al., 2020)~~
217 ~~al., 2020~~). One cultured *Tridacna squamosa* shell (**TSM1**) was obtained from the National Center
218 for Mariculture, Eilat. Species were determined following shell characteristics of the local
219 population as cited in ~~(Roa-Quiaoit, 2005)~~ ~~Roa-Quiaoit (2005)~~.

220 All shells were sectioned along the axis of maximum growth after removing epibionts using a
221 metal brush (see **Fig. 1G-I**). Original microstructure and preservation of the original aragonite
222 mineralogy of all specimens was confirmed using Scanning Electron Microscopy and X-ray
223 Diffraction Spectroscopy following ~~(Gannon et al., 2017)~~ ~~Gannon et al. (2017)~~ and ~~(Kontoyannis~~
224 ~~and Vagenas, 2000)~~ ~~Kontoyannis and Vagenas (2000)~~; ~~(see details in (Killam et al., 2020))~~. Shell
225 segments were partially embedded in Araldite 2020 epoxy resin (Huntsman Corp., Woodlands,
226 TX, USA) before being sectioned in direction of maximum growth using a slow-rotating saw
227 equipped with a thin wafered saw blade ($\varnothing < 1$ mm). Parallel cross sections produced 5-10 mm
228 thick sections that were polished using progressively finer SiC polishing disks.

229

230 2.3 Microscopy and photography

231 Polished surfaces of all 11 cross sections (5 *Pecten*, 6 *Tridacna*) were imaged using an Epson®
232 1850 flatbed scanner (Seiko Epson Corp., Nagano, Japan) at a pixel resolution of 6400 dpi (± 4
233 μm pixel size) as well as by stitching micrographs made using a KEYENCE VHX-5000 digital
234 microscope using x250 magnification together into composite images (see **S1**). Cross sections

235 were imaged both before and after trace element analyses to allow the trace element profiles to
236 be referenced relative to the cross sections.

237

238 2.4 LA-ICP-MS analyses

239 Elemental ratios were based on measuring ratios of the isotopes ^{25}Mg , ^{87}Sr , ^{55}Mn and ^{137}Ba to
240 ^{43}Ca along profiles through all shell cross sections using Laser Ablation – Inductively Coupled
241 Plasma – Mass Spectrometry (LA-ICP-MS). Measurements were carried out on a laser ablation
242 system (ESI NWR193UC; Elemental Scientific, Omaha, NE, USA) coupled to a quadrupole ICP-
243 MS (iCap-Q, Thermo Fisher Scientific, Waltham, MA, USA) at the Royal Netherlands Institute for
244 Sea Research (NIOZ). Operation parameters are provided in **S11**.

245

246
247 Scan lines were programmed on the polished shell cross-sections in direction of growth as close
248 as possible to the outer edge of the shell, with the circular LA-ICP-MS spot oriented parallel to
249 the growth lines (with a width of 20 μm in scanning direction, see **Fig. 1J**; **S11**). For the pectinids,
250 care was taken to target the outer portion of the outermost shell layer (oOSL) and avoid sampling
251 of the inner portion of the outer shell layer (iOSL) or inner shell layer (ISL), which was
252 demonstrated to have a different chemical composition (see Freitas et al., 2009). For the
253 tridacnids, profiles were placed within the OSL close to (within 100 μm of) the outer edge of the
254 shell in a first analytical session. However, since spikes of high Mg/Ca and Mn/Ca ratios were
255 observed in these results, parallel transects placed \sim 100 μm further towards the inside of the
256 shell were measured through all tridacnid shells to verify whether these spikes in Mg and Mn were
257 reproducible further inward (see **S2**). The combination of laser scan speed ($4 \mu\text{m} * \text{s}^{-1}$) and ICP-
258 MS run cycle time ("sweep time": 109 ms) yielded a mean spatial sampling resolution of 0.44 μm ,
259 determined as the arithmetic mean without taking into account the round shape of the laser spot.
260 However, note that the width of the LA-ICP-MS spot size in scanning direction (20 μm) caused
261 smoothing of the LA-ICP-MS signal, reducing the effective spatial sampling resolution. As a result,
262 each 0.44 μm wide segment of the shells in growth direction is sampled 45 times while the spot
263 moves across the shell. We tested the effect of this smoothing on a virtual record with
264 characteristics similar to the Sr/Ca record obtained by (Sano et al., 2012) (see **section 3.3 and**
265 **S13**). All scan lines in pectinids and tridacnids were repeated a second time at the exact same
266 location using a faster scan rate of 10 $\mu\text{m} * \text{s}^{-1}$ to assess repeatability of the elemental signals
267 (see **S2**).

268 Data reduction was performed using an adapted version of the data reduction software SILLS
269 (Signal Integration for Laboratory Laser Systems; (Guillong et al., 2008)) in Matlab. Raw LA-ICP-
270 MS data were calibrated using NIST610, (National Institute of Standards and Technologies,

271 Gaithersburg, MD, USA) using the reference values reported in the GeoReM database ((Jochum
272 et al., 2005, 2011)). Quality control reference materials BAS CRM 752-393 (Bureau of Analyzed
273 Samples, Middlesbrough, UK), RS3 and one matrix-matched carbonate standard (MACS-3;
274 United States Geological Survey, Reston, VA, USA; (Wilson et al., 2008)) were used to monitor
275 the quality of the measurement. Details on the accuracy of the LA-ICP-MS trace element results
276 relative to preferred values for the check standards is provided in S12.

277 To increase the stability of the ICP-MS signal and to correct for drift, ^{43}Ca was used as internal
278 standard. Calcium concentrations were assumed to be constant (38 wt%) throughout the
279 LAICPMS profiles within the same shell layer. External drift-correction using repeated
280 measurements on the JCp1 standard was applied. ~~if~~ The element/Ca drift was less than $\geq 5\%$
281 during the analytical sequence. Drift during a single transect was found to be negligible.

282

283 2.5 Age models

284 Trace element profiles in *P. maximus* shells were internally dated using daily striae visible on the
285 outer shell surface (**Fig. 4E1D**). Daily increment widths (perpendicular distances between
286 successive striae) were counted and measured multiple times, both on the outside of the shell
287 using the focus-stacked images (see **section 2.3**) and by counting and measuring the distance
288 between growth layers in cross sections through the “valleys” of the shells (**PM2_2** and **PM3_2**;
289 see **S3**) by different persons. Positions of daily striae on the outside of the shells were plotted
290 relative to distance along the LA-ICP-MS scan line using manual alignment of striae and the LA-
291 ICP-MS path on microscope composites of cross sections through the shells, taking into account
292 the curvature of growth lines with distance away from the outer shell surface (see **S3**). The timing
293 of shell formation was determined by backdating the daily striae from the ventral margin (last
294 visible stria mineralized on the date of shell collection, i.e., November 15, 2019), and by linearly

295 interpolating the timing of measurements located between daily growth lines based on their
296 distance from daily striae positions (**S5**).

297 Trace element profiles from *Tridacna* shells were also dated using layer counting. Polished cross
298 sections through all tridacnids were imaged using UV luminescence (see Fig. 1J and S4) and
299 stained with Mutvei solution (Schöne et al., 2005c; Killam et al., 2021) to facilitate this counting.

300 However, despite staining and luminescence techniques, the expression of daily and semi-diurnal
301 (half-daily, or 12 h rhythmic) growth markings were insufficiently clear to count individual growth
302 lines along the full (multi-year) growth period recorded in all the shells. Therefore, we opted for a
303 hybrid method in which we measured the width of daily and semi-diurnal increments in parts of
304 cross sections of each shell where they were well developed and used these measurements in
305 combination with the annual growth breaks (which are easily recognized on the shell) to create
306 age models for all specimens. ~~age models were constructed based on parts of the shell where~~
307 ~~daily and tidal layers could be identified with confidence. The median widths of daily or semi-~~
308 ~~diurnal increments were determined on these cross sections and compared to the width of annual~~
309 ~~increments identified based on growth breaks visible on the outer margin of the shell.~~ The
310 distinction between diurnal (24_h) and tidal (~12_h) pacing of growth increments was made based
311 on the width of small-scale increments relative to the width of annual increments in the shell. A
312 von Bertalanffy growth model (Von Bertalanffy, 1957) was constructed for each specimen based
313 on the annual growth (ΔL) inferred from (semi-)diurnal growth line counting and the maximum
314 shell height (L_{inf}) known for these species in the Red Sea from the literature (Roa-Quiaoit, 2005;
315 Mohammed et al., 2019):

316
$$L_t = L_{inf} * (1 - e^{-kt}), \text{ with } k = -\ln\left(\frac{\Delta L}{L_{inf}}\right)$$

317 In this formula, L_t is the shell height at time t and k is the growth constant (Brody growth coefficient;
318 (Munro, 1982)). Since cross sections through the tridacnids were made through the shell hinge

319 (in direction of the shell height) and literature values for L_{inf} are reported with reference to shell
320 length (measured parallel to the shell hinge), allometric data on *T. maxima*, *T. squamosa* and *T.*
321 *squamosina* from the literature was used to convert L_{inf} values (which are commonly reported as
322 shell length) to shell height and make them relevant for the direction in which the trace element
323 profiles were measured on the cross sections (Roa-Quiaoit, 2005; Richter et al., 2008;
324 Mohammed et al., 2019). Uncertainties on the annual growth increment widths (ΔL) were
325 calculated from the standard error of the mean width of daily and semi-diurnal growth increments
326 on which ΔL is based, and uncertainties on the values for L_{inf} were taken from variability in the
327 values in the literature. Both sources of uncertainty were propagated through the growth model
328 using the variance formula (Ku, 1966) to obtain error envelopes on age-distance relationships
329 (growth curves) of tridacnids (see **S5**). All data processing steps described in this manuscript are
330 carried out using the open-source computational software package R (R Core Team, 2013), and
331 scripts detailing these calculations are provided in **S6** and deposited on the open-access software
332 repository GitHub (<https://zenodo.org/record/6603175>)

333

334 2.6 Spectral analysis

335 Spectral analysis on the LA-ICP-MS data was used to isolate trace element variability at the sub-
336 annual scale. All trace element profiles were first detrended using a LOESS filter with a span of
337 0.2 times the length of the record to remove longer term (i.e., seasonal to multi-annual) trends.
338 The detrended series were linearly resampled in the time domain before applying the Multi-Taper
339 Method (MTM; (Thomson, 1982)) to extract dominant frequencies from the data. Spectral analysis
340 was carried out using the “astrochron” package (Meyers, 2014) in R ((R Core Team, 2013); see
341 script in **S6**). The significance of relevant periodicities was tested using a combination of “red
342 noise” estimation and a harmonic F-test (see (Meyers, 2012)). To visualize the evolution of

343 periodic behavior across the shells, wavelet analysis was applied on all trace element profiles
344 using the “dplR” package in R (see **S6**).

345

346 2.7 Extracting high-resolution variability

347 After detrending and spectral analysis, all trace element profiles were smoothed using a Savitzky-
348 Golay filter with a width of 21 datapoints (8.4 μm ; equivalent to a timespan of $\sim 1\text{-}5\text{ h}$; **S6**) to
349 remove high-frequency measurement noise within our LA-ICP-MS spot size. The Savitzky-Golay
350 filter was used because it preserves the tendency of the trace element profile and therefore retains
351 a larger fraction of the amplitude of periodicity close to the width of the filter compared to simpler
352 smoothing techniques (e.g. moving average; (Savitzky and Golay, 1964)). The 21-point window
353 size was chosen to smooth out the maximum amount of instrumental noise without losing
354 periodicity larger than half the width of the laser spot (0.22 μm ; equivalent to 23 datapoints).
355 Statistically significant (see **section 2.6**) variability in daily ($\sim 22\text{-}36\text{ h}$; centered on the 24 h diurnal
356 cycle) and ~~tidal~~ semi-diurnal ($\sim 8\text{-}14\text{ h}$; centered on the 12.4 h tidal cycle) frequency bands was
357 extracted from the trace element records using a combination of bandpass filtering (using the
358 “bandpass” function in the “astrochron” R package) and stacking (see **S6**). Trace element data
359 was stacked along bandpass filters using the following procedure: Maxima and minima in the
360 bandpass filter were used as tie points to reference each datapoint of the smoothed dataset
361 relative to its position within the cycle on a scale from 0 to 1. These relative positions were then
362 used to divide the data into 10 bins (bin 1 contains positions 0 – 0.1, bin 2 contains data from
363 positions 0.1 – 0.2, etc.), ~~giving the~~ providing stacked data a resolution of 0.1 times the length of
364 the cycle under investigation. The full breakdown of variability within and between bins created in
365 the stacking routine is provided in **S7**. Different sources of variance in the trace element records
366 were isolated by sequentially determining the variance left in the trace element records after each
367 of the data treatment steps explained above (see example in **S7**). This procedure allowed us to

368 quantify the amount of variance in each trace element profile explained by either diurnal or semi-
369 diurnal variability.

370 3. Results

371 3.1 Trace element data

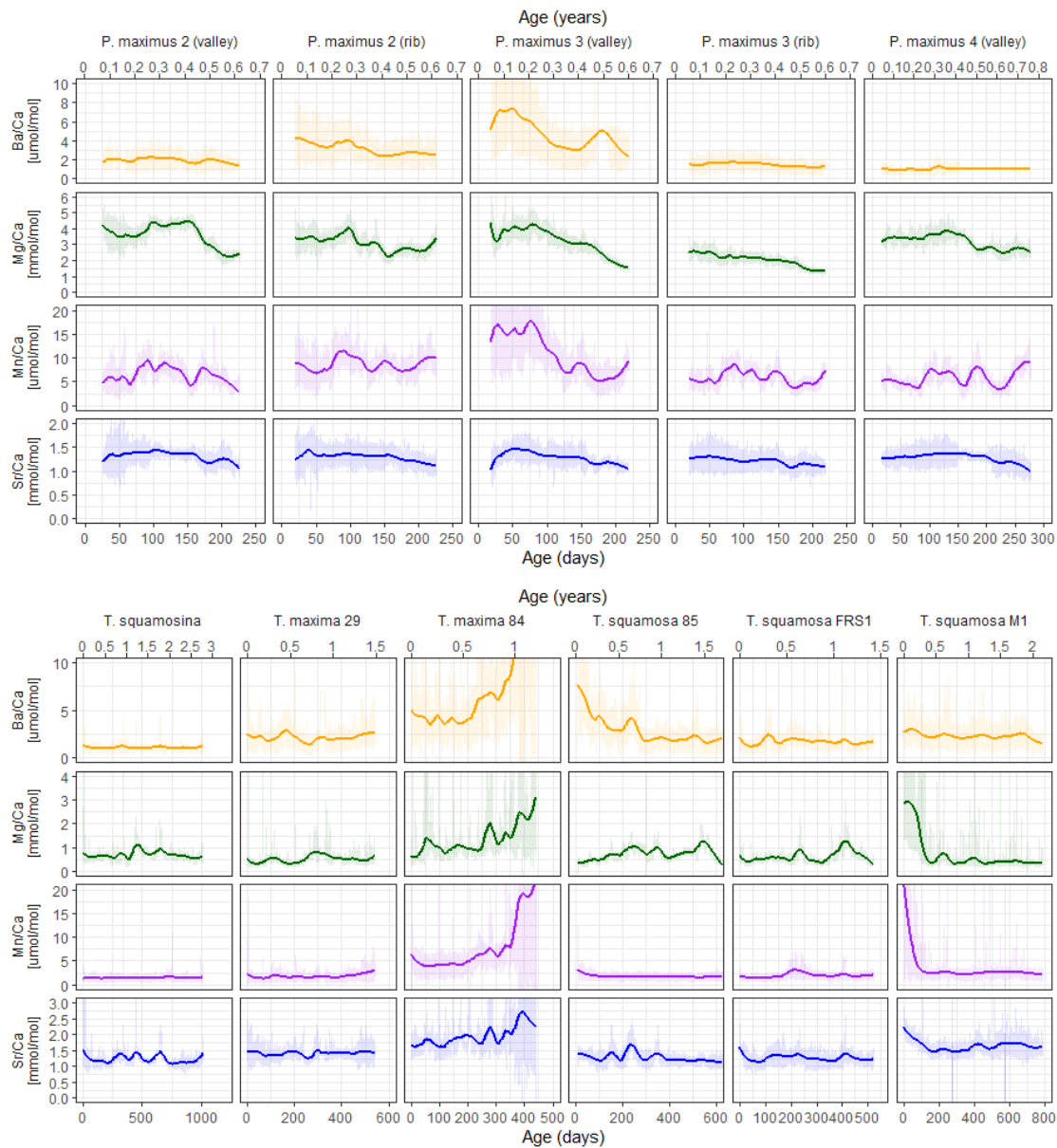
372 LA-ICP-MS line scans yielded profiles of Sr/Ca, Mg/Ca, Mn/Ca and Ba/Ca in growth direction on
373 11 cross-sections through shells of *P. maximus*, *T. maxima*, *T. squamosa* and *T. squamosina*
374 (**Fig. 2**; see **S0** for raw data of all scans). ~~Trace element profiles of consecutive line scans on the~~
375 ~~same transect show high repeatability: s~~Sub-millimeter scale patterns in Sr/Ca, Mg/Ca, Mn/Ca,
376 and Ba/Ca are highly repeated repeatablereproducible between consecutive line scans on the
377 same LA-ICP-MS transect; R^2 values ~~between trace element results of time-equivalent shell~~
378 ~~samples~~ typically exceed 0.8, and ~~the~~ mean element ratio differences between time equivalent
379 samples in different line scans are typically <0.05 mmol/mol for Mg/Ca (<5 % relative to mean
380 value), <0.02 mmol/mol for Sr/Ca (<2 % relative to mean value), <0.5 μ mol/mol for Mn/Ca (<10
381 % relative to mean value) and <0.2 μ mol/mol for Ba/Ca (<8 % relative to mean value; is less than
382 0.05 mmol/mol for the most variable profiles (Mg/Ca, with lower differences for the lower-
383 concentration Mn/Ca and Ba/Ca records; see **S2**). Remeasured transects further away from the
384 outer shell surface in tridacnids (see **section 2.4**) differ more from the original transects than
385 those measured on the exact same locality in the shell: R^2 values between parallel lines in different
386 localities are 0.3 – 0.5 for Mg/Ca and Sr/Ca and <0.3 for Mn/Ca and Ba/Ca, reflecting intra-shell
387 variability in trace element composition in the tridacnids (**S2**). Overall, sub-millimeter scale
388 patterns in trace element composition are reproduced in parallel line scans, ~~and the mean offset~~
389 ~~between the lines was always less than 0.2 mmol/mol.~~
390 ~~Pectinid and tridacnid shells contain similar mean Sr/Ca and Ba/Ca ratios (Sr/Ca of 1.3 ± 0.3 and~~
391 ~~1.5 ± 0.6 mmol/mol respectively; Ba/Ca of 2.8 ± 2.5 and 3.0 ± 5.1 μ mol/mol respectively;~~
392 ~~uncertainty is calculated as 1σ). Mean Mg/Ca and Mn/Ca ratios are higher in *P. maximus* than in~~
393 ~~*Tridacna* species (Mg/Ca = 3.1 ± 0.9 and 0.7 ± 0.9 mmol/mol; Mn/Ca = 7.8 ± 4.7 and 2.7 ± 7.8~~
394 ~~μ mol/mol; 1σ ; **Figure 2**; **S4**).~~ Differences between tridacnid specimens generally exceed the

395 differences between tridacnids and pectinids (1σ of Ba/Ca among all tridacnid specimens = 2.1
396 $\mu\text{mol/mol}$). Individual records like those in **TM84** and **PM3_1** show large variability (especially in
397 Ba/Ca and Mn/Ca) compared to other specimens of the same species. Inter-specimen variability
398 is higher in tridacnid shells than in pectinids (inter-specimen relative standard deviations as a
399 fraction of mean ratio for Ba/Ca: 0.74 vs 0.64, Mg/Ca: 0.37 vs 0.20, Sr/Ca: 0.19 vs 0.03 and
400 Mn/Ca: 0.78 vs 0.33 for tridacnids and pectinids, respectively). **Figure 2** shows that this variability
401 between tridacnids is not readily explained by differences between species, but mostly reflects
402 differences in the trends within the records, with some specimens (e.g., **TM84**, **TSM1** and **TS85**)
403 showing trends in composition towards the end of the record (see also **S8**). Trace element
404 compositions in tridacnid shells are significantly more skewed towards higher values than in
405 pectinids (mean skewness per element and per specimen is 9.7 for tridacnids and 0.9 for
406 pectinids), reflecting the high peaks in trace element composition observed in tridacnid profiles,
407 especially near the ventral margin (e.g., specimens **TM84**, **TSM1** and **TS85**; see **section 2.4**; **Fig.**
408 **2**; **S8**). Finally, “rib” and “valley” segments through the same specimen of *P. maximus* show similar
409 patterns in trace elements, but absolute concentrationselement-to-calciumal ratios (especially of
410 Ba/Ca and Mn/Ca) can be quite different, highlighting heterogeneity within the shells of *P.*
411 *maximus* (**Fig. 2**).

412 ~~Plots of trace element variability reveal dominant high-frequency variability superimposed on~~
413 ~~seasonal-scale patterns (Figure 2).~~ Trace element profiles in pectinids, reflecting only one
414 growing season, show ~~a typical seasonal pattern in~~ Sr/Ca and Mg/Ca ~~with~~ maxima ~~in the~~
415 ~~elemental ratio~~ in the middle of the profile ~~(corresponding to the summer).~~, while Mn/Ca and Ba/Ca
416 ~~in pectinids~~ are more variable, showing multiple peaks in the same growth year. Peaks in Mn/Ca
417 and Ba/Ca are synchronous between profiles through the same specimen, but not between
418 specimens, ~~possibly showing that growth resumed on different days for different specimens after~~
419 ~~the winter stop.~~ Like in the pectinid profiles, Tridacnid Mg/Ca, and Sr/Ca ratios ~~in tridacnids~~ show

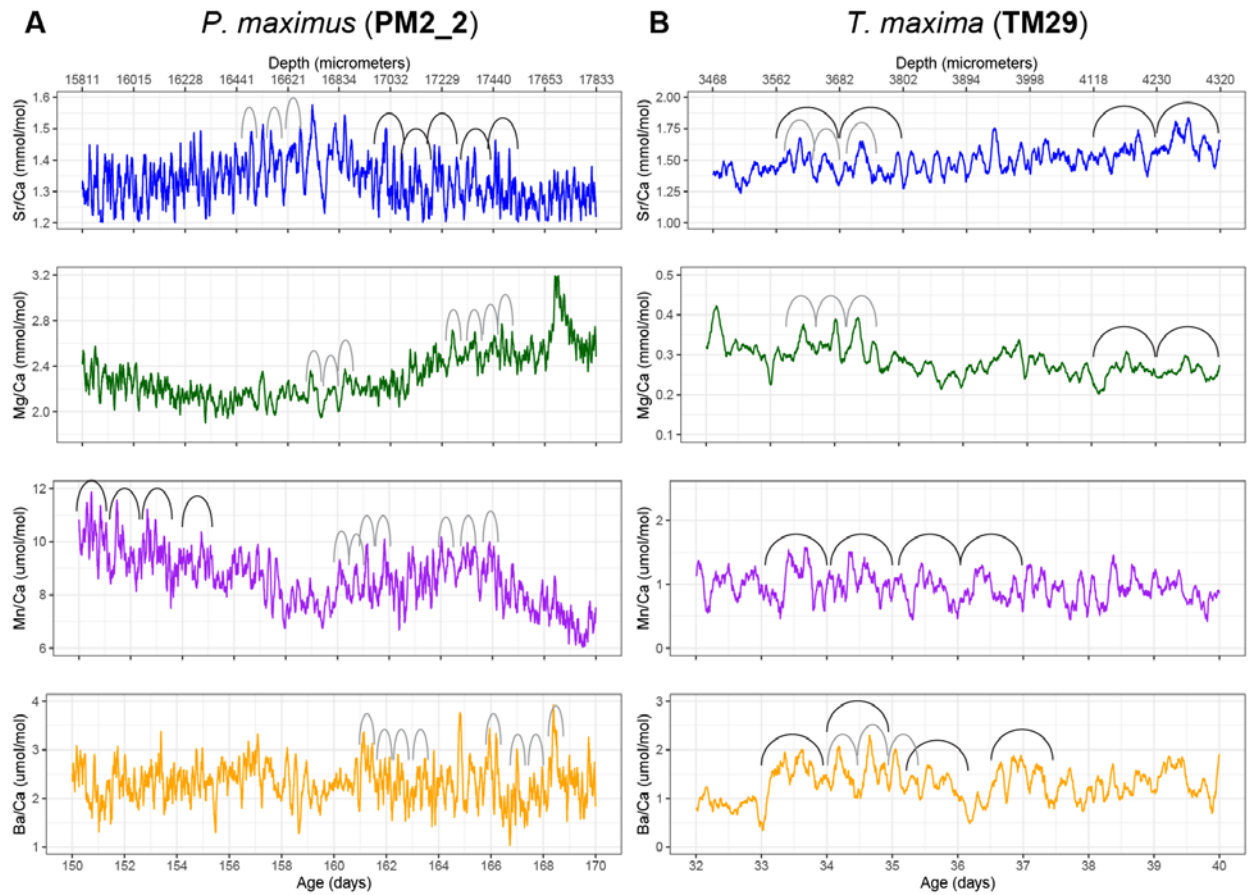
420 ~~similar patterns, with~~ one or two distinct cycles per growth year. Mn/Ca and Ba/Ca ratios in
421 tridacnids show more regular annual or biannual variability than pectinids (most notably specimen
422 SQSA1). It must be noted, however, that *P. maximus* shells only recorded one growth season,
423 limiting the interpretation of seasonal growth patterns.

424 Plots of trace element variability zoomed in on smaller sections of the record reveal dominant
425 high-frequency variability superimposed on seasonal-scale patterns (Figure 3). Both tridacnid
426 and pectinid LA-ICP-MS records show distinct high-frequency cyclicity in all analyzed studied trace
427 element-to-Ca ratios with amplitudes on nearly the same order of magnitude as the longer-term
428 variability described by the records on a seasonal to multi-annual scale (Fig. 2). ~~However, higher~~
429 ~~frequency variability in tridacnid ratio profiles is characterized by more extreme peaks, especially~~
430 ~~in Mg/Ca, skewing the distribution of trace element values. Mn/Ca and Ba/Ca appear to be less~~
431 ~~variable in tridacnid shells than in pectinids, except for specimen TM84, which shows a sharp~~
432 ~~increase in Mn and Ba towards the end of its lifetime. Mn/Ca and Ba/Ca ratios in tridacnids show~~
433 ~~more regular annual or biannual variability than pectinids (most notably specimen SQSA1). It~~
434 ~~must be noted, however, that *P. maximus* shells only recorded one growth season, limiting the~~
435 ~~interpretation of seasonal growth patterns.~~



436

437 Figure 2: Overview of LA-ICP-MS results of Sr/Ca (blue), Mg/Ca (green), Mn/Ca (purple) and
 438 Ba/Ca (orange) in pectinid (upper panel) and tridacnid (lower panel) specimens. Vertical axes are
 439 equal for plots positioned next to each other (but different for the two groups of tridacnid and
 440 pectinid plots). Shaded lines show raw LA-ICP-MS data while solid lines indicate 0.2 span LOESS
 441 fits through the data highlighting monthly-scale variability. A direct comparison of trace elemental
 442 ratios between specimens is provided in **S8**.



443 **Figure 3:** Plots showing samples of semi-diurnal and daily variability in Savitzky-Golay filtered
 444 trace element ratios in selected intervals through *P. maximus* specimen **PM2_2** (A; 51-point filter)
 445 and *T. maxima* specimen **TM29** (B; 21-point filter). Filters isolate hour to daily scale variability
 446 while filtering out the higher-order measurement noise. Arches indicate examples of the
 447 expression of daily (black) and semi-diurnal (grey) cycles in the records.
 448

449
450
451
452
453
454
455
456
457
458
459
460
461
462
463
464
465
466
467
468
469
470
471
472

3.2 Age models

Growth line counting in the *P. maximus* shells was repeated multiple times on both the outer shell surface and in cross sections through the shell by different persons (**Table 1**; **S3**). The variability in counting results shows that the growth lines were not always equally easy to distinguish. In **PM2** and **PM3**, the most likely number of increments (228 and 220 respectively) was ~~counted confirmed~~ in both cross sections and on the outside of the shell, ~~with other analyses yielding both higher and lower numbers.~~ In **PM4**, ~~counts on the outside and on the one available cross section were very close (Table 1).~~ In this case, the counting in the cross section (278 increments) was chosen over the slightly lower count on the outside of the shell (272-273 increments) as reference since the LA-ICP-MS profile was measured on the same cross section and could be directly linked to the counted increments. Note that, while the consistency in daily counts between specimens from the same year and environment is encouraging, inter-specimen variability in the onset of spring growth or the onset of the winter stop (potentially prior to the collection date of November 15th, 2019) places some uncertainty on the absolute date assigned to *P. maximus* shell sections (Chauvaud et al., 2005). ~~The fact that the mean increment width between the *P. maximus* specimens which grew in the same year in the same environment is highly consistent lends confidence to the layer counting result (Table 1). The difference in number of days of growth between specimens can be caused either by variability in the day on which seasonal growth commenced (in spring) or the day on which the winter growth stop commenced (in autumn; Chauvaud et al., 1998). The sampling date (November 15th, 2019) does not preclude the onset of winter growth cessation before the time of sampling.~~ The age-distance relationships (growth curves) resulting from the sclerochronology are shown in **S5**.

473 **Table 1: Growth increments counting in *P. maximus***

Specimen	Increments counted on outer surface	Increments counted in cross sections	Mean <u>daily</u> increment width [$\mu\text{m} \pm 1\sigma$]
PM2	226, 228 , 234, 241	227, 228 , 233	249 \pm 19
PM3	220 , 226, 243	213, 220 , 220	249 \pm 22
PM4	272, 273	278	247 \pm 4

474

475

476 Layer counting in tridacnid shells yielded estimates of semi-diurnal, daily and annual growth
477 (**Table 2; S4**). Annual growth rates calculated from layer counting are highly consistent between
478 specimens from the same species from the same environment (within 1 mm/yr; Table 2), lending
479 confidence to the growth line counting results. The von Bertalanffy growth models based on these
480 growth line countings are plotted in **S5**. Statistics of the parameters (L_{inf} and k) of these growth
481 models and their uncertainty are provided in **S4**.

482

483 **Table 2: Growth line counting in *Tridacna* shells.** Column 3 shows the total number of
 484 increments counted in the specimen, column 4 shows their median width and column 5 shows
 485 the width of an annual increment in the specimen. Note that increments could not be counted over
 486 the entire growth period of the shells, so the numbers in column 3 represent representative
 487 numbers of increments counted in those parts of the shells where they were distinct enough for
 488 counting (see **section 2.5**). Increment timing (semi-diurnal vs diurnal) was established based on
 489 the relative difference between ~~small~~ increment width and ~~annual increment width~~ the distance
 490 between annual growth breaks measured on the outside of the shells.

Specimen	Species	# counted increments	Median increment width [μm]	Annual growth [mm]	Increment timing
TM29	<i>T. maxima</i>	274	26.5	27.9	Semi-diurnal
TM84	<i>T. maxima</i>	109	39.1	26.6	Diurnal
TS85	<i>T. squamosa</i>	310	40.3	20.2	Diurnal
TSFRS1	<i>T. squamosa</i>	225	23.3	20.1	Semi-diurnal
TSM1	<i>T. squamosa</i>	180	33.3	20.6	Diurnal
SQSA1	<i>T. squamosina</i>	153	22.3	14.9	Diurnal

491

492

493 3.3 Growth rates and temporal sampling resolution

494 Growth rates are highly similar between specimens of the same species (**Table 1 and Table 2;**
495 **S3-5**), with *P. maximus* achieving the highest growth rates (~ 220 growth days * ~ 250 $\mu\text{m}/\text{d} \approx 55$
496 mm/yr ; **Table 1**), followed by *T. maxima* (~ 27 mm/yr ; **Table 2**), *T. squamosa* (~ 20 mm/yr ; **Table**
497 **2**) and *T. squamosina* (15 mm/yr ; **Table 2**). ~~The~~ Dividing the width of the daily increments (e.g.,
498 250 μm for *P. maximus*) by spatial LA-ICP-MS sampling resolution of 0.44 μm (see **section 2.4**),
499 these growth rates would seem to translate age models reveal that the average to a temporal
500 resolution of ~~the LA-ICP-MS line scans was~~ 0.04_h, 0.24_h, 0.44_h and 0.27_h for *P. maximus*, *T.*
501 *maxima*, *T. squamosa* and *T. squamosina*, respectively. ~~These estimates were calculated by~~
502 dividing the width of the daily increments (e.g., 250 μm for *P. maximus*) by the resolution of the
503 LAICPMS data (0.4 μm) to obtain the number of LAICPMS measurements per day (e.g., 625
504 pts/day for *P. maximus*, yielding a mean sampling resolution of 0.04h). Note that However, the our
505 LA-ICP-MS slit spot size is wider (20 μm in sampling direction) than the spatial sample resolution,
506 causing causes some significant smoothing, reducing the frequency that can be resolved on the
507 scale of this very fine temporal resolution. Nevertheless, our test applying the LA-ICP-MS settings
508 on a virtual Sr/Ca dataset with the characteristics of the diurnal record by (Sano et al., 2012) and
509 growth rates equivalent to our specimens (see **S13**) reveals that our analytical methodology can
510 easily resolve daily variability even in our slowest-growing specimen (*T. sSquamosina* **SQSA1**),
511 conserving at least 75 % of the signal amplitude. The LA-ICP-MS profiles record trace element
512 variability during growth periods ranging between 220 days (for **PM3**) and 1041 days (for **SQSA1**).

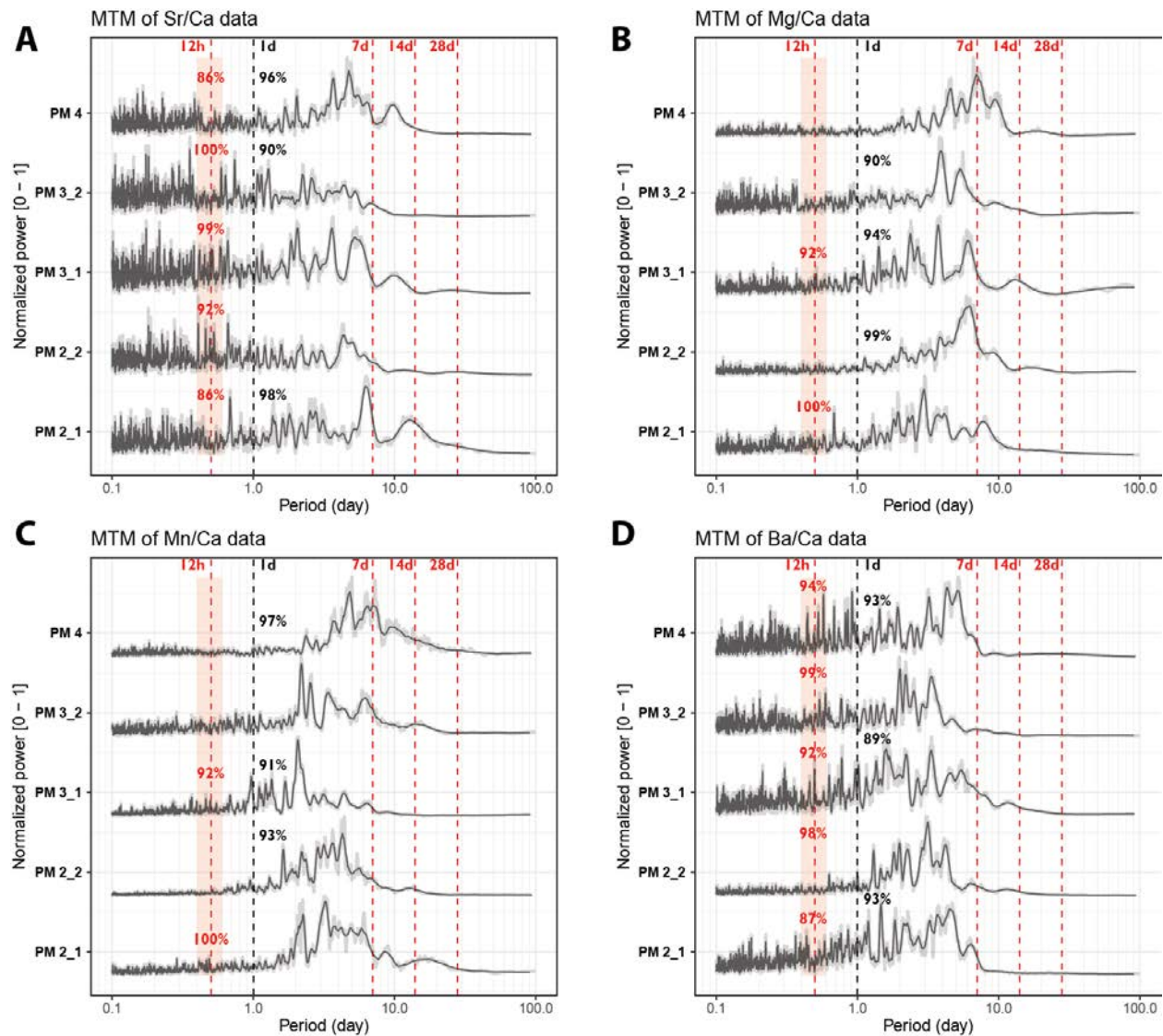
513

514 ~~3.3~~ 3.4 Spectral analysis

515 Normalized power spectra and significance level of daily and tidal periodicities in pectinid and
516 tridacnid records are shown in **Figure 3-4** and **Figure 45**, respectively. Full spectral analysis

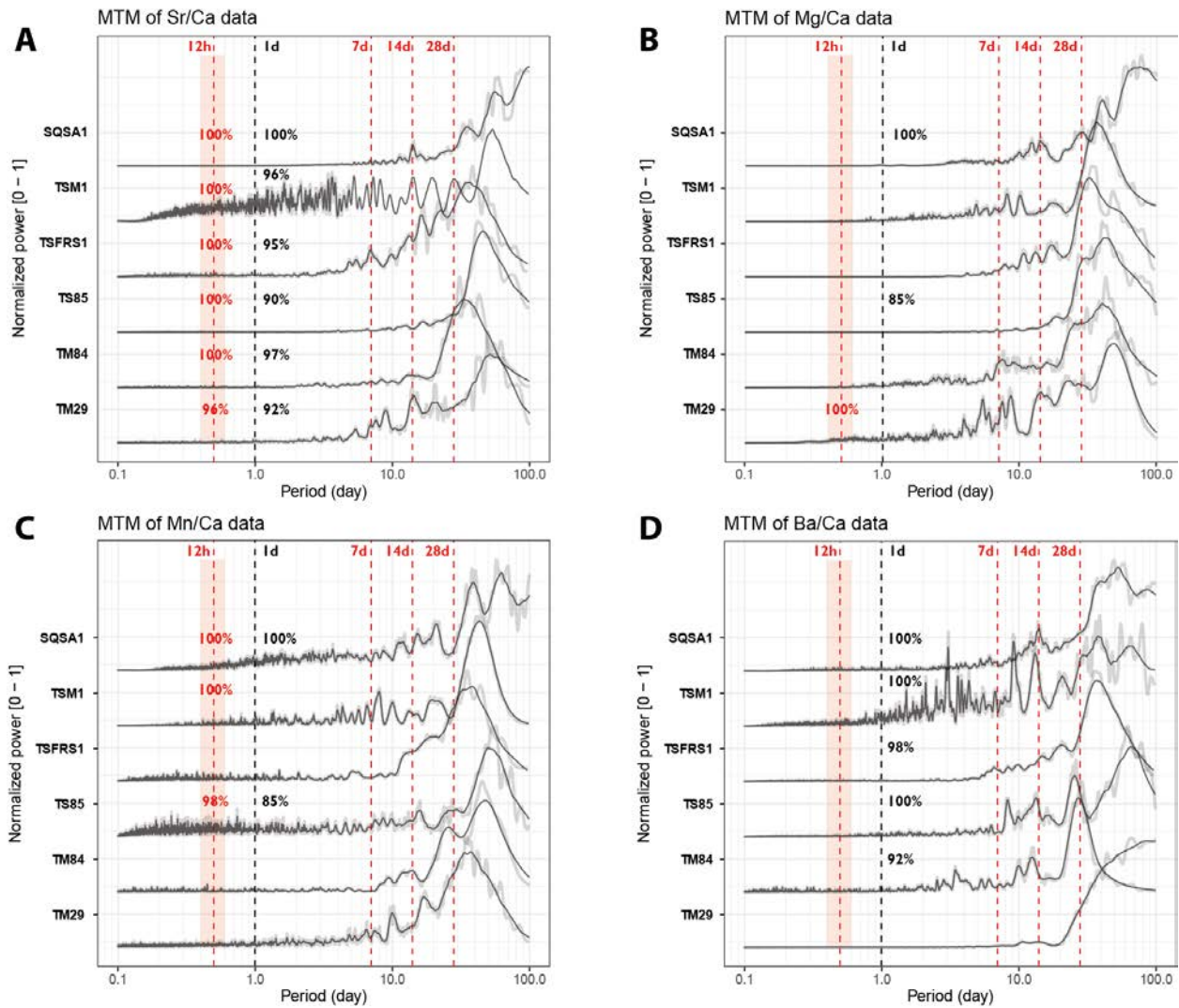
517 results for all trace element records in all specimens are provided in **S9**. All *P. maximus* power
518 spectra (**Fig. 43**) reveal semi-diurnal (12_h) periodicity in Sr/Ca and Ba/Ca with >_86_% statistical
519 significance. Only sections through the ribs of the shells (**PM2_1** and **PM3_1**) show semi-diurnal
520 periodicity in Mg/Ca and Mn/Ca (>_90_% significance). Daily periodicity is present in some, but not
521 all pectinid profiles, ~~but there seems to be no consistent pattern in the presence of diurnal~~
522 ~~variability between specimens, between sections through ribs or valleys in the shell or between~~
523 ~~trace element records. Most power spectra of trace element profiles in p~~Most pectinid trace
524 element records also contain ~~show peaks associated with~~ multi-day tidal periodicities, ~~the most~~
525 ~~dominant being a 7-day period, with weaker expression of cyclicity associated with the fortnightly~~
526 ~~(14d) cycle or lunar month (28d)~~including strong 7-day periodicities and weaker cyclicity
527 associated with 14-day and 28-day cycles. The latter is partly suppressed by the 0.2 span LOESS
528 filter (equivalent to a 44-56 day period depending on the length of the record) applied on the
529 records to remove the seasonal trend from the records. However, these lower frequency cycles
530 are clearly visible in the wavelets (see **S9**).

531 ~~A much more consistent expression of diurnal periodicity is found in the t~~Iridacnid trace element
532 profiles ~~compared to these in~~show more consistent daily periodicity than ~~the~~ pectinid records
533 (**Fig. 54**). Especially Sr/Ca and Ba/Ca records through nearly all tridacnid specimens exhibit
534 strong (>_90_% confidence level) power in the daily period, while daily cyclicity is weaker in Mn/Ca
535 and Mg/Ca records ~~exhibit much less periodicity~~. Sr/Ca records in the tridacnids also contain a
536 significant (>_96_%) semi-diurnal component, whose tidal origin seems clear in most specimens
537 by peaks in power in the longer (7_d, 14_d and 28_d) tidal components.



538

539 **Figure 34:** Multi-taper method spectrograms of Sr/Ca (A), Mg/Ca (B), Mn/Ca (C) and Ba/Ca (D)
 540 records through the five pectinid cross sections after detrending (see section 2.6). All spectra are
 541 normalized by dividing by the highest power peak and plotted on the same horizontal axis. Grey
 542 shaded lines show raw data while solid black lines plot 21-point moving average smoothed
 543 curves. Red vertical dashed lines highlight the expected periods of tidal variability while black
 544 vertical dashed lines indicate 1-day periodicities. Significance levels of peaks on these periods
 545 (see section 2.6 and (Meyers, 2012)) are rounded to the nearest whole percentage point.



546

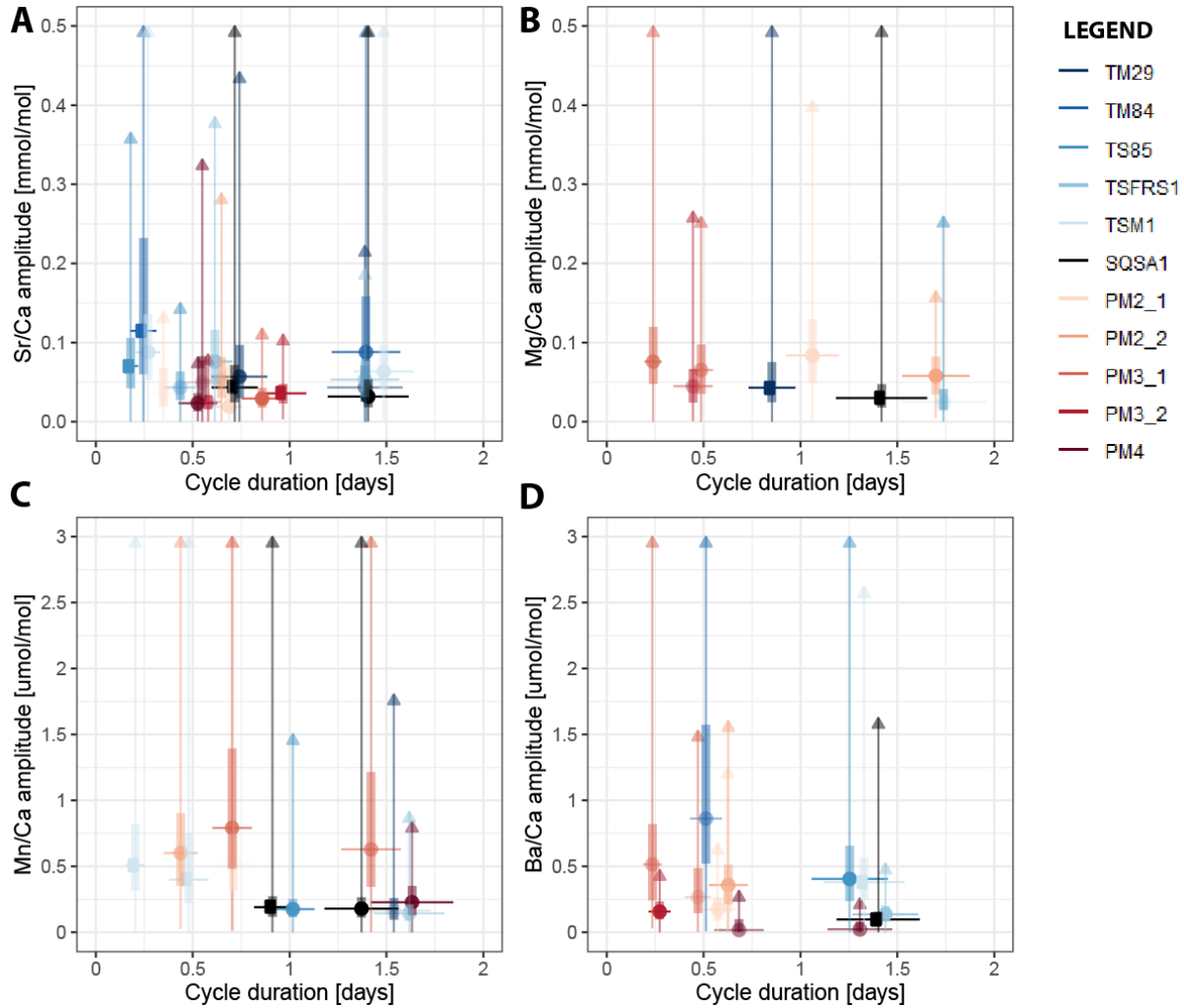
547 **Figure 45:** Multi-taper method spectrograms of Sr/Ca (A), Mg/Ca (B), Mn/Ca (C) and Ba/Ca (D)
 548 records through the six tridacnid cross sections after detrending (see section 2.6). All spectra are
 549 normalized by dividing by the highest power peak and plotted on the same horizontal axis. Grey
 550 shaded lines show raw data while solid black lines plot 21-point moving average smoothed
 551 curves. Red vertical dashed lines highlight the expected periods of tidal variability while black
 552 vertical dashed lines indicate 1-day periodicities. Significance levels of peaks on these periods
 553 (see section 2.6 and (Meyers, 2012)) are rounded to the nearest whole percentage point.

554

555 ~~3.4~~ 3.5 Variance decomposition

556 Variability at the daily (24_h) and ~~tidal~~semi-diurnal (12_h) scale in all trace element records through
557 all specimens was extracted using bandpass filtering (**section 2.7**; see **S9** and **S10**). The median
558 amplitude of variability within these stacks was plotted against the median period of the variability
559 per element and per specimen to highlight dominant periodicities in the trace element data
560 (**Figure 65**). As noted in the spectral analysis results (**section 3.34**), trace element composition
561 in tridacnid shells is more strongly controlled by daily variability than in pectinid shells (**Fig. 56**;
562 **S10**). The difference is especially noticeable in Sr/Ca and Ba/Ca ratios, which show a clear divide
563 between daily periodicity in tridacnid shells and tidal periodicity in pectinids (see **Fig. 56**). The
564 differences in Mg/Ca and Mn/Ca ratios are less ~~clear~~obvious.

565



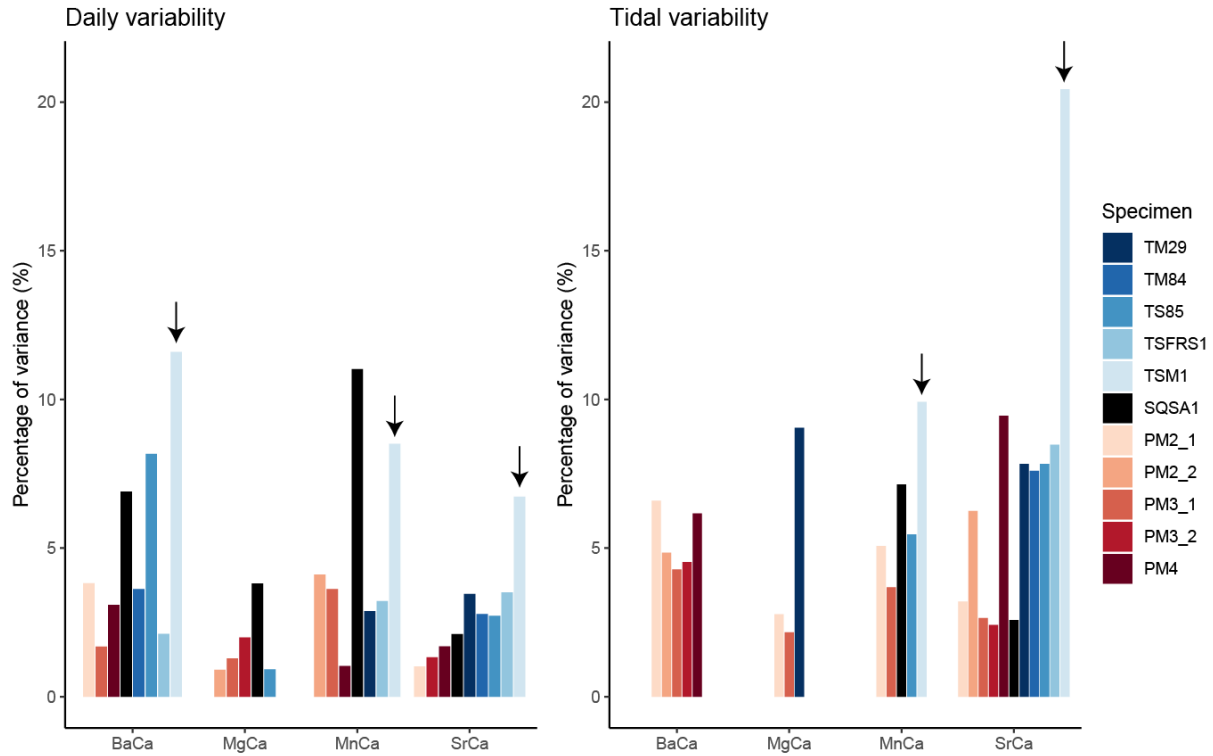
566

567 **Figure 56:** Cross plot showing the amplitude of variability of dominant spectral periods in Sr/Ca
 568 (A), Mg/Ca (B), Mn/Ca (C) and Ba/Ca (D) against the period (duration) of the cycle. Round
 569 symbols indicate the median amplitude of the cycle, while vertical bars and lines show interquartile
 570 differences and ranges in the amplitude over the record. Horizontal bars indicate the width of the
 571 bandpass filter used to extract periodic variability. Colors highlight different specimens (see
 572 legend).

573

574 An example of the distribution of normalized variability within the trace element records after each
575 data processing step is shown in **S7**. ~~From this example~~ it is clear shows that a large fraction of
576 the variance in the records (73_% in this record after trimming outliers) is explained by low-
577 frequency (seasonal scale) variability (**S7**). Of the remaining smoothed and detrended dataset, at
578 most 20_% of the variance is explained by daily and tidal (semi-diurnal) periodicity (see **Figure 76**
579 and **Table 3**). A full decomposition of variance in all trace element records through all specimens
580 is provided in **S7**. **Figure 65** and **Figure 6A-7A** ~~shows~~ that, overall, the variance explained by
581 daily periodicity is higher in tridacnids than in pectinids (Wilcoxon signed rank test; $W = 44$; $p =$
582 0.009). The difference between species is smaller for tidal variability (**Fig. 76B**). There is no clear
583 difference in relative dominance of ~~tidal~~ semi-diurnal variability between trace element records,
584 but daily variability is more strongly expressed in Ba/Ca and Mn/Ca records, especially in tridacnid
585 shells. Finally, *T. squamosa* specimen **TSM1**, which grew under a sunshade, does not exhibit
586 significantly lower daily periodicity compared to the other tridacnid specimens.

587



588

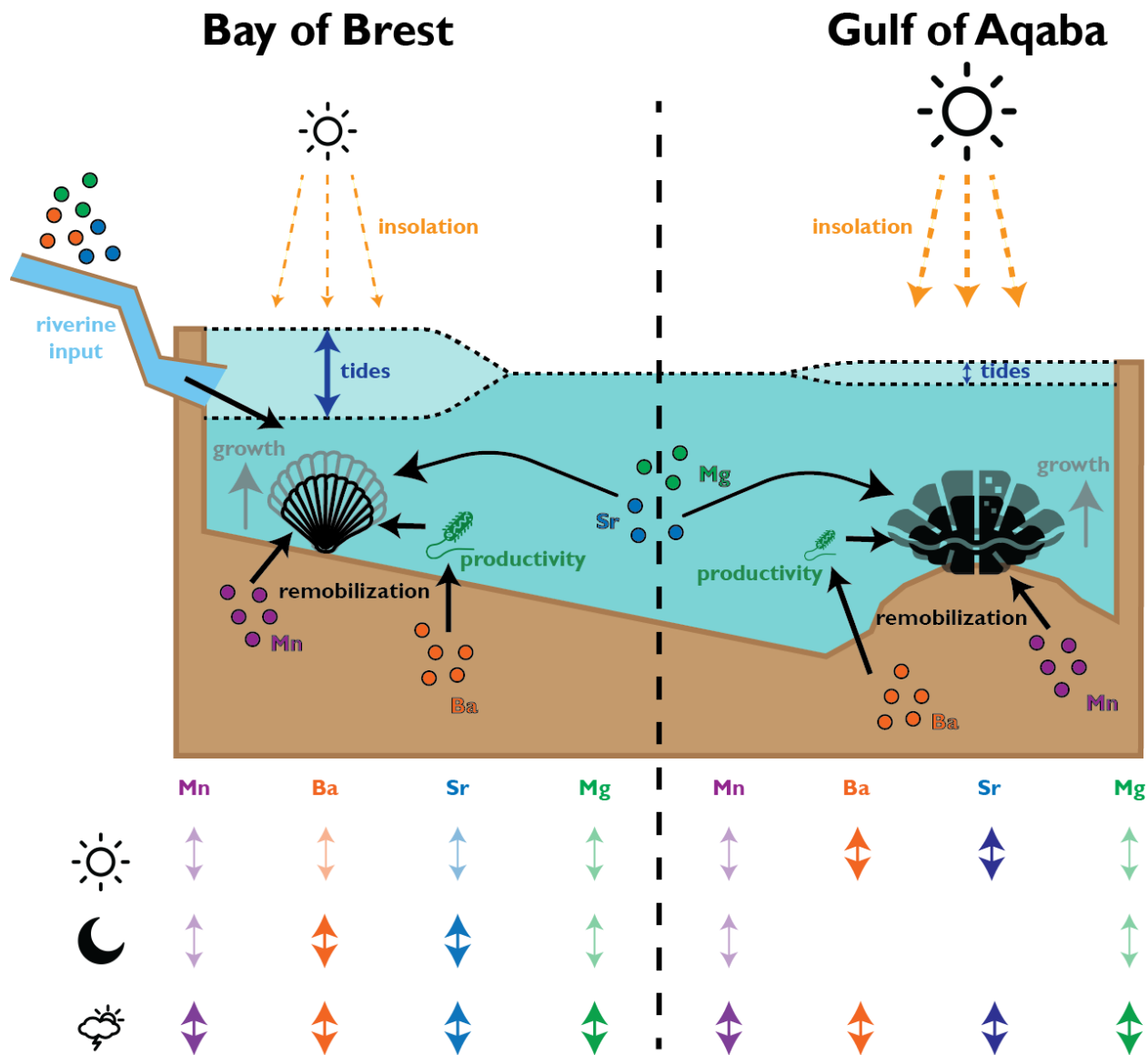
589 **Figure 67:** Summary of relative variance (in %) of significant daily (left) and tidal (right) variability
 590 extracted from trace element records. Colors highlight different specimens (see legend). Note that
 591 the *T. squamosa* specimen **TSM1** which grew under a sunshade is highlighted with a black arrow.

592

593 **Table 3:** Overview of the relative (in %) variance associated with daily and tidal variability in all
 594 trace element records through all specimens. Empty cells represent records for which no
 595 significant tidal or daily periodicity was found (see **Fig. 4-53-4**).

	Daily variance				Tidal variance			
	[% relative to detrended record]				[% relative to detrended record]			
	Ba/Ca	Mg/Ca	Mn/Ca	Sr/Ca	Ba/Ca	Mg/Ca	Mn/Ca	Sr/Ca
PM2_1	3.8 %			1.0 %	6.6 %	2.8 %	5.1 %	3.2 %
PM2_2		0.9 %	4.1 %		4.9 %			6.3 %
PM3_1	1.7 %	1.3 %	3.6 %		4.3 %	2.2 %	3.7 %	2.7 %
PM3_2		2.0 %		1.3 %	4.5 %			2.4 %
PM4	3.1 %		1.0 %	1.7 %	6.2 %			9.5 %
TM29			2.9 %	3.5 %		9.0 %		7.8 %
TM84	3.6 %			2.8 %				7.6 %
TS85	8.1 %	0.9 %		2.7 %			5.5 %	7.8 %
TSFRS1	2.1 %		3.2 %	3.5 %				8.5 %
TSM1	12 %		8.5 %	6.7 %			10 %	20 %
SQSA1	6.9 %	3.8 %	11 %	2.1 %			7.1 %	2.6 %

596



597

598 **Figure 78:** Schematic overview of environmental parameters interpreted to affect shell growth
 599 and composition of pectinids in the Bay of Brest and tridacnids in the Gulf of Aqaba. The table at
 600 the bottom provides a schematic qualitative overview of the amount of variance in the trace
 601 element records of the taxa is explained by daily (sun symbol), tidal (moon symbol) or aperiodic
 602 (cloud symbol) variability in the environment.

603

4. Discussion

4.1 Compositional differences between pectinids and tridacnids

Pectinid and tridacnid shells are characterized by similar mean Sr/Ca and Ba/Ca ratios (Sr/Ca of 1.3 ± 0.3 and 1.5 ± 0.6 mmol/mol respectively; Ba/Ca of 2.8 ± 2.5 and 3.0 ± 5.1 $\mu\text{mol/mol}$ respectively; uncertainty is calculated as 1σ). Mean Mg/Ca and Mn/Ca ratios are higher in *P. maximus* than in *Tridacna* species (Mg/Ca = 3.1 ± 0.9 and 0.7 ± 0.9 mmol/mol; Mn/Ca = 7.8 ± 4.7 and 2.7 ± 7.8 $\mu\text{mol/mol}$; 1σ ; **Figure 2; S4**). The incorporation of higher concentrations of the elements Mg and Mn, which have a lower ionic radius than Sr and Ba, in calcitic pectinid shells compared to aragonitic tridacnid shells makes sense given the higher partition coefficient of these elements in calcite than in aragonite (Day and Henderson, 2013; Wassenburg et al., 2016).

Differences between tridacnid specimens generally exceed the differences between tridacnids and pectinids (1σ of Ba/Ca among all tridacnid specimens = $2.1 \mu\text{mol/mol}$), suggesting large inter-species differences. However, individual records such as those in **TM84** and **PM3_1** show large variability (especially in Ba/Ca and Mn/Ca) compared to other specimens of the same species. Inter-specimen variability is higher in tridacnid shells than in pectinids (inter-specimen relative standard deviations as a fraction of mean ratio for Ba/Ca: 0.74 vs 0.64 $\mu\text{mol/mol}$, Mg/Ca: 0.37 vs 0.20 mmol/mol, Sr/Ca: 0.19 vs 0.03 mmol/mol and Mn/Ca: 0.78 vs 0.33 $\mu\text{mol/mol}$ for tridacnids and pectinids, respectively). **Figure 2** shows that this variability between tridacnids is not readily explained by differences between species, but mostly reflects differences in the trends within the records, with some specimens (e.g., **TM84**, **TSM1** and **TS85**) showing trends in composition towards the end of the record (see also **S8**). It thus seems that inter-specimen differences, perhaps driven by growth stress, are dominant drivers of trace element variability in giant clams. This interpretation is corroborated by the observation that trace element compositions in tridacnid shells are significantly more skewed towards higher values than in pectinids (mean skewness per element and per specimen is 9.7 for tridacnids and 0.9 for pectinids). This skewness reflects the

629 high peaks in trace element composition observed in tridacnid profiles, especially near the ventral
630 margin (e.g., specimens **TM84**, **TSM1** and **TS85**; see **section 2.4**; **Fig. 2**; **S8**), which hint towards
631 growth disturbances at the individual level.

632 4.2.4 Trace element variability in *P. maximus*

633 4.2.4.1 Comparison with previous studies

634 Trace element concentrations in *P. ~~Maximus-maximus~~* analyzed in this study are in close
635 agreement with concentrations found in wild (live collected) pectinid shells in the literature (Lorrain
636 et al., 2005; Barats et al., 2008; Poitevin et al., 2020; Fröhlich et al., 2022) (~~Lorrain et al., 2005;~~
637 ~~Barats et al., 2008; Poitevin et al., 2020; Fröhlich et al., 2022~~). In these studies, Sr/Ca shows a
638 strong link with calcification rate (as measured by the width of daily shell increments; (Lorrain et
639 al., 2005) ~~Lorrain et al., 2005~~), although previous studies did not assess variability on the (sub-
640)daily scale. The long-term trends in our Sr/Ca records seem to confirm this correlation, with
641 higher values being recorded in the middle of the growing season (day 50-150; **Fig. 2**) when
642 growth rates are highest (see **S5**). Previous studies demonstrate that Mg/Ca ratios in pectinid
643 shells are at most partially related to temperature and/or salinity (Lorrain et al., 2005;
644 Poitevin et al., 2020). The fact that the studied *P. maximus* specimens, which all grew during
645 the same year in the same environment, do not show a synchronous Mg/Ca pattern (**Fig. 2**)
646 corroborates this previous work and argues against a straightforward temperature
647 dependence for Mg/Ca in *P. maximus* ~~There is some discussion on the dependence of Mg/Ca~~
648 ~~ratios in pectinid shells to temperature and/or salinity (Lorrain et al., 2005; Poitevin et al., 2020).~~
649 ~~This study's individuals that grew during the same year in the same environment do not show a~~
650 ~~synchronous Mg/Ca pattern (**Fig. 2**), arguing against a simple temperature dependence for Mg/Ca~~
651 ~~in *P. maximus*.~~ In addition, the lack of strict coherence between profiles of Mg/Ca (and other
652 elements) in parallel transects through *P. maximus* shells (e.g., **PM2_1** and **PM2_2**; **Fig. 2**) hints
653 at compositional heterogeneity within the shells, in agreement with findings by (Lorrain et al.,

654 2005) ~~hints at compositional heterogeneity within the shells~~. Low correlations between profiles
655 through the same shell at the daily scale are also partly driven by small misalignments of the
656 timing of shell formation between the transects at the sub-millimeter scale and variations in the
657 height of trace element peaks, especially in Mn/Ca and Ba/Ca, which are higher further towards
658 the outside of the shell (**S2**).

659 There is evidence suggesting that Mg content varies in mollusk shells in function of the amount
660 of organic matter in the biomineral (Dauphin et al., 2003; Richard, 2009; Tanaka et al., 2019)
661 ~~(Dauphin et al., 2003; Richard, 2009; Tanaka et al., 2019)~~. Contrarily, Mn is known to be taken
662 up in thermodynamic equilibrium in the mineral fraction of bivalve shells (Onuma et al., 1979;
663 Soldati et al., 2016) ~~(Onuma et al., 1979; Soldati et al., 2016)~~, and Mn/Ca ratios in *P. maximus*
664 have been shown to faithfully record fluctuations of dissolved Mn in the coastal environment
665 driven by riverine input and redox conditions (Barats et al., 2008) ~~(Barats et al., 2008)~~. Similarly,
666 there is strong evidence that Ba/Ca ratios in *P. maximus* (and other mollusks) record changes in
667 Ba available in the environment linked to primary productivity (e.g., (Gillikin et al., 2008; Thébault
668 et al., 2009; Fröhlich et al., 2022) ~~Gillikin et al., 2008; Thébault et al., 2009; Fröhlich et al., 2022~~).
669 Interestingly, our results (Fig. 2) show that background Ba/Ca values are not equal in the shells
670 of *P. maximus* and tridacnid specimens grown in the same environment. This contradicts the
671 assessment by (Gillikin et al., 2005) that background Ba/Ca concentrations are a function of
672 environmental conditions and can be consistently subtracted from Ba/Ca records to separate
673 peak from background values. This–The suggested relationship between Ba/Ca and primary
674 productivity would explain the skewed (skewness > 1; **S8**) character of the Ba/Ca records and the
675 correlation between Ba/Ca and Mn/Ca in ~~our~~ the studied *P. maximus* specimens, as the reducing
676 conditions following peaks in primary productivity favor the remobilization of Mn into the water
677 column causing short-lived simultaneous increases in Ba/Ca and Mn/Ca in the shells (Dehairs et
678 al., 1989; Barats et al., 2008, 2009) ~~(Dehairs et al., 1989; Barats et al., 2008; 2009)~~.

679 4.2.2 -Short-term changes in shell composition in *tridacnids P. maximus*

680 In the context of the high-resolution trace element variability central to this study, it seems
681 plausible that short-term changes in the environment of the Bay of Brest were drivers of Mn/Ca
682 and Ba/Ca variability in *P. maximus* shells, while Mg/Ca and Sr/Ca composition is mostly driven
683 by changes in calcification rate. This would suggest that the significant tidal (12_h) component in
684 Ba/Ca and Mn/Ca records through *P. maximus* (**Fig. 43**) is driven directly by redox changes over
685 the strong tidal cycle in the Bay of Brest (see_(Polsenaere et al., 2021)-~~Polsenaere et al., 2021~~)
686 and resuspension of Ba and Mn due to tidal currents_(Hily et al., 1992)-~~(Hily et al., 1992)~~, while
687 tidal rhythms in Mg/Ca and Sr/Ca may be a consequence of the scallop's calcification response
688 to changes in its environment (e.g., temperature, salinity and light availability) through the large
689 (up to 7_m range) tidal cycle (**Fig. 87**). The latter corroborates with previous studies in other calcitic
690 mollusk shells which demonstrated that Mg incorporation on short timescales is driven by the
691 metabolic response to subtle changes in the environment_(Lazareth et al., 2007)-~~(Lazareth et al.,~~
692 ~~2007)~~. Finally, care must be taken to interpret trace element variability in *P. maximus* shells, since
693 large intra-shell gradients in Mg/Ca, Sr/Ca and Mn/Ca have previously been observed in this
694 species, making trace element composition highly dependent on the location of measurements
695 relative to the outer shell surface or positioning relative to striae on the shell surface_(Freitas et
696 al., 2009)-~~(Freitas et al., 2009)~~. Even though the LA-ICP-MS line scans in this study targeted
697 exclusively the oOSL of *P. maximus* specimens, variability in elemental ratios resulting from small
698 changes in the distance of the line scan from the outer edge of the shell cannot be fully excluded
699 (Richard, 2009)-~~(Richard, 2009)~~.

700

701 4.2.3 Trace element variability in tridacnids

702 4.23.1 Comparison with previous studies

703 Results for Sr/Ca, Mg/Ca and Ba/Ca in this study's tridacnid specimens broadly corroborate trace
704 element results in other tridacnid studies (e.g., (Elliot et al., 2009; Sano et al., 2012; Yan et al.,
705 2013; Warter et al., 2018) ~~Elliot et al., 2009; Sano et al., 2012; Yan et al., 2013; Warter et al.,~~
706 ~~2018~~). While data on Mn/Ca in the OSL of tridacnids is scarce, the Mn/Ca ratios in tridacnids in
707 this study (mean Mn/Ca = 7.8 ± 4.7 $\mu\text{mol/mol}$) are similar to LA-ICP-MS Mn/Ca data
708 available in the literature ((Warter et al., 2015), 4-10 $\mu\text{mol/mol}$), but significantly lower than Mn/Ca
709 values measured using total digestion Atomic Absorption Spectrometry ((Madkour, 2005), ~30
710 $\mu\text{mol/mol}$). The main difference between the techniques is that LA-ICP-MS (both in this study as
711 in (Warter et al., 2015)) sampled shell layers where growth lines were visible and did not include
712 pre-treatment, while the total digestion study (Madkour, 2005) removed organic matter by roasting
713 the shells at 200°C prior to bulk shell analysis. Given that Mn in bivalve shells is typically
714 associated with the mineral fraction of the shell (Soldati et al., 2016), ~~The~~ the difference in results
715 may therefore hint at differences between shell layers within tridacnids, or differences in Mn
716 concentration between the organic and mineral fractions in the shells. Bivalve shells typically
717 contain between 1% and 5% organic matter (Marin and Luquet, 2004), with tridacnid shells being
718 notable for their low organic matter content (< 1%; (Taylor and Layman, 1972; Agbaje et al.,
719 2017) ~~Agbaje et al., 2017; Taylor and Layman, 1972~~). ~~Given that most Mn in bivalve shells is~~
720 ~~typically associate with the mineral fraction of the shell (Soldati et al., 2016), it~~ It thus seems
721 unlikely that ~~such a large~~ the fraction of differences in Mn/Ca ratio between bulk analyses
722 (Madkour, 2005) and in situ analysis ((Warter et al., 2015); this study) could originate from
723 variations within the organic matrix, which only constitutes such a small fraction of the shell.
724 Therefore, we consider a difference in Mn concentration between shell layers in tridacnids more
725 likely. The lack of consistent trace element offsets between the tridacnid species under study here
726 (*T. maxima*, *T. squamosa* and *T. squamosina*) confirms the chemical similarities of shells tridacnid
727 species found in previous studies (e.g., *T. gigas*; (Elliot et al., 2009; Yan et al., 2013) ~~Elliot et al.,~~
728 ~~2009; Yan et al., 2013~~; *T. crocea*; (Warter et al., 2018); *T. derasa*; (Sano et al., 2012)).

729 4.23.2 Short-term variability in Sr/Ca paced to the day-night cycle
730 Sr/Ca in tridacnids is ~~thought~~ hypothesized to be strongly controlled by light intensity through a
731 circadian rhythm linked to the day-night cycle (Sano et al., 2012; Warter et al., 2018). This would
732 explain the strong daily periodicity in Sr/Ca records through all tridacnids in this study. This daily
733 periodicity may be caused by the ctenidium in tridacnids working on a daily rhythm to keep the
734 acid-base balance in the hemolymph of the clams to offset the CO₂ depletion by photosymbionts
735 (which is paced to the day-night cycle of light availability). In the process, Ca²⁺-channels and
736 Na⁺/H⁺-exchangers work to keep the charge balance in the internal fluid and provide nutrients and
737 ions for shell mineralization, letting in compatible trace elements such as Sr²⁺ (Ip and Chew,
738 2021). This mechanism follows the biomineralization model by (Carré et al., 2006) and is
739 supported by the high affinity of Sr²⁺ with Ca-channels (Hagiwara and Byerly, 1981) and the high
740 ionic fluxes supported by this pathway, allowing enough membrane permeability to support the
741 fast shell formation in tridacnids (Coimbra et al., 1988; Sather and McCleskey, 2003). Following
742 this line of reasoning, the preconcentration of Sr²⁺ in the extrapallial fluid through Ca-channels
743 should have a larger effect on shell Sr/Ca ratios in tridacnids than the discrimination against Sr²⁺
744 (or other trace elements) through shell organic matrix during mineralization of the shell from this
745 fluid (as proposed in (Gillikin et al., 2005)) . This model could explain the indirect link between
746 trace element ~~uptake~~ incorporation into the shell ~~in~~ of tridacnids and the day-night cycle without
747 a direct causal relationship between trace element concentration and light availability (as
748 demonstrated by the strong daily cycle in trace elements in the shaded **TSM1** specimen). It is
749 worth noting that experiments on freshwater bivalves (e.g., *Corbicula fluminea*; (Zhao et al.,
750 2017)) revealed that a closure of the Ca²⁺ channels did not influence Sr concentrations in the
751 shell, arguing against a kinetic effect on Sr partitioning into the shell.

752 4.23.3 Tidal vs. diurnal variability

753 Our spectral analysis does not allow us to distinguish between the expression of the solar day (24
754 h) and lunar day (~24.8 h) because the width of the bandpass filters used to extract periodicities
755 (~22–36 h) encompass both frequencies. While we cannot exclude the possibility that some of
756 the daily (24 h frequency band) periodicity in tridacnid records is an expression of the lunar cycle,
757 it seems unlikely for most records except Sr/Ca, because the expression of the other lunar ~~cycles~~
758 periodicities (most notably the ~12 h cycle) is much weaker in tridacnids compared to the pectinids
759 (see Fig. 6-7). Nevertheless, it remains possible that the diurnal cycle in Sr/Ca in tridacnids,
760 previously interpreted as a response to the day-night cycle, is in fact caused by a circadian rhythm
761 paced to the lunar day. Additionally, vertical mixing, a major driver of sea surface temperature
762 changes in the northern Gulf of Aqaba, is shown to be driven by a combination of surface wind
763 intensity (which has strong daily variability) and the presence of tidal currents (Carlson et al.,
764 2014). It is therefore possible that changes in local surface water temperature partly control the
765 observed (semi-)diurnal variability in trace element concentrations in Red Sea tridacnids.

766 4.23.4 Seasonal variability and temperature relationships

767 On longer (seasonal) timescales, Sr/Ca in tridacnids has been suggested as a temperature proxy
768 similar to the well-known Sr/Ca-Sea Surface Temperature relationship in tropical corals (Lough,
769 2010; Yan et al., 2013). However, significantly lower Sr/Ca ratios in tridacnids compared to coral
770 aragonite (1.5 – 2.0 mmol/mol vs. 7.5 – 9.5 mmol/mol in corals; (Elliot et al., 2009); **Fig. 2**) suggest
771 that tridacnids exert a large degree of biological control on the Sr concentration in their shells,
772 either ~~possibly~~ through the light-sensitive photosymbiosis-calcification relationship outlined above
773 (section 4.3.2) or otherwise through active Sr removal from the biomineralization site by Sr-
774 binding organic molecules (following the model proposed by (Gillikin et al., 2005)). Similarly,
775 Mg/Ca ratios in tridacnids were previously thought to primarily record water temperature (e.g.,
776 (Batenburg et al., 2011)) but our detailed investigation shows ~~here~~ large differences in Mg
777 concentration within tridacnid shells- and a strong anticorrelation of Mg with sulfur compounds

778 associated with the organic matrix in the shell (see **section 4.2.11**; (Dauphin et al., 2003)), has
779 been put forward as evidence for a strong control of calcification and microstructure on Mg
780 composition in tridacnid shells (Yoshimura et al., 2014). However, evidence from studies on
781 foraminifera calcification demonstrate that the sulfur in biocarbonates is not organically bound
782 and that the covariation with Mg might instead be caused by lattice distortion due to incorporation
783 of Mg favoring simultaneous S incorporation (van Dijk et al., 2017). If this is also the case in
784 tridacnids, the Mg/Ca-S/Ca covariance observed in previous studies might not preclude the use
785 of Mg/Ca as a temperature proxy. In that case, more detailed calibration studies (e.g. using
786 controlled growth experiments; (Warter et al., 2018)) are required to establish this proxy.

787 4.2.3.5 Ba/Ca and Mn/Ca in tridacnids

788 As in the pectinids, Ba/Ca ratios in tridacnids likely reflect changes in Ba concentration in the
789 environment, which can be caused by river input, upwelling of comparatively nutrient-rich waters
790 or blooms of Ba-rich phytoplankton (Vander Putten et al., 2000; Elliot et al., 2009). Given that Mn
791 is mostly associated with the mineral fraction of bivalve shells and seems to fractionate into the
792 shell close to equilibrium with seawater (Onuma et al., 1979; Soldati et al., 2016), Mn/Ca ratios in
793 tridacnids likely reflect the availability of dissolved Mn in the water column, as in other mollusk
794 taxa (e.g., (Barats et al., 2009); see **section 4.24**). This assumption is supported by the correlation
795 between Mn/Ca and Ba/Ca measured in this study (**Fig. 2**), suggesting that both records are
796 influenced on seasonal timescales by variability in nutrient availability and redox conditions (*sensu*
797 (Dehairs et al., 1989)). Part of this correlation between Mn/Ca and Ba/Ca is driven by synchronous
798 increases in both elements near the start and end of the profiles through tridacnid shells (**Fig. 2**).
799 These changes may reflect a decrease of control on shell composition during periods of stress,
800 or alternatively reflect periods of slower growth which cause more primitive microstructures
801 (characterized by higher concentrations of trace elements) to be formed (Warter et al., 2018).

802 4.2.6 Environmental changes in the Gulf of Aqaba

803 Given that the Gulf of Aqaba is oligotrophic, seasonally stratified, and lacks significant riverine
804 input (Nassar et al., 2014; Manasrah et al., 2019)(~~Nassar et al., 2014; Manasrah et al., 2018~~), the
805 variability in nutrient concentrations and redox conditions driving Mn/Ca and Ba/Ca variability in
806 tridacnids are likely driven by convective overturning. The tidal amplitude is much smaller than in
807 the Bay of Brest (<_1 m; (Manasrah et al., 2019)) and is unlikely to drive significant short-term
808 fluctuations in sea water chemistry. This may therefore explain the lack of tidal (12_h) periodicity
809 in Ba/Ca and Mn/Ca in tridacnids (**Fig. 5-6**) . Nevertheless, tidal rhythms have been observed in
810 the behavior and growth of deep-sea bivalves living far below the direct influence of tides on the
811 environment, proving that such patterns can be recorded by the animals through their circadian
812 rhythm (Schöne and Giere, 2005; Nedoncelle et al., 2013; Mat et al., 2020)(~~Schöne and Giere,~~
813 ~~2005; Nedoncelle et al., 2013; Mat et al., 2020~~). In this case, the daily cycle seems to have been
814 more important for Ba/Ca in tridacnids, plausibly by driving diurnal changes in primary productivity
815 in the Gulf of Aqaba. Alternatively, the daily periodicity found in tridacnid shell chemistry may in
816 fact be a response to the lunar day (~24.8_h) cycle, which is imprinted in the shell's chemical
817 composition through periodic exposure of the clams to extreme heat or air (subaerial exposure)
818 in their shallow water environment during exceptionally low tides. The stress induced from this
819 exposure could have affected calcification and incorporation of trace elements (see
820 **above section 4.3.5**).

821 Interestingly, Sr/Ca ratios in tridacnids do exhibit tidal periodicity (**Table 2; Fig. 3**), perhaps driven
822 by a circadian rhythm in calcification linked to the tidal cycle, or by subtle changes in water
823 temperature driven by tidal currents (Carlson et al., 2014). This 12_h periodic behavior is not
824 observed in previous studies of Sr/Ca ratios in tridacnids (Sano et al., 2012; Warter et al., 2018).
825 A recent valvometric study on tridacnids found a 12_h period in activity, which supports the
826 hypothesis that a circadian rhythm paced to the tidal cycle could influence shell calcification
827 (Killam and Clapham, 2018b). Significant daily fluctuations in solar radiation (up to 1500 W m⁻²;

828 (Manasrah et al., 2019)) likely exerted ~~a dominant~~ control on the calcification of tridacnids in the
829 Red Sea, explaining the strong diurnal periodicity in Sr/Ca and Ba/Ca records in this study (see
830 **Fig. 67** and **Fig. 98**). As in the (non-symbiotic) pectinid data, it seems likely that the majority of
831 Mn/Ca and Ba/Ca variability in tridacnids directly reflects changes in the chemistry of the sea
832 water and its constituents (e.g., particulate organic matter) while Mg/Ca and Sr/Ca variations are
833 driven by changes in calcification and microstructure. The latter may be indirectly influenced by
834 light intensity through photosynthesis by the symbionts, or by circadian rhythms paces to the
835 diurnal or tidal cycle.

836

837 **4.3.4** Role of photosymbiosis on high-frequency chemical variability

838 **4.3.4.1** Effect of symbiosis on ~~calcification~~ shell formation

839 While the amplitude of diurnal variability in trace element concentrations does not vary much
840 between the symbiotic tridacnids and the non-symbiotic pectinids (**Fig. 56**), the amount of
841 variance in the trace element records explained by daily cyclicity is up to twice as high in tridacnids
842 (**Fig. 76**; **Table 3**). This suggests that the 24_h cycle has a much larger relative influence on trace
843 element composition (especially Sr/Ca and Ba/Ca) in tridacnids than in pectinids. This seems to
844 point towards a role of the photosymbionts in calcification by tridacnids, such as through symbiont-
845 mediated diurnal variation in the pH of the extrapallial fluid (Ip et al., 2006), as well as active
846 transport of HCO_3^- for calcification (Chew et al., 2019) and as a C supply to the symbionts from
847 the host (Boo et al., 2021). Given the differences in absolute-elemental ratios between these two
848 groups of bivalves, comparing variance yields a more robust assessment of the relative
849 importance of tidal or diurnal variability on shell composition than looking at the absolute size
850 (amplitude) of the chemical cycle. While the difference in variance is clear, the importance of
851 diurnal cyclicity on the photosymbiotic tridacnids is not as big as one might expect. Rarely more

852 than 10_% of the variance is explained by day-night variability (**Table 3**). This seems to contradict
853 the large daily Sr/Ca amplitudes found in (Warter et al., 2018) and the trace element fluctuations
854 found in (de Winter et al., 2020), which rival the seasonal cycle in these trace element ratios in
855 terms of amplitude. However, the percentages in **Table 3** relate to the amount of variation in the
856 complete records through these individuals and therefore also contain areas of the shell where
857 daily cyclicality is less pronounced, while values in previous studies often reflect maximum
858 amplitudes recorded in parts of the shell with exceptionally clear daily increments.

859 4.34.2 Effect of differences in the environment

860 It seems plausible that part of the difference in diurnal variability between pectinids and tridacnids
861 is explained by a difference in the environment between the Gulf of Aqaba and the Bay of Brest,
862 rather than the presence of photosymbionts. The diurnal insolation cycle in the Gulf of Aqaba is
863 larger than in the Bay of Brest (1500 vs 546 W^*m^{-2} maximum summer irradiance; (Roberts et al.,
864 2018; Manasrah et al., 2019)). If calcification in pectinids would be equally sensitive to sunlight,
865 this difference may explain much of the difference between the species. In this scenario, part of
866 the strong tidal component in the pectinid trace element data may be explained by the influence
867 of differences in water depth on the penetration of sunlight through the murky waters of the Bay
868 of Brest (Roberts et al., 2018). In fact, tidal movement can cause strong non-linear amplification
869 or reduction of the solar irradiance at the sea floor of the Bay of Brest by factors exceeding 10,
870 especially outside the summer months, which in turn has a significant effect on primary
871 productivity in the water column (Roberts et al., 2018). This tidal effect is likely to be much weaker
872 in the Gulf of Aqaba, given its comparatively low tidal amplitude, clear oligotrophic waters, and
873 much stronger and less seasonal day-night cycle (Manasrah et al., 2019). Indeed, even in non-
874 photosymbiotic bivalves, light and food availability are demonstrated to be major drivers of the
875 animal's behavior (e.g., (Ballesta-Artero et al., 2017)). The combination of the daily and tidal
876 cycles on solar irradiance at depth and photosynthesis in the Bay of Brest may therefore pose an

877 alternative pathway for strong tidal cyclicity in the trace element composition of pectinids in this
878 study and account for part of the twofold increase in daily variability in tridacnids compared to the
879 pectinids (**Fig. 6-77-8; Table 3**).

880 4.34.3 Effect of direct insolation

881 Specimen **TSM1** poses an interesting case study for investigating the link between sunlight and
882 calcification in tridacnids, since it grew under a sunshade and therefore experienced a dampened
883 diurnal variability in insolation compared to other giant clams in the area. The fact that this
884 specimen exhibits similar or even higher diurnal variability in shell chemistry (**Fig. 67**) argues
885 against a direct influence of the rate of photosynthesis itself on calcification. Instead, it seems that
886 daily chemical variability is mostly an expression of circadian rhythm in tridacnids, which is
887 strongly (evolutionarily) coupled to the day-night cycle to optimize the symbiosis with primary
888 producers in its mantle, possibly through respiration rhythms carried out by the ctenidium (see
889 **section 4.32**; (Ip and Chew, 2021)). Symbionts have been shown to directly aid in calcification ~~in~~
890 ~~terms of~~through proton pumping (Armstrong et al., 2018), influencing internal acid-base chemistry
891 (Ip et al., 2006), and valvometric studies show the clams bask in sunlight in daylight hours and
892 close partially at night when symbiosis is likely reduced (Schwartzmann et al., 2011). This
893 conclusion is further supported by the lack of a clear difference in diurnal cyclicity between trace
894 element records in *T. maxima*, *T. squamosa* and *T. squamosina* (**Fig. 67; Table 3**), even though
895 the degree of reliance on photosymbiosis is demonstrated to be highly variable between these
896 species (Killam et al., 2020). Therefore, it seems unlikely that sub-daily resolved trace element
897 records in tridacnids can be used as quantitative recorders of paleo-insolation, as was originally
898 suggested by (Sano et al., 2012). While the degree of symbiotic activity may not be clearly
899 recorded in the daily amplitude of trace element oscillations, the ~~greater~~ consistency of daily
900 periodic signal in the studied giant clams could relate to the direct biological control exerted by
901 the symbionts on the hosts' rhythms of calcification. Light exposure in giant clams promotes

902 expression of genes coding for proteins involved in Ca^{2+} , H^+ and HCO_3^- transport in the mantles
903 of giant clams (Ip et al., 2017; Chew et al., 2019), with the expression proposed to be at least
904 partially mediated by photosensing on the part of the symbionts themselves (Ip et al., 2017).
905 Differences between the daily consistency (spectral power) of photosymbiotic and non-
906 photosymbiotic trace element profiles might still allow paleontologists to use the presence of
907 strong daily periodicity as a proxy for photosymbiosis in the fossil record (as suggested by (de
908 Winter et al., 2020)). However, the small differences found between pectinids and tridacnids in
909 this study and the comparatively large influence of environmental variability show that such
910 records should be interpreted with caution. Future studies could measure photosynthetic activity
911 of the symbionts in tridacnids and attempt to relate this to the trace element composition of the
912 shell in an attempt to isolate the direct effect of photosymbiosis on shell composition.

913

914 4.45 Aperiodic drivers of shell chemistry

915 4.45.1 Circadian and behavioral changes

916 Even after controlling for instrumental noise, most (~ 90%) of the variance observed in our trace
917 element records is not directly related to the diurnal or tidal cycle. This suggests that aperiodic
918 events at the scale of hours to days play an important role in the calcification of pectinids and
919 tridacnids. Given the large difference in ecological niche (e.g., photosymbiotic versus non-
920 symbiotic) between these taxa, and the difference between the environment in which they grew,
921 this observation suggests that calcification of bivalves at the (sub-)daily scale may-is generally be
922 dominated by aperiodic variability in calcification or in the environment. Part of this unaccounted
923 variability may be caused by variability in the animal's behavior, as documented by observations
924 of siphon and valve gape activity in cultured or monitored specimens of a variety of bivalve taxa
925 (Rodland et al., 2006; Ballesta-Artero et al., 2017). While these experiments revealed quasi-

926 periodic (3-7 minute and 60–90 minute periods) behavior unassociated with the tidal or daily cycle,
927 records of activity of the ~~individuals~~ bivalves also reveal less regular patterns on the scale of ~~2~~
928 24 h which may contribute to the aperiodic variance in trace element records (Rodland et al.,
929 2006). Another example of aperiodic behavior potentially influencing shell chemistry is rapid valve
930 adduction or “coughing” observed in both pectinids and tridacnids, which serves as a mechanism
931 for expelling respiratory CO₂ and faeces from the pallial cavity or to evade predation attempts
932 (Robson et al., 2012; Soo and Todd, 2014). This behavior could resuspend sediment and produce
933 pulses of Mn and Ba at the sediment-water interface which are recorded as short-term, aperiodic
934 variability in these elements in the shell. The temporal sampling resolution (~~>1h~~ several hours) of
935 our trace element records after smoothing out measurement noise does not allow us to resolve
936 the types of periodic variability at the sub-hourly scale cited in these previous studies, meaning
937 that aperiodic variability in behavior and aliasing of these ultradian patterns likely contribute to the
938 aperiodic variability in our trace element records. On longer (sub-)seasonal timescales, activity in
939 bivalves is shown to be highly dependent on food and light availability ~~((Ballesta-Artero et al.,~~
940 ~~2017))~~, suggesting that aperiodic, short-term changes in these environmental factors could be a
941 main driver of shell growth and composition and explain a large part of the variance in the trace
942 element records which is not explained by ultradian changes in the animal's behavior.

943 4.45.2 Short-term environmental changes and paleoweather

944 Outside of regular fluctuations caused by tidal, daily, and seasonal cycles, changes in light and
945 food availability at the hourly to daily scale are probably linked to circulation and weather
946 phenomena. Previous studies show that enhanced vertical mixing during weather events such as
947 storms, algal bloom events after wind-driven upwelling and pseudoperiodic dust deposition can
948 temporarily increase the concentration of dissolved metals in surface waters, resuspend organic
949 matter and temporarily increase primary productivity. (Lin et al., 2003; Al-Najjar et al., 2007; Iluz
950 et al., 2009; Al-Taani et al., 2015; Komagoe et al., 2018) ~~(Lin et al., 2003; Al-Najjar et al., 2007;~~

951 ~~Huz et al., 2009; Al-Taani et al., 2015; Komagoe et al., 2018~~). This will in turn lead to a shallowing
952 of the redoxcline through increased organic matter load at the sediment-water interface, which
953 can be recorded in the composition of giant clam shells (Yan et al., 2020). Interestingly, data in
954 (Yan et al., 2020) suggest that recording an extreme weather event in *Tridacna* requires wind
955 speeds exceeding 20 km/h, a threshold which is almost never reached in the comparatively quiet
956 Gulf of Aqaba (Manasrah et al., 2019), while such events are common in the stormier Bay of Brest
957 (Hily et al., 1992; Chauvaud et al., 2005). This difference is also reflected in the periodicity of shell
958 composition, with the tridacnids having overall higher percentages of their variance explained by
959 daily and tidal variability than pectinids (Fig. 3 and 7), showing that aperiodic (potentially weather-
960 controlled) variability in shell composition has a stronger influence on the pectinids which grew in
961 the stormier Bay of Brest. highlights another difference between the environments of pectinid and
962 tridacnid specimens investigated in this study which could contribute to the variable expression
963 of periodicity in the trace element composition of their shells. A plausible scenario therefore
964 emerges in which aperiodic weather events cause short-term variability in both the chemistry and
965 physical properties of the water column. These changes are subsequently recorded in bivalve
966 shells, either directly because the weather events resuspend, remobilize or deliver trace elements
967 like Mn and Ba (e.g., (Dehairs et al., 1989; Gillikin et al., 2008; Mahé et al., 2010)), or indirectly
968 because environmental stress associated with the event affects behavior and shell calcification,
969 resulting in a change in the incorporation of alkali-group cations (e.g., Mg and Sr) into the shell
970 biomineral ((Carré et al., 2006; Takesue et al., 2008); **Fig. 87**). Our results therefore highlight the
971 potential of high-resolution trace element records in bivalve shells to record short-term circulation
972 changes and weather events, while prescribing caution in interpreting such records until the effect
973 of true environmental changes on the sub-daily scale can be separated from aperiodic ultradian
974 or behavioral patterns.

975

976 5. Conclusions

977 Our high-resolution trace element records reveal that short-term variability on the tidal or daily
978 scale is recorded in the Mg, Sr, Mn, and Ba composition of shells of fast-growing mollusk species.
979 The application of spectral analysis and variance decomposition on these trace element records
980 is a useful tool to assess the influence of periodicity in the shallow marine environment on
981 calcification in mollusk shells. Our statistical analysis reveals that tidal and daily variability ~~each~~
982 on average account for less than 10_% of trace element variance in pectinids and tridacnids. In
983 photosymbiotic giant clam shells, the amount of variance in Sr and Ba paced to the daily cycle is
984 two times higher than in the non-photosymbiotic pectinids, suggesting that photosymbiosis in
985 giant clams exerts some control on trace element composition in their shells. However, since only
986 ~10_% of the trace element variability in tridacnids is explained by diurnal variability, the
987 recognition of photosymbiosis in the fossil record from diurnal variability in fossil shell composition
988 will be complicated. In addition, differences between the mid-latitude environment of the pectinids
989 and the tropical environment of the tridacnids likely account for part of the difference in trace
990 element composition between the taxa.

991 ~~We~~ propose that Ba and Mn composition in pectinids and tridacnids reflect short-term variability
992 in primary productivity and sea water chemistry which control the mobility of these elements.
993 Concentrations of Mg and Sr are likely controlled by short-term changes in growth and metabolic
994 rate of the mollusks, which may be indirectly controlled by changes in their environment through
995 circadian rhythms or behavior, explaining the pacing of trace element composition to the tidal and
996 diurnal cycle. Most of the variance in trace element records in both taxa are not related to periodic
997 behavior at the 12_h or 24_h scale, likely recording aperiodic events in the environment related to
998 weather-scale phenomena or circadian patterns. We thus conclude that mollusk shell carbonate
999 is a promising archive for recording weather-scale variability in shallow marine environments

1000 across latitudes, potentially recording weather-scale phenomena in deep time, as long as these
1001 environmental effects can be separated by the influence of the ~~animal's~~ behavior of the animal.

1002

1003 **Code availability**

1004 Scripts used for data processing and to create figures in this manuscript were uploaded to an
1005 open-access repository on GitHub (https://github.com/nielsjdewinter/TE_circadian) and linked
1006 through Zenodo (<https://zenodo.org/record/6603175>).

1007

1008 **Data availability**

1009 Supplementary data and figures referenced in this contribution were uploaded to the online open-
1010 access repository Zenodo (<https://doi.org/10.5281/zenodo.6602894>).

1011

1012 **Author contribution**

1013 NJW designed the experiment after discussion with BRS, DK and LF. LF, DK, BRS and JT
1014 collected the samples. LF, DK and NJW together prepared samples for analyses and constructed
1015 shell chronologies using growth line counting. WB, LN, GJR and NJW carried out the LA-ICP-MS
1016 analyses and data processing. NJW designed and carried out the statistical analyses and wrote
1017 the R scripts guided by feedback from LN, BK, LN, WB and GJR. NJW wrote the first draft of the
1018 manuscript. All authors contributed to the writing process towards the final version of the
1019 manuscript.

1020

1021 **Competing interests**

1022 The authors declare that they have no conflict of interest.

1023 **Acknowledgements**

1024 The authors would like to thank Leonard Bik for his help with sample preparation and Maarten
1025 Zeilmans for his help with high-resolution imaging of the samples at Utrecht University. This study
1026 is part of the UNBIAS project, jointly funded by a Flemish Research Foundation (FWO;
1027 12ZB220N) post-doctoral fellowship (NJW) and a MSCA Individual Fellowship (H2020-MSCA-IF-
1028 2018; 843011 – UNBIAS; awarded to NJW). GJR and LKD acknowledge funding from the
1029 Netherlands Earth System Science Center (NESSC; grant no. 024.002.001) from the Dutch
1030 Ministry for Education, Culture and Science (gravitation grant no. NWO 024.002.001). BRS
1031 acknowledges funding from the Deutsche Forschungsgemeinschaft (DFG; SCHO_#793/21
1032 [\[HIPPO\]+ SCHO 793/23](#)). JT acknowledges funding from the French National Research Agency
1033 (ANR; ANR-18-CE92-0036-01) awarded within the framework of the French-German
1034 collaborative project HIPPO (High-resolution Primary Production multiprOxy archives).

1035

1036 **References**

- 1037 Agbaje, O. B. A., Wirth, R., Morales, L. F. G., Shirai, K., Kosnik, M., Watanabe, T., and Jacob, D. E.:
1038 Architecture of crossed-lamellar bivalve shells: the southern giant clam (*Tridacna derasa*, Röding, 1798),
1039 *R. Soc. Open Sci.*, 4, 170622, <https://doi.org/10.1098/rsos.170622>, 2017.
- 1040 Al-Aasm, I. S. and Veizer, J.: Diagenetic stabilization of aragonite and low-Mg calcite, I. Trace elements in
1041 rudists, *J. Sediment. Res.*, 56, 138–152, 1986a.
- 1042 Al-Aasm, I. S. and Veizer, J.: Diagenetic stabilization of aragonite and low-Mg calcite, II. Stable isotopes in
1043 rudists, *J. Sediment. Res.*, 56, 1986b.
- 1044 Al-Najjar, T., Badran, M. I., Richter, C., Meyerhoefer, M., and Sommer, U.: Seasonal dynamics of
1045 phytoplankton in the Gulf of Aqaba, Red Sea, *Hydrobiologia*, 579, 69–83,
1046 <https://doi.org/10.1007/s10750-006-0365-z>, 2007.
- 1047 Al-Taani, A. A., Rashdan, M., and Khashashneh, S.: Atmospheric dry deposition of mineral dust to the
1048 Gulf of Aqaba, Red Sea: Rate and trace elements, *Mar. Pollut. Bull.*, 92, 252–258,
1049 <https://doi.org/10.1016/j.marpolbul.2014.11.047>, 2015.

- 1050 Anand, P. and Elderfield, H.: Variability of Mg/Ca and Sr/Ca between and within the planktonic
1051 foraminifers *Globigerina bulloides* and *Globorotalia truncatulinoides*, *Geochem. Geophys. Geosystems*,
1052 6, <https://doi.org/10.1029/2004GC000811>, 2005.
- 1053 Armstrong, E. J., Roa, J. N., Stillman, J. H., and Tresguerres, M.: Symbiont photosynthesis in giant clams is
1054 promoted by V-type H⁺-ATPase from host cells, *J. Exp. Biol.*, 221, jeb177220,
1055 <https://doi.org/10.1242/jeb.177220>, 2018.
- 1056 Ballesta-Artero, I., Witbaard, R., Carroll, M. L., and van der Meer, J.: Environmental factors regulating
1057 gaping activity of the bivalve *Arctica islandica* in Northern Norway, *Mar. Biol.*, 164, 116, 2017.
- 1058 Barats, A., Amouroux, D., Pécheyran, C., Chauvaud, L., and Donard, O. F. X.: High-Frequency Archives of
1059 Manganese Inputs To Coastal Waters (Bay of Seine, France) Resolved by the LA-ICP-MS Analysis of
1060 Calcitic Growth Layers along Scallop Shells (*Pecten maximus*), *Environ. Sci. Technol.*, 42, 86–92,
1061 <https://doi.org/10.1021/es0701210>, 2008.
- 1062 Barats, A., Amouroux, D., Chauvaud, L., Pécheyran, C., Lorrain, A., Thébaud, J., Church, T. M., and
1063 Donard, O. F. X.: High frequency Barium profiles in shells of the Great Scallop *Pecten maximus*: a
1064 methodical long-term and multi-site survey in Western Europe, *Biogeosciences*, 6, 157–170,
1065 <https://doi.org/10.5194/bg-6-157-2009>, 2009.
- 1066 Batenburg, S. J., Reichart, G.-J., Jilbert, T., Janse, M., Wesselingh, F. P., and Renema, W.: Interannual
1067 climate variability in the Miocene: High resolution trace element and stable isotope ratios in giant clams,
1068 *Palaeogeogr. Palaeoclimatol. Palaeoecol.*, 306, 75–81, 2011.
- 1069 Black, B. A.: Climate-driven synchrony across tree, bivalve, and rockfish growth-increment chronologies
1070 of the northeast Pacific, *Mar. Ecol. Prog. Ser.*, 378, 37–46, 2009.
- 1071 Boo, M. V., Chew, S. F., and Ip, Y. K.: The colorful mantle of the giant clam *Tridacna squamosa* expresses
1072 a homolog of electrogenic sodium: Bicarbonate cotransporter 2 that mediates the supply of inorganic
1073 carbon to photosynthesizing symbionts, *PloS One*, 16, e0258519,
1074 <https://doi.org/10.1371/journal.pone.0258519>, 2021.
- 1075 Bougeois, L., De Rafélis, M., Reichart, G.-J., De Nooijer, L. J., Nicollin, F., and Dupont-Nivet, G.: A high
1076 resolution study of trace elements and stable isotopes in oyster shells to estimate Central Asian Middle
1077 Eocene seasonality, *Chem. Geol.*, 363, 200–212, 2014.
- 1078 Carlson, D. F., Fredj, E., and Gildor, H.: The annual cycle of vertical mixing and restratification in the
1079 Northern Gulf of Eilat/Aqaba (Red Sea) based on high temporal and vertical resolution observations,
1080 *Deep Sea Res. Part Oceanogr. Res. Pap.*, 84, 1–17, <https://doi.org/10.1016/j.dsr.2013.10.004>, 2014.
- 1081 Carré, M., Bentaleb, I., Bruguier, O., Ordinola, E., Barrett, N. T., and Fontugne, M.: Calcification rate
1082 influence on trace element concentrations in aragonitic bivalve shells: Evidences and mechanisms,
1083 *Geochim. Cosmochim. Acta*, 70, 4906–4920, <https://doi.org/10.1016/j.gca.2006.07.019>, 2006.
- 1084 Chauvaud, L., Lorrain, A., Dunbar, R. B., Paulet, Y.-M., Thouzeau, G., Jean, F., Guarini, J.-M., and
1085 Mucciarone, D.: Shell of the Great Scallop *Pecten maximus* as a high-frequency archive of
1086 paleoenvironmental changes, *Geochem. Geophys. Geosystems*, 6, 2005.

- 1087 Checa, A. G., Esteban-Delgado, F. J., and Rodríguez-Navarro, A. B.: Crystallographic structure of the
1088 foliated calcite of bivalves, *J. Struct. Biol.*, 157, 393–402, 2007.
- 1089 Chew, S. F., Koh, C. Z., Hiong, K. C., Choo, C. Y., Wong, W. P., Neo, M. L., and Ip, Y. K.: Light-enhanced
1090 expression of Carbonic Anhydrase 4-like supports shell formation in the fluted giant clam *Tridacna*
1091 *squamosa*, *Gene*, 683, 101–112, 2019.
- 1092 Cochran, J. K., Kallenberg, K., Landman, N. H., Harries, P. J., Weinreb, D., Turekian, K. K., Beck, A. J., and
1093 Cobban, W. A.: Effect of diagenesis on the Sr, O, and C isotope composition of late Cretaceous mollusks
1094 from the Western Interior Seaway of North America, *Am. J. Sci.*, 310, 69–88,
1095 <https://doi.org/10.2475/02.2010.01>, 2010.
- 1096 Cohen, A. L., Owens, K. E., Layne, G. D., and Shimizu, N.: The Effect of Algal Symbionts on the Accuracy of
1097 Sr/Ca Paleotemperatures from Coral, *Science*, 296, 331–333, <https://doi.org/10.1126/science.1069330>,
1098 2002.
- 1099 Coimbra, J., Machado, J., Fernandes, P. L., Ferreira, H. G., and Ferreira, K. G.: Electrophysiology of the
1100 Mantle of *Anodonta Cygnea*, *J. Exp. Biol.*, 140, 65–88, <https://doi.org/10.1242/jeb.140.1.65>, 1988.
- 1101 Coimbra, R., Huck, S., de Winter, N. J., Heimhofer, U., and Claeys, P.: Improving the detection of shell
1102 alteration: Implications for sclerochronology, *Palaeogeogr. Palaeoclimatol. Palaeoecol.*, 559, 109968,
1103 <https://doi.org/10.1016/j.palaeo.2020.109968>, 2020.
- 1104 Comboul, M., Emile-Geay, J., Evans, M. N., Mirnateghi, N., Cobb, K. M., and Thompson, D. M.: A
1105 probabilistic model of chronological errors in layer-counted climate proxies: applications to annually
1106 banded coral archives, *Clim. Past*, 10, 825–841, 2014.
- 1107 Crippa, G., Grieshaber, E., Checa, A. G., Harper, E. M., Roda, M. S., and Schmahl, W. W.: Orientation
1108 patterns of aragonitic crossed-lamellar, fibrous prismatic and myostracal microstructures of modern
1109 *Glycymeris* shells, *J. Struct. Biol.*, 212, 107653, 2020.
- 1110 Dauphin, Y., Cuif, J., Doucet, J., Salomé, M., Susini, J., and Williams, C.: In situ mapping of growth lines in
1111 the calcitic prismatic layers of mollusc shells using X-ray absorption near-edge structure (XANES)
1112 spectroscopy at the sulphur K-edge, *Mar. Biol.*, 142, 299–304, 2003.
- 1113 Day, C. C. and Henderson, G. M.: Controls on trace-element partitioning in cave-analogue calcite,
1114 *Geochim. Cosmochim. Acta*, 120, 612–627, <https://doi.org/10.1016/j.gca.2013.05.044>, 2013.
- 1115 DeCarlo, T. M. and Cohen, A. L.: Dissepiments, density bands and signatures of thermal stress in *Porites*
1116 skeletons, *Coral Reefs*, 36, 749–761, <https://doi.org/10.1007/s00338-017-1566-9>, 2017.
- 1117 Dehairs, F., Baeyens, W., and Van Gansbeke, D.: Tight coupling between enrichment of iron and
1118 manganese in North Sea suspended matter and sedimentary redox processes: Evidence for seasonal
1119 variability, *Estuar. Coast. Shelf Sci.*, 29, 457–471, [https://doi.org/10.1016/0272-7714\(89\)90080-2](https://doi.org/10.1016/0272-7714(89)90080-2), 1989.
- 1120 van Dijk, I., de Nooijer, L. J., Boer, W., and Reichart, G.-J.: Sulfur in foraminiferal calcite as a potential
1121 proxy for seawater carbonate ion concentration, *Earth Planet. Sci. Lett.*, 470, 64–72, 2017.

- 1122 Dunbar, R. B. and Wellington, G. M.: Stable isotopes in a branching coral monitor seasonal temperature
1123 variation, *Nature*, 293, 453–455, 1981.
- 1124 Eggins, S., De Deckker, P., and Marshall, J.: Mg/Ca variation in planktonic foraminifera tests: implications
1125 for reconstructing palaeo-seawater temperature and habitat migration, *Earth Planet. Sci. Lett.*, 212,
1126 291–306, [https://doi.org/10.1016/S0012-821X\(03\)00283-8](https://doi.org/10.1016/S0012-821X(03)00283-8), 2003.
- 1127 Elliot, M., Welsh, K., Chilcott, C., McCulloch, M., Chappell, J., and Ayling, B.: Profiles of trace elements
1128 and stable isotopes derived from giant long-lived *Tridacna gigas* bivalves: potential applications in
1129 paleoclimate studies, *Palaeogeogr. Palaeoclimatol. Palaeoecol.*, 280, 132–142, 2009.
- 1130 Freitas, P. S., Clarke, L. J., Kennedy, H., Richardson, C. A., and others: Ion microprobe assessment of the
1131 heterogeneity of Mg/Ca, Sr/Ca and Mn/Ca ratios in *Pecten maximus* and *Mytilus edulis* (bivalvia) shell
1132 calcite precipitated at constant temperature, *Biogeosciences Discuss.*, 6, 1267, 2009.
- 1133 Fröhlich, L., Siebert, V., Walliser, E. O., Thébaud, J., Jochum, K. P., Chauvaud, L., and Schöne, B. R.: Ba/Ca
1134 profiles in shells of *Pecten maximus* – A proxy for specific primary producers rather than bulk
1135 phytoplankton, *Chem. Geol.*, 120743, <https://doi.org/10.1016/j.chemgeo.2022.120743>, 2022.
- 1136 Gannon, M. E., Pérez-Huerta, A., Aharon, P., and Street, S. C.: A biomineralization study of the Indo-
1137 Pacific giant clam *Tridacna gigas*, *Coral Reefs*, 36, 503–517, <https://doi.org/10.1007/s00338-016-1538-5>,
1138 2017.
- 1139 García-March, J. R., Sanchís Solsona, M. Á., and García-Carrascosa, A. M.: Shell gaping behaviour of *Pinna*
1140 *nobilis* L., 1758: circadian and circalunar rhythms revealed by in situ monitoring, *Mar. Biol.*, 153, 689–
1141 698, <https://doi.org/10.1007/s00227-007-0842-6>, 2008.
- 1142 Gilbert, P. U., Bergmann, K. D., Myers, C. E., Marcus, M. A., DeVol, R. T., Sun, C.-Y., Blonsky, A. Z., Tamre,
1143 E., Zhao, J., and Karan, E. A.: Nacre tablet thickness records formation temperature in modern and fossil
1144 shells, *Earth Planet. Sci. Lett.*, 460, 281–292, 2017.
- 1145 Gillikin, D. P., Lorrain, A., Navez, J., Taylor, J. W., André, L., Keppens, E., Baeyens, W., and Dehairs, F.:
1146 Strong biological controls on Sr/Ca ratios in aragonitic marine bivalve shells, *Geochem. Geophys.*
1147 *Geosystems*, 6, <https://doi.org/10.1029/2004GC000874>, 2005.
- 1148 Gillikin, D. P., Lorrain, A., Paulet, Y.-M., André, L., and Dehairs, F.: Synchronous barium peaks in high-
1149 resolution profiles of calcite and aragonite marine bivalve shells, *Geo-Mar. Lett.*, 28, 351–358, 2008.
- 1150 Goodwin, D. H., Paul, P., and Wissink, C. L.: MoGroFunGen: A numerical model for reconstructing intra-
1151 annual growth rates of bivalve molluscs, *Palaeogeogr. Palaeoclimatol. Palaeoecol.*, 276, 47–55,
1152 <https://doi.org/10.1016/j.palaeo.2009.02.026>, 2009.
- 1153 Guillaume Olivier, M., Leroux, E., Rabineau, M., Le Hir, P., Granjeon, D., Chataigner, T., Beudin, A., and
1154 Muller, H.: Numerical modelling of a Macrotidal Bay over the last 9,000 years: An interdisciplinary
1155 methodology to understand the influence of sea-level variations on tidal currents in the Bay of Brest,
1156 *Cont. Shelf Res.*, 231, 104595, <https://doi.org/10.1016/j.csr.2021.104595>, 2021.

- 1157 Guillong, M., Meier, D. L., Allan, M. M., Heinrich, C. A., and Yardley, B. W. D.: SILLS: A Matlab-based
 1158 program for the reduction of laser ablation ICP–MS data of homogenous materials and inclusions,
 1159 Mineral. Assoc. Can. Short Course, 40, 328–333, 2008.
- 1160 Hagiwara, S. and Byerly, L.: Calcium channel, *Annu. Rev. Neurosci.*, 4, 69–125, 1981.
- 1161 Hallmann, N., Schöne, B. R., Strom, A., and Fiebig, J.: An intractable climate archive—Sclerochronological
 1162 and shell oxygen isotope analyses of the Pacific geoduck, *Panopea abrupta* (bivalve mollusk) from
 1163 Protection Island (Washington State, USA), *Palaeogeogr. Palaeoclimatol. Palaeoecol.*, 269, 115–126,
 1164 2008.
- 1165 Hily, C., Potin, P., and Floc’h, J.-Y.: Structure of subtidal algal assemblages on soft-bottom sediments:
 1166 fauna/flora interactions and role of disturbances in the Bay of Brest, France, *Mar. Ecol. Prog. Ser.*, 85,
 1167 115–130, 1992.
- 1168 Höche, N., Peharda, M., Walliser, E. O., and Schöne, B. R.: Morphological variations of crossed-lamellar
 1169 ultrastructures of *Glycymeris bimaculata* (*Bivalvia*) serve as a marine temperature proxy, *Estuar. Coast.
 1170 Shelf Sci.*, 237, 106658, <https://doi.org/10.1016/j.ecss.2020.106658>, 2020.
- 1171 Höche, N., Walliser, E. O., de Winter, N. J., Witbaard, R., and Schöne, B. R.: Temperature-induced
 1172 microstructural changes in shells of laboratory-grown *Arctica islandica* (*Bivalvia*), *PLoS One*, 16,
 1173 e0247968, 2021.
- 1174 Huyghe, D., de Rafelis, M., Ropert, M., Mouchi, V., Emmanuel, L., Renard, M., and Lartaud, F.: New
 1175 insights into oyster high-resolution hinge growth patterns, *Mar. Biol.*, 166, 48, 2019.
- 1176 Huyghe, D., Daëron, M., de Rafelis, M., Blamart, D., Sébilo, M., Paulet, Y.-M., and Lartaud, F.: Clumped
 1177 isotopes in modern marine bivalves, *Geochim. Cosmochim. Acta*, 316, 41–58,
 1178 <https://doi.org/10.1016/j.gca.2021.09.019>, 2021.
- 1179 Iluz, D., Dishon, G., Capuzzo, E., Meeder, E., Astoreca, R., Montecino, V., Znachor, P., Ediger, D., and
 1180 Marra, J.: Short-term variability in primary productivity during a wind-driven diatom bloom in the Gulf of
 1181 Eilat (Aqaba), *Aquat. Microb. Ecol.*, 56, 205–215, <https://doi.org/10.3354/ame01321>, 2009.
- 1182 Inoue, M., Nakamura, T., Tanaka, Y., Suzuki, A., Yokoyama, Y., Kawahata, H., Sakai, K., and Gussone, N.: A
 1183 simple role of coral-algal symbiosis in coral calcification based on multiple geochemical tracers,
 1184 *Geochim. Cosmochim. Acta*, 235, 76–88, <https://doi.org/10.1016/j.gca.2018.05.016>, 2018.
- 1185 Ip, Y. K. and Chew, S. F.: Light-Dependent Phenomena and Related Molecular Mechanisms in Giant
 1186 Clam–Dinoflagellate Associations: A Review, *Front. Mar. Sci.*, 8, 2021.
- 1187 Ip, Y. K., Loong, A. M., Hiong, K. C., Wong, W. P., Chew, S. F., Reddy, K., Sivaloganathan, B., and
 1188 Ballantyne, J. S.: Light induces an increase in the pH of and a decrease in the ammonia concentration in
 1189 the extrapallial fluid of the giant clam *Tridacna squamosa*, *Physiol. Biochem. Zool.*, 79, 656–664, 2006.
- 1190 Ip, Y. K., Koh, C. Z., Hiong, K. C., Choo, C. Y., Boo, M. V., Wong, W. P., Neo, M. L., and Chew, S. F.:
 1191 Carbonic anhydrase 2-like in the giant clam, *Tridacna squamosa*: characterization, localization, response
 1192 to light, and possible role in the transport of inorganic carbon from the host to its symbionts, *Physiol.
 1193 Rep.*, 5, e13494, 2017.

- 1194 Ivany, L. C.: Reconstructing paleoseasonality from accretionary skeletal carbonates—challenges and
1195 opportunities, *Paleontol. Soc. Pap.*, 18, 133–166, 2012.
- 1196 Ivany, L. C. and Judd, E. J.: Deciphering Temperature Seasonality in Earth’s Ancient Oceans, *Annu. Rev.*
1197 *Earth Planet. Sci.*, 50, 123–152, <https://doi.org/10.1146/annurev-earth-032320-095156>, 2022.
- 1198 Jablonski, D., Roy, K., Valentine, J. W., Price, R. M., and Anderson, P. S.: The Impact of the Pull of the
1199 Recent on the History of Marine Diversity, *Science*, 300, 1133–1135,
1200 <https://doi.org/10.1126/science.1083246>, 2003.
- 1201 Jablonski, D., Huang, S., Roy, K., and Valentine, J. W.: Shaping the latitudinal diversity gradient: new
1202 perspectives from a synthesis of paleobiology and biogeography, *Am. Nat.*, 189, 1–12, 2017.
- 1203 Jochum, K. P., Willbold, M., Raczek, I., Stoll, B., and Herwig, K.: Chemical Characterisation of the USGS
1204 Reference Glasses GSA-1G, GSC-1G, GSD-1G, GSE-1G, BCR-2G, BHVO-2G and BIR-1G Using EPMA, ID-
1205 TIMS, ID-ICP-MS and LA-ICP-MS, *Geostand. Geoanalytical Res.*, 29, 285–302,
1206 <https://doi.org/10.1111/j.1751-908X.2005.tb00901.x>, 2005.
- 1207 Jochum, K. P., Weis, U., Stoll, B., Kuzmin, D., Yang, Q., Raczek, I., Jacob, D. E., Stracke, A., Birbaum, K.,
1208 and Frick, D. A.: Determination of reference values for NIST SRM 610–617 glasses following ISO
1209 guidelines, *Geostand. Geoanalytical Res.*, 35, 397–429, 2011.
- 1210 Jones, D. S.: Sclerochronology: reading the record of the molluscan shell: annual growth increments in
1211 the shells of bivalve molluscs record marine climatic changes and reveal surprising longevity, *Am. Sci.*,
1212 71, 384–391, 1983.
- 1213 Jones, D. S. and Quitmyer, I. R.: Marking Time with Bivalve Shells: Oxygen Isotopes and Season of Annual
1214 Increment Formation, *PALAIOS*, 11, 340–346, <https://doi.org/10.2307/3515244>, 1996.
- 1215 Judd, E. J., Wilkinson, B. H., and Ivany, L. C.: The life and time of clams: Derivation of intra-annual growth
1216 rates from high-resolution oxygen isotope profiles, *Palaeogeogr. Palaeoclimatol. Palaeoecol.*, 490, 70–
1217 83, 2018.
- 1218 Killam, D., Thomas, R., Al-Najjar, T., and Clapham, M.: Interspecific and Intrashell Stable Isotope
1219 Variation Among the Red Sea Giant Clams, *Geochem. Geophys. Geosystems*, 21, e2019GC008669,
1220 <https://doi.org/10.1029/2019GC008669>, 2020.
- 1221 Killam, D., Al-Najjar, T., and Clapham, M.: Giant clam growth in the Gulf of Aqaba is accelerated
1222 compared to fossil populations, *Proc. R. Soc. B Biol. Sci.*, 288, 20210991,
1223 <https://doi.org/10.1098/rspb.2021.0991>, 2021.
- 1224 Killam, D. E. and Clapham, M. E.: Identifying the ticks of bivalve shell clocks: Seasonal growth in relation
1225 to temperature and food supply, *PALAIOS*, 33, 228–236, <https://doi.org/10.2110/palo.2017.072>, 2018a.
- 1226 Killam, D. E. and Clapham, M. E.: IDENTIFYING THE TICKS OF BIVALVE SHELL CLOCKS: SEASONAL
1227 GROWTH IN RELATION TO TEMPERATURE AND FOOD SUPPLY, *PALAIOS*, 33, 228–236,
1228 <https://doi.org/10.2110/palo.2017.072>, 2018b.

- 1229 Klein, R. T., Lohmann, K. C., and Thayer, C. W.: Bivalve skeletons record sea-surface temperature and
1230 $\delta^{18}\text{O}$ via Mg/Ca and $^{18}\text{O}/^{16}\text{O}$ ratios, *Geology*, 24, 415–418, 1996.
- 1231 Komagoe, T., Watanabe, T., Shirai, K., Yamazaki, A., and Uematu, M.: Geochemical and Microstructural
1232 Signals in Giant Clam *Tridacna maxima* Recorded Typhoon Events at Okinotori Island, Japan, *J. Geophys.*
1233 *Res. Biogeosciences*, 123, 1460–1474, <https://doi.org/10.1029/2017JG004082>, 2018.
- 1234 Kontoyannis, C. G. and Vagenas, N. V.: Calcium carbonate phase analysis using XRD and FT-Raman
1235 spectroscopy, *Analyst*, 125, 251–255, <https://doi.org/10.1039/A908609I>, 2000.
- 1236 Ku, H. H.: Notes on the use of propagation of error formulas, *J. Res. Natl. Bur. Stand.*, 70, 263–273, 1966.
- 1237 Lazareth, C. E., Vander Putten, E., André, L., and Dehairs, F.: High-resolution trace element profiles in
1238 shells of the mangrove bivalve *Isognomon ehippium*: a record of environmental spatio-temporal
1239 variations?, *Estuar. Coast. Shelf Sci.*, 57, 1103–1114, 2003.
- 1240 Lazareth, C. E., Guzman, N., Poitrasson, F., Candaudap, F., and Ortlieb, L.: Nyctemeral variations of
1241 magnesium intake in the calcitic layer of a Chilean mollusk shell (*Concholepas concholepas*,
1242 *Gastropoda*), *Geochim. Cosmochim. Acta*, 71, 5369–5383, 2007.
- 1243 Lazier, A. V., SMITH, J. E., RISK, M. J., and SCHWARCZ, H. P.: The skeletal structure of *Desmophyllum*
1244 *cristagalli*: the use of deep-water corals in sclerochronology, *Lethaia*, 32, 119–130, 1999.
- 1245 Lin, I., Liu, W. T., Wu, C.-C., Wong, G. T. F., Hu, C., Chen, Z., Liang, W.-D., Yang, Y., and Liu, K.-K.: New
1246 evidence for enhanced ocean primary production triggered by tropical cyclone, *Geophys. Res. Lett.*, 30,
1247 <https://doi.org/10.1029/2003GL017141>, 2003.
- 1248 Lorrain, A., Gillikin, D. P., Paulet, Y.-M., Chauvaud, L., Le Mercier, A., Navez, J., and André, L.: Strong
1249 kinetic effects on Sr/Ca ratios in the calcitic bivalve *Pecten maximus*, *Geology*, 33, 965–968, 2005.
- 1250 Lough, J. M.: Climate records from corals, *WIREs Clim. Change*, 1, 318–331,
1251 <https://doi.org/10.1002/wcc.39>, 2010.
- 1252 Madkour, H. A.: Distribution and relationships of heavy metals in the giant clam (*Tridacna maxima*) and
1253 associated sediments from different sites in the Egyptian Red Sea Coast, *توزيع وعلاقات العناصر الثقيلة في*
1254 *2005, الكائن الصدفي الكبير (نراى داكنا مكسيما (والرواسب المصاحبة من مناطق مختلفة للساحل المصرى للبحر الاحمر*
- 1255 Mahé, K., Bellamy, E., Lartaud, F., and Rafélis, M. de: Calcein and manganese experiments for marking
1256 the shell of the common cockle (*Cerastoderma edule*): tidal rhythm validation of increments formation,
1257 *Aquat. Living Resour.*, 23, 239–245, <https://doi.org/10.1051/alr/2010025>, 2010.
- 1258 Manasrah, R., Abu-Hilal, A., and Rasheed, M.: Physical and Chemical Properties of Seawater in the Gulf
1259 of Aqaba and Red Sea, in: *Oceanographic and Biological Aspects of the Red Sea*, edited by: Rasul, N. M.
1260 A. and Stewart, I. C. F., Springer International Publishing, Cham, 41–73, [https://doi.org/10.1007/978-3-](https://doi.org/10.1007/978-3-319-99417-8_3)
1261 [319-99417-8_3](https://doi.org/10.1007/978-3-319-99417-8_3), 2019.
- 1262 Marin, F. and Luquet, G.: Molluscan shell proteins, *Comptes Rendus Palevol*, 3, 469–492,
1263 <https://doi.org/10.1016/j.crpv.2004.07.009>, 2004.

- 1264 Mat, A. M., Sarrazin, J., Markov, G. V., Apremont, V., Dubreuil, C., Eché, C., Fabioux, C., Klopp, C.,
1265 Sarradin, P.-M., Tanguy, A., Huvet, A., and Matabos, M.: Biological rhythms in the deep-sea
1266 hydrothermal mussel *Bathymodiolus azoricus*, *Nat. Commun.*, 11, 3454,
1267 <https://doi.org/10.1038/s41467-020-17284-4>, 2020.
- 1268 Meibom, A., Stage, M., Wooden, J., Constantz, B. R., Dunbar, R. B., Owen, A., Grumet, N., Bacon, C. R.,
1269 and Chamberlain, C. P.: Monthly Strontium/Calcium oscillations in symbiotic coral aragonite: Biological
1270 effects limiting the precision of the paleotemperature proxy, *Geophys. Res. Lett.*, 30,
1271 <https://doi.org/10.1029/2002GL016864>, 2003.
- 1272 Meyers, S. R.: Seeing red in cyclic stratigraphy: Spectral noise estimation for astrochronology,
1273 *Paleoceanography*, 27, 2012.
- 1274 Meyers, S. R.: Astrochron: An R package for astrochronology, [http://cran.r-](http://cran.r-project.org/package=astrochron)
1275 [project.org/package=astrochron](http://cran.r-project.org/package=astrochron), 2014.
- 1276 Mohammed, T. A. A., Mohamed, M. H., Zamzamy, R. M., and Mahmoud, M. A. M.: Growth rates of the
1277 giant clam *Tridacna maxima* (Röding, 1798) reared in cages in the Egyptian Red Sea, *Egypt. J. Aquat. Res.*,
1278 45, 67–73, <https://doi.org/10.1016/j.ejar.2019.02.003>, 2019.
- 1279 Munro, J. L.: Estimation of the parameters of the von Bertalanffy growth equation from recapture data
1280 at variable time intervals, *ICES J. Mar. Sci.*, 40, 199–200, <https://doi.org/10.1093/icesjms/40.2.199>,
1281 1982.
- 1282 Nassar, M. Z., Mohamed, H. R., Khiray, H. M., and Rashedy, S. H.: Seasonal fluctuations of phytoplankton
1283 community and physico-chemical parameters of the north western part of the Red Sea, Egypt, *Egypt. J.*
1284 *Aquat. Res.*, 40, 395–403, <https://doi.org/10.1016/j.ejar.2014.11.002>, 2014.
- 1285 Nedoncelle, K., Lartaud, F., de Rafelis, M., Boulila, S., and Le Bris, N.: A new method for high-resolution
1286 bivalve growth rate studies in hydrothermal environments, *Mar. Biol.*, 160, 1427–1439,
1287 <https://doi.org/10.1007/s00227-013-2195-7>, 2013.
- 1288 Onuma, N., Masuda, F., Hirano, M., and Wada, K.: Crystal structure control on trace element partition in
1289 molluscan shell formation, *Geochem. J.*, 13, 187–189, 1979.
- 1290 Pandolfi, J. M. and Kiessling, W.: Gaining insights from past reefs to inform understanding of coral reef
1291 response to global climate change, *Curr. Opin. Environ. Sustain.*, 7, 52–58,
1292 <https://doi.org/10.1016/j.cosust.2013.11.020>, 2014.
- 1293 Pannella, G.: Tidal growth patterns in recent and fossil mollusc bivalve shells: a tool for the
1294 reconstruction of paleotides, *Naturwissenschaften*, 63, 539–543, 1976.
- 1295 Petersen, S. V., Tabor, C. R., Lohmann, K. C., Poulsen, C. J., Meyer, K. W., Carpenter, S. J., Erickson, J. M.,
1296 Matsunaga, K. K., Smith, S. Y., and Sheldon, N. D.: Temperature and salinity of the Late Cretaceous
1297 western interior seaway, *Geology*, 44, 903–906, 2016.
- 1298 Poitevin, P., Chauvaud, L., Pécheyran, C., Lazure, P., Jolivet, A., and Thébault, J.: Does trace element
1299 composition of bivalve shells record ultra-high frequency environmental variations?, *Mar. Environ. Res.*,
1300 158, 104943, <https://doi.org/10.1016/j.marenvres.2020.104943>, 2020.

- 1301 Polsenaere, P., Deflandre, B., Thouzeau, G., Rigaud, S., Cox, T., Amice, E., Bec, T. L., Bihannic, I., and
1302 Maire, O.: Comparison of benthic oxygen exchange measured by aquatic Eddy Covariance and Benthic
1303 Chambers in two contrasting coastal biotopes (Bay of Brest, France), *Reg. Stud. Mar. Sci.*, 43, 101668,
1304 <https://doi.org/10.1016/j.rsma.2021.101668>, 2021.
- 1305 Popov, S. V.: Formation of bivalve shells and their microstructure, *Paleontol. J.*, 48, 1519–1531,
1306 <https://doi.org/10.1134/S003103011414010X>, 2014.
- 1307 R Core Team: R: A language and environment for statistical computing. R Foundation for Statistical
1308 Computing, 2013.
- 1309 Richard, M.: Analyse de la composition élémentaire de *Pecten maximus* par HR-ICP-MS Element 2:
1310 développements méthodologiques et interprétations écologiques., PhD Thesis, Université de Bretagne
1311 occidentale-Brest, 2009.
- 1312 Richardson, C. A., Crisp, D. J., Runham, N. W., and Gruffydd, L. D.: The use of tidal growth bands in the
1313 shell of *Cerastoderma edule* to measure seasonal growth rates under cool
1314 temperate and sub-arctic conditions, *J. Mar. Biol. Assoc. U. K.*, 60, 977–989,
1315 <https://doi.org/10.1017/S002531540004203X>, 1980.
- 1316 Richter, C., Roa-Quiaoit, H., Jantzen, C., Al-Zibdah, M., and Kochzius, M.: Collapse of a new living species
1317 of giant clam in the Red Sea, *Curr. Biol.*, 18, 1349–1354, 2008.
- 1318 Roa-Quiaoit, H.: Ecology and culture of giant clams (Tridacnidae) in the Jordanian sector of the Gulf of
1319 Aqaba, Red Sea, <Httpelibsuebuni-BremendedissdocsE-Diss1340PHDROAQpdf>, 2005.
- 1320 Roberts, E. M., Bowers, D. G., and Davies, A. J.: Tidal modulation of seabed light and its implications for
1321 benthic algae, *Limnol. Oceanogr.*, 63, 91–106, <https://doi.org/10.1002/lno.10616>, 2018.
- 1322 Robson, A. A., Chauvaud, L., Wilson, R. P., and Halsey, L. G.: Small actions, big costs: the behavioural
1323 energetics of a commercially important invertebrate, *J. R. Soc. Interface*, 9, 1486–1498,
1324 <https://doi.org/10.1098/rsif.2011.0713>, 2012.
- 1325 Rodland, D. L., Schöne, B. R., Helama, S., Nielsen, J. K., and Baier, S.: A clockwork mollusc: Ultradian
1326 rhythms in bivalve activity revealed by digital photography, *J. Exp. Mar. Biol. Ecol.*, 334, 316–323,
1327 <https://doi.org/10.1016/j.jembe.2006.02.012>, 2006.
- 1328 Sano, Y., Kobayashi, S., Shirai, K., Takahata, N., Matsumoto, K., Watanabe, T., Sowa, K., and Iwai, K.: Past
1329 daily light cycle recorded in the strontium/calcium ratios of giant clam shells, *Nat. Commun.*, 3, 761,
1330 <https://doi.org/10.1038/ncomms1763>, 2012.
- 1331 Sather, W. A. and McCleskey, E. W.: Permeation and selectivity in calcium channels, *Annu. Rev. Physiol.*,
1332 65, 133–159, 2003.
- 1333 Savitzky, A. and Golay, M. J.: Smoothing and differentiation of data by simplified least squares
1334 procedures., *Anal. Chem.*, 36, 1627–1639, 1964.

- 1335 Schöne, B. R. and Giere, O.: Growth increments and stable isotope variation in shells of the deep-sea
1336 hydrothermal vent bivalve mollusk *Bathymodiolus brevior* from the North Fiji Basin, Pacific Ocean, Deep
1337 Sea Res. Part Oceanogr. Res. Pap., 52, 1896–1910, 2005.
- 1338 Schöne, B. R. and Gillikin, D. P.: Unraveling environmental histories from skeletal diaries — Advances in
1339 sclerochronology, *Palaeogeogr. Palaeoclimatol. Palaeoecol.*, 373, 1–5,
1340 <https://doi.org/10.1016/j.palaeo.2012.11.026>, 2013.
- 1341 Schöne, B. R., Castro, A. D. F., Fiebig, J., Houk, S. D., Oschmann, W., and Kröncke, I.: Sea surface water
1342 temperatures over the period 1884–1983 reconstructed from oxygen isotope ratios of a bivalve mollusk
1343 shell (*Arctica islandica*, southern North Sea), *Palaeogeogr. Palaeoclimatol. Palaeoecol.*, 212, 215–232,
1344 2004.
- 1345 Schöne, B. R., Fiebig, J., Pfeiffer, M., Gleß, R., Hickson, J., Johnson, A. L., Dreyer, W., and Oschmann, W.:
1346 Climate records from a bivalved *Methuselah* (*Arctica islandica*, Mollusca; Iceland), *Palaeogeogr.*
1347 *Palaeoclimatol. Palaeoecol.*, 228, 130–148, 2005a.
- 1348 Schöne, B. R., Houk, S. D., Castro, A. D. F., Fiebig, J., Oschmann, W., Kröncke, I., Dreyer, W., and
1349 Gosselck, F.: Daily growth rates in shells of *Arctica islandica*: assessing sub-seasonal environmental
1350 controls on a long-lived bivalve mollusk, *Palaios*, 20, 78–92, 2005b.
- 1351 Schöne, B. R., Dunca, E., Fiebig, J., and Pfeiffer, M.: Mutvei's solution: An ideal agent for resolving
1352 microgrowth structures of biogenic carbonates, *Palaeogeogr. Palaeoclimatol. Palaeoecol.*, 228, 149–166,
1353 <https://doi.org/10.1016/j.palaeo.2005.03.054>, 2005c.
- 1354 Schöne, B. R., Zhang, Z., Jacob, D., Gillikin, D. P., Tütken, T., Garbe-Schönberg, D., and SOLDATI, A.: Effect
1355 of organic matrices on the determination of the trace element chemistry (Mg, Sr, Mg/Ca, Sr/Ca) of
1356 aragonitic bivalve shells (*Arctica islandica*)—Comparison of ICP-OES and LA-ICP-MS data, *Geochem. J.*,
1357 44, 23–37, 2010.
- 1358 Schwartzmann, C., Durrieu, G., Sow, M., Ciret, P., Lazareth, C. E., and Massabuau, J.-C.: In situ giant clam
1359 growth rate behavior in relation to temperature: A one-year coupled study of high-frequency
1360 noninvasive valvometry and sclerochronology, *Limnol. Oceanogr.*, 56, 1940–1951,
1361 <https://doi.org/10.4319/lo.2011.56.5.1940>, 2011.
- 1362 Service Hydrographique et Océanographique de la Marine - Géoportail:
1363 <https://www.geoportail.gouv.fr/>, last access: 28 June 2022.
- 1364 Sinclair, D. J., Kinsley, L. P. J., and McCulloch, M. T.: High resolution analysis of trace elements in corals
1365 by laser ablation ICP-MS, *Geochim. Cosmochim. Acta*, 62, 1889–1901, [https://doi.org/10.1016/S0016-](https://doi.org/10.1016/S0016-7037(98)00112-4)
1366 [7037\(98\)00112-4](https://doi.org/10.1016/S0016-7037(98)00112-4), 1998.
- 1367 Soldati, A. L., Jacob, D. E., Glatzel, P., Swarbrick, J. C., and Geck, J.: Element substitution by living
1368 organisms: the case of manganese in mollusc shell aragonite, *Sci. Rep.*, 6, 1–9, 2016.
- 1369 Soo, P. and Todd, P. A.: The behaviour of giant clams (*Bivalvia: Cardiidae: Tridacninae*), *Mar. Biol.*, 161,
1370 2699–2717, <https://doi.org/10.1007/s00227-014-2545-0>, 2014.

- 1371 Surge, D., Lohmann, K. C., and Dettman, D. L.: Controls on isotopic chemistry of the American oyster,
1372 *Crassostrea virginica*: implications for growth patterns, *Palaeogeogr. Palaeoclimatol. Palaeoecol.*, 172,
1373 283–296, 2001.
- 1374 Takesue, R. K., Bacon, C. R., and Thompson, J. K.: Influences of organic matter and calcification rate on
1375 trace elements in aragonitic estuarine bivalve shells, *Geochim. Cosmochim. Acta*, 72, 5431–5445, 2008.
- 1376 Tanaka, K., Okaniwa, N., Miyaji, T., Murakami-Sugihara, N., Zhao, L., Tanabe, K., Schöne, B. R., and Shirai,
1377 K.: Microscale magnesium distribution in shell of the Mediterranean mussel *Mytilus galloprovincialis*: An
1378 example of multiple factors controlling Mg/Ca in biogenic calcite, *Chem. Geol.*, 511, 521–532,
1379 <https://doi.org/10.1016/j.chemgeo.2018.10.025>, 2019.
- 1380 Taylor, J. D. and Layman, M.: The mechanical properties of bivalve (Mollusca) shell structures,
1381 *Palaeontology*, 15, 73–87, 1972.
- 1382 Thébault, J., Chauvaud, L., L’Helguen, S., Clavier, J., Barats, A., Jacquet, Sé., PÉcheyran, C., and
1383 Amouroux, D.: Barium and molybdenum records in bivalve shells: Geochemical proxies for
1384 phytoplankton dynamics in coastal environments?, *Limnol. Oceanogr.*, 54, 1002–1014,
1385 <https://doi.org/10.4319/lo.2009.54.3.1002>, 2009.
- 1386 Thébault, J., Jolivet, A., Waeles, M., Tabouret, H., Sabarot, S., PÉcheyran, C., Leynaert, A., Jochum, K. P.,
1387 Schöne, B. R., Fröhlich, L., Siebert, V., Amice, E., and Chauvaud, L.: Scallop shells as geochemical archives
1388 of phytoplankton-related ecological processes in a temperate coastal ecosystem, *Limnol. Oceanogr.*, 67,
1389 187–202, <https://doi.org/10.1002/lno.11985>, 2022.
- 1390 Thomson, D. J.: Spectrum estimation and harmonic analysis, *Proc. IEEE*, 70, 1055–1096, 1982.
- 1391 Tierney, J. E., Poulsen, C. J., Montañez, I. P., Bhattacharya, T., Feng, R., Ford, H. L., Hönisch, B., Inglis, G.
1392 N., Petersen, S. V., Sagoo, N., Tabor, C. R., Thirumalai, K., Zhu, J., Burls, N. J., Foster, G. L., Goddérís, Y.,
1393 Huber, B. T., Ivany, L. C., Turner, S. K., Lunt, D. J., McElwain, J. C., Mills, B. J. W., Otto-Bliesner, B. L.,
1394 Ridgwell, A., and Zhang, Y. G.: Past climates inform our future, *Science*, 370,
1395 <https://doi.org/10.1126/science.aay3701>, 2020.
- 1396 Tran, D., Nadau, A., Durrieu, G., Ciret, P., Parisot, J.-P., and Massabuau, J.-C.: Field chronobiology of a
1397 molluscan bivalve: how the moon and sun cycles interact to drive oyster activity rhythms, *Chronobiol.*
1398 *Int.*, 28, 307–317, 2011.
- 1399 Tran, D., Perrigault, M., Ciret, P., and Payton, L.: Bivalve mollusc circadian clock genes can run at tidal
1400 frequency, *Proc. R. Soc. B Biol. Sci.*, 287, 20192440, <https://doi.org/10.1098/rspb.2019.2440>, 2020.
- 1401 Vander Putten, E., Dehairs, F., Keppens, E., and Baeyens, W.: High resolution distribution of trace
1402 elements in the calcite shell layer of modern *Mytilus edulis*: Environmental and biological controls,
1403 *Geochim. Cosmochim. Acta*, 64, 997–1011, 2000.
- 1404 Vermeij, G. J.: The evolution of molluscan photosymbioses: a critical appraisal, *Biol. J. Linn. Soc.*, 109,
1405 497–511, 2013.
- 1406 Von Bertalanffy, L.: Quantitative laws in metabolism and growth, *Q. Rev. Biol.*, 32, 217–231, 1957.

- 1407 Warter, V. and Müller, W.: Daily growth and tidal rhythms in Miocene and modern giant clams revealed
1408 via ultra-high resolution LA-ICPMS analysis—A novel methodological approach towards improved
1409 sclerochemistry, *Palaeogeogr. Palaeoclimatol. Palaeoecol.*, 465, 362–375, 2017.
- 1410 Warter, V., MÜLLER, W., WESSELINGH, F. P., TODD, J. A., and RENEMA, W.: LATE MIOCENE SEASONAL
1411 TO SUBDECADAL CLIMATE VARIABILITY IN THE INDO-WEST PACIFIC (EAST KALIMANTAN, INDONESIA)
1412 PRESERVED IN GIANT CLAMS, *PALAIOS*, 30, 66–82, <https://doi.org/10.2110/palo.2013.061>, 2015.
- 1413 Warter, V., Erez, J., and Müller, W.: Environmental and physiological controls on daily trace element
1414 incorporation in *Tridacna crocea* from combined laboratory culturing and ultra-high resolution LA-ICP-
1415 MS analysis, *Palaeogeogr. Palaeoclimatol. Palaeoecol.*, 496, 32–47,
1416 <https://doi.org/10.1016/j.palaeo.2017.12.038>, 2018.
- 1417 Wassenburg, J. A., Scholz, D., Jochum, K. P., Cheng, H., Oster, J., Immenhauser, A., Richter, D. K., Häger,
1418 T., Jamieson, R. A., Baldini, J. U. L., Hoffmann, D., and Breitenbach, S. F. M.: Determination of aragonite
1419 trace element distribution coefficients from speleothem calcite–aragonite transitions, *Geochim.*
1420 *Cosmochim. Acta*, 190, 347–367, <https://doi.org/10.1016/j.gca.2016.06.036>, 2016.
- 1421 Wichern, N. M. A., de Winter, N. J., Johnson, A. L. A., Goolaerts, S., Wesselingh, F., Hamers, M. F., Kaskes,
1422 P., Claeys, P., and Ziegler, M.: The fossil bivalve *Angulus benedeni benedeni*: a potential
1423 seasonally resolved stable isotope-based climate archive to investigate Pliocene temperatures in the
1424 southern North Sea basin, *EGU sphere*, 1–53, <https://doi.org/10.5194/egusphere-2022-951>, 2022.
- 1425 Wilson, S. A., Koenig, A. E., and Orklid, R.: Development of microanalytical reference material (MACS-3)
1426 for LA-ICP-MS analysis of carbonate samples, *Geochim. Cosmochim. Acta Suppl.*, 72, A1025, 2008.
- 1427 de Winter, N. J. and Claeys, P.: Micro X-ray fluorescence (μ XRF) line scanning on Cretaceous rudist
1428 bivalves: A new method for reproducible trace element profiles in bivalve calcite, *Sedimentology*, 64,
1429 231–251, <https://doi.org/10.1111/sed.12299>, 2017.
- 1430 de Winter, N. J., Goderis, S., Dehairs, F., Jagt, J. W., Fraaije, R. H., Van Malderen, S. J., Vanhaecke, F., and
1431 Claeys, P.: Tropical seasonality in the late Campanian (late Cretaceous): Comparison between multiproxy
1432 records from three bivalve taxa from Oman, *Palaeogeogr. Palaeoclimatol. Palaeoecol.*, 485, 740–760,
1433 2017.
- 1434 de Winter, N. J., Vellekoop, J., Vorrsselmans, R., Golreihan, A., Soete, J., Petersen, S. V., Meyer, K. W.,
1435 Casadio, S., Speijer, R. P., and Claeys, P.: An assessment of latest Cretaceous Pycnodonte vesicularis
1436 (Lamarck, 1806) shells as records for palaeoseasonality: a multi-proxy investigation, *Clim. Past*, 14, 725–
1437 749, 2018.
- 1438 de Winter, N. J., Goderis, S., Malderen, S. J. M. V., Sinnesael, M., Vansteenberge, S., Snoeck, C., Belza, J.,
1439 Vanhaecke, F., and Claeys, P.: Subdaily-Scale Chemical Variability in a *Torreites Sanchezi* Rudist Shell:
1440 Implications for Rudist Paleobiology and the Cretaceous Day-Night Cycle, *Paleoceanogr.*
1441 *Paleoclimatology*, 35, e2019PA003723, <https://doi.org/10.1029/2019PA003723>, 2020.
- 1442 de Winter, N. J., Müller, I. A., Kocken, I. J., Thibault, N., Ullmann, C. V., Farnsworth, A., Lunt, D. J., Claeys,
1443 P., and Ziegler, M.: Absolute seasonal temperature estimates from clumped isotopes in bivalve shells
1444 suggest warm and variable greenhouse climate, *Commun. Earth Environ.*, 2, 1–8,
1445 <https://doi.org/10.1038/s43247-021-00193-9>, 2021a.

- 1446 de Winter, N. J., Agterhuis, T., and Ziegler, M.: Optimizing sampling strategies in high-resolution
1447 paleoclimate records, *Clim. Past*, 17, 1315–1340, <https://doi.org/10.5194/cp-17-1315-2021>, 2021b.
- 1448 de Winter, N. J., Witbaard, R., Kocken, I. J., Müller, I. A., Guo, J., Goudsmit, B., and Ziegler, M.:
1449 Temperature Dependence of Clumped Isotopes ($\Delta 47$) in Aragonite, *Geophys. Res. Lett.*, 49,
1450 e2022GL099479, <https://doi.org/10.1029/2022GL099479>, 2022.
- 1451 Winter, N. J. de, Sikkeleras, S. van, Goudsmit-Hazevoort, B., Boer, W., Nooijer, L. de, Reichart, G.-J.,
1452 Claeys, P., and Witbaard, R.: Tracing timing of growth in cultured mollusks using strontium spiking, 2022.
- 1453 Wisshak, M., Correa, M. L., Gofas, S., Salas, C., Taviani, M., Jakobsen, J., and Freiwald, A.: Shell
1454 architecture, element composition, and stable isotope signature of the giant deep-sea oyster
1455 *Neopycnodonte zibrowii* sp. n. from the NE Atlantic, *Deep Sea Res. Part Oceanogr. Res. Pap.*, 56, 374–
1456 407, 2009.
- 1457 Witbaard, R., Jenness, M. I., Van Der Borg, K., and Ganssen, G.: Verification of annual growth increments
1458 in *Arctica islandica* L. from the North Sea by means of oxygen and carbon isotopes, *Neth. J. Sea Res.*, 33,
1459 91–101, [https://doi.org/10.1016/0077-7579\(94\)90054-X](https://doi.org/10.1016/0077-7579(94)90054-X), 1994.
- 1460 Xing, Q., Zhang, L., Li, Y., Zhu, X., Li, Y., Guo, H., Bao, Z., and Wang, S.: Development of Novel Cardiac
1461 Indices and Assessment of Factors Affecting Cardiac Activity in a Bivalve Mollusc *Chlamys farreri*, *Front.*
1462 *Physiol.*, 10, 2019.
- 1463 Yan, H., Shao, D., Wang, Y., and Sun, L.: Sr/Ca profile of long-lived *Tridacna gigas* bivalves from South
1464 China Sea: A new high-resolution SST proxy, *Geochim. Cosmochim. Acta*, 112, 52–65,
1465 <https://doi.org/10.1016/j.gca.2013.03.007>, 2013.
- 1466 Yan, H., Liu, C., An, Z., Yang, W., Yang, Y., Huang, P., Qiu, S., Zhou, P., Zhao, N., Fei, H., Ma, X., Shi, G.,
1467 Dodson, J., Hao, J., Yu, K., Wei, G., Yang, Y., Jin, Z., and Zhou, W.: Extreme weather events recorded by
1468 daily to hourly resolution biogeochemical proxies of marine giant clam shells, *Proc. Natl. Acad. Sci.*, 117,
1469 7038–7043, <https://doi.org/10.1073/pnas.1916784117>, 2020.
- 1470 Yoshimura, T., Suzuki, A., Tamenori, Y., and Kawahata, H.: Micro-X-ray fluorescence-based comparison
1471 of skeletal structure and P, Mg, Sr, O and Fe in a fossil of the cold-water coral *Desmophyllum* sp., NW
1472 Pacific, *Geo-Mar. Lett.*, 34, 1–9, 2014.
- 1473 Zhao, L., Schöne, B. R., and Mertz-Kraus, R.: Controls on strontium and barium incorporation into
1474 freshwater bivalve shells (*Corbicula fluminea*), *Palaeogeogr. Palaeoclimatol. Palaeoecol.*, 465, 386–394,
1475 <https://doi.org/10.1016/j.palaeo.2015.11.040>, 2017.
- 1476
- 1477 ~~Agbaje, O. B. A., Wirth, R., Morales, L. F. G., Shirai, K., Kosnik, M., Watanabe, T., and Jacob, D.~~
1478 ~~E.: Architecture of crossed-lamellar bivalve shells: the southern giant clam (*Tridacna derasa*,~~
1479 ~~Röding, 1798), 4, 170622, <https://doi.org/10.1098/rsos.170622>, n.d.~~
- 1480 ~~Al-Aasm, I. S. and Veizer, J.: Diagenetic Stabilization of Aragonite and Low-mg Calcite, I. Trace~~
1481 ~~Elements in Rudists, 56, 1986a.~~

1482 Al-Aasm, I. S. and Veizer, J.: Diagenetic stabilization of aragonite and low-Mg calcite, II. Stable
1483 isotopes in rudists, 56, 1986b.

1484 Al-Najjar, T., Badran, M. I., Richter, C., Meyerhoefer, M., and Sommer, U.: Seasonal dynamics of
1485 phytoplankton in the Gulf of Aqaba, Red Sea, *Hydrobiologia*, 579, 69–83,
1486 <https://doi.org/10.1007/s10750-006-0365-z>, 2007.

1487 Al-Taani, A. A., Rashdan, M., and Khashashneh, S.: Atmospheric dry deposition of mineral dust
1488 to the Gulf of Aqaba, Red Sea: Rate and trace elements, *Marine Pollution Bulletin*, 92, 252–258,
1489 <https://doi.org/10.1016/j.marpolbul.2014.11.047>, 2015.

1490 Armstrong, E. J., Roa, J. N., Stillman, J. H., and Tresguerres, M.: Symbiont photosynthesis in
1491 giant clams is promoted by V-type H⁺-ATPase from host cells, *Journal of Experimental Biology*,
1492 221, jeb177220, <https://doi.org/10.1242/jeb.177220>, 2018.

1493 Ballesta-Artero, I., Witbaard, R., Carroll, M. L., and van der Meer, J.: Environmental factors
1494 regulating gaping activity of the bivalve *Arctica islandica* in Northern Norway, *Mar Biol*, 164, 116,
1495 <https://doi.org/10.1007/s00227-017-3144-7>, 2017.

1496 Barats, A., Amouroux, D., Pécheyran, C., Chauvaud, L., and Donard, O. F. X.: High-Frequency
1497 Archives of Manganese Inputs To Coastal Waters (Bay of Seine, France) Resolved by the
1498 LA-ICP-MS Analysis of Calcitic Growth Layers along Scallop Shells (*Pecten maximus*), *Environ.*
1499 *Sci. Technol.*, 42, 86–92, <https://doi.org/10.1021/es0701210>, 2008.

1500 Barats, A., Amouroux, D., Chauvaud, L., Pécheyran, C., Lorrain, A., Thébault, J., Church, T. M.,
1501 and Donard, O. F. X.: High frequency Barium profiles in shells of the Great Scallop *Pecten*
1502 *maximus*: a methodical long-term and multi-site survey in Western Europe, 6, 157–170,
1503 <https://doi.org/10.5194/bg-6-157-2009>, 2009.

1504 Batenburg, S. J., Reichart, G. J., Jilbert, T., Janse, M., Wesselingh, F. P., and Renema, W.:
1505 Interannual climate variability in the Miocene: High resolution trace element and stable isotope
1506 ratios in giant clams, *Palaeogeography, Palaeoclimatology, Palaeoecology*, 306, 75–81,
1507 <https://doi.org/10.1016/j.palaeo.2011.03.031>, 2011.

1508 Black, B. A.: Climate-driven synchrony across tree, bivalve, and rockfish growth-increment
1509 chronologies of the northeast Pacific, 378, 37–46, 2009.

1510 Boo, M. V., Chew, S. F., and Ip, Y. K.: The colorful mantle of the giant clam *Tridacna squamosa*
1511 expresses a homolog of electrogenic sodium: Bicarbonate cotransporter 2 that mediates the
1512 supply of inorganic carbon to photosynthesizing symbionts, *PLoS One*, 16, e0258519,
1513 <https://doi.org/10.1371/journal.pone.0258519>, 2021.

1514 Bougeois, L., de Rafélis, M., Reichart, G. J., de Nooijer, L. J., Nicollin, F., and Dupont-Nivet, G.:
1515 A high resolution study of trace elements and stable isotopes in oyster shells to estimate Central
1516 Asian Middle Eocene seasonality, *Chemical Geology*, 363, 200–212,
1517 <https://doi.org/10.1016/j.chemgeo.2013.10.037>, 2014.

1518 Carlson, D. F., Fredj, E., and Gildor, H.: The annual cycle of vertical mixing and restratification in
1519 the Northern Gulf of Eilat/Aqaba (Red Sea) based on high temporal and vertical resolution
1520 observations, *Deep Sea Research Part I: Oceanographic Research Papers*, 84, 1–17,
1521 <https://doi.org/10.1016/j.dsr.2013.10.004>, 2014.

1522 Carré, M., Bentaleb, I., Bruguier, O., Ordinola, E., Barrett, N. T., and Fontugne, M.: Calcification
1523 rate influence on trace element concentrations in aragonitic bivalve shells: evidences and
1524 mechanisms, 70, 4906–4920, 2006.

1525 Chauvaud, L., Thouzeau, G., and Paulet, Y.-M.: Effects of environmental factors on the daily
1526 growth rate of *Pecten maximus* juveniles in the Bay of Brest (France), *Journal of Experimental*
1527 *Marine Biology and Ecology*, 227, 83–111, [https://doi.org/10.1016/S0022-0984\(97\)00263-3](https://doi.org/10.1016/S0022-0984(97)00263-3),
1528 1998.

1529 Chauvaud, L., Lorrain, A., Dunbar, R. B., Paulet, Y.-M., Thouzeau, G., Jean, F., Guarini, J.-M.,
1530 and Mucciarone, D.: Shell of the Great Scallop *Pecten maximus* as a high-frequency archive of
1531 paleoenvironmental changes, 6, <https://doi.org/10.1029/2004GC000890>, 2005.

1532 Checa, A. G., Esteban-Delgado, F. J., and Rodríguez-Navarro, A. B.: Crystallographic structure
1533 of the foliated calcite of bivalves, 157, 393–402, 2007.

1534 Chew, S. F., Koh, C. Z., Hiong, K. C., Choo, C. Y., Wong, W. P., Neo, M. L., and Ip, Y. K.: Light-
1535 enhanced expression of Carbonic Anhydrase 4-like supports shell formation in the fluted giant
1536 clam *Tridacna squamosa*, 683, 101–112, 2019.

1537 Cochran, J. K., Kallenberg, K., Landman, N. H., Harries, P. J., Weinreb, D., Turekian, K. K., Beck,
1538 A. J., and Cobban, W. A.: Effect of diagenesis on the Sr, O, and C isotope composition of late
1539 Cretaceous mollusks from the Western Interior Seaway of North America, 310, 69–88,
1540 <https://doi.org/10.2475/02.2010.01>, 2010.

1541 Cohen, A. L., Owens, K. E., Layne, G. D., and Shimizu, N.: The Effect of Algal Symbionts on the
1542 Accuracy of Sr/Ca Paleotemperatures from Coral, 296, 331–333,
1543 <https://doi.org/10.1126/science.1069330>, 2002.

1544 Coimbra, R., Huck, S., de Winter, N. J., Heimhofer, U., and Claeys, P.: Improving the detection
1545 of shell alteration: Implications for sclerochronology, *Palaeogeography, Palaeoclimatology,*
1546 *Palaeoecology*, 559, 109968, <https://doi.org/10.1016/j.palaeo.2020.109968>, 2020.

1547 Comboul, M., Emile-Geay, J., Evans, M. N., Mirnateghi, N., Cobb, K. M., and Thompson, D. M.:
1548 A probabilistic model of chronological errors in layer-counted climate proxies: applications to
1549 annually banded coral archives, 10, 825–841, 2014.

1550 Crippa, G., Grieshaber, E., Checa, A. G., Harper, E. M., Roda, M. S., and Schmahl, W. W.:
1551 Orientation patterns of aragonitic crossed-lamellar, fibrous prismatic and myostracal
1552 microstructures of modern *Glycymeris* shells, 212, 107653, 2020.

1553 Dauphin, Y., Cuif, J., Doucet, J., Salomé, M., Susini, J., and Williams, C.: In situ mapping of
1554 growth lines in the calcitic prismatic layers of mollusc shells using X-ray absorption near-edge
1555 structure (XANES) spectroscopy at the sulphur K-edge, *Marine Biology*, 142, 299–304,
1556 <https://doi.org/10.1007/s00227-002-0950-2>, 2003.

1557 DeCarlo, T. M. and Cohen, A. L.: Dissepiments, density bands and signatures of thermal stress
1558 in *Porites* skeletons, *Coral Reefs*, 36, 749–761, <https://doi.org/10.1007/s00338-017-1566-9>,
1559 2017.

1560 Dehairs, F., Baeyens, W., and Van Gansbeke, D.: Tight coupling between enrichment of iron and
1561 manganese in North Sea suspended matter and sedimentary redox processes: Evidence for

1562 seasonal variability, *Estuarine, Coastal and Shelf Science*, 29, 457–471,
1563 [https://doi.org/10.1016/0272-7714\(89\)90080-2](https://doi.org/10.1016/0272-7714(89)90080-2), 1989.

1564 Dunbar, R. B. and Wellington, G. M.: Stable isotopes in a branching coral monitor seasonal
1565 temperature variation, 293, 453–455, 1981.

1566 Elliot, M., Welsh, K., Chilcott, C., McCulloch, M., Chappell, J., and Ayling, B.: Profiles of trace
1567 elements and stable isotopes derived from giant long-lived *Tridacna gigas* bivalves: Potential
1568 applications in paleoclimate studies, *Palaeogeography, Palaeoclimatology, Palaeoecology*, 280,
1569 132–142, <https://doi.org/10.1016/j.palaeo.2009.06.007>, 2009.

1570 Freitas, P. S., Clarke, L. J., Kennedy, H., and Richardson, C. A.: Ion microprobe assessment of
1571 the heterogeneity of Mg/Ca, Sr/Ca and Mn/Ca ratios in *Pecten maximus* and *Mytilus edulis*
1572 (bivalvia) shell calcite precipitated at constant temperature, 6, 1209–1227,
1573 <https://doi.org/10.5194/bg-6-1209-2009>, 2009.

1574 Fröhlich, L., Siebert, V., Walliser, E. O., Thébaud, J., Jochum, K. P., Chauvaud, L., and Schöne,
1575 B. R.: Ba/Ca profiles in shells of *Pecten maximus* – A proxy for specific primary producers rather
1576 than bulk phytoplankton, *Chemical Geology*, 120743,
1577 <https://doi.org/10.1016/j.chemgeo.2022.120743>, 2022.

1578 Gannon, M. E., Pérez-Huerta, A., Aharon, P., and Street, S. C.: A biomineralization study of the
1579 Indo-Pacific giant clam *Tridacna gigas*, *Coral Reefs*, 36, 503–517,
1580 <https://doi.org/10.1007/s00338-016-1538-5>, 2017.

1581 García-March, J. R., Sanchis-Solsona, M. Á., and García-Carrascosa, A. M.: Shell gaping
1582 behaviour of *Pinna nobilis* L., 1758: circadian and circalunar rhythms revealed by in situ
1583 monitoring, *Mar Biol*, 153, 689–698, <https://doi.org/10.1007/s00227-007-0842-6>, 2008.

1584 Gilbert, P. U., Bergmann, K. D., Myers, C. E., Marcus, M. A., DeVol, R. T., Sun, C.-Y., Blonsky,
1585 A. Z., Tamre, E., Zhao, J., and Karan, E. A.: Nacre tablet thickness records formation temperature
1586 in modern and fossil shells, 460, 281–292, 2017.

1587 Gillikin, D. P., Lorrain, A., Paulet, Y.-M., André, L., and Dehairs, F.: Synchronous barium peaks
1588 in high-resolution profiles of calcite and aragonite marine bivalve shells, *Geo-Mar Lett*, 28, 351–
1589 358, <https://doi.org/10.1007/s00367-008-0111-9>, 2008.

1590 Goodwin, D. H., Paul, P., and Wissink, C. L.: MoGroFunGen: A numerical model for reconstructing
1591 intra-annual growth rates of bivalve molluscs, *Palaeogeography, Palaeoclimatology,*
1592 *Palaeoecology*, 276, 47–55, <https://doi.org/10.1016/j.palaeo.2009.02.026>, 2009.

1593 Guillaume Olivier, M., Leroux, E., Rabineau, M., Le Hir, P., Granjeon, D., Chataigner, T., Beudin,
1594 A., and Muller, H.: Numerical modelling of a Macrotidal Bay over the last 9,000 years: An
1595 interdisciplinary methodology to understand the influence of sea-level variations on tidal currents
1596 in the Bay of Brest, *Continental Shelf Research*, 231, 104595,
1597 <https://doi.org/10.1016/j.csr.2021.104595>, 2021.

1598 Guillong, M., Meier, D. L., Allan, M. M., Heinrich, C. A., and Yardley, B. W. D.: M.GUILLONG,
1599 D.L. MEIER, M.M. ALLAN, C.A. HEINRICH & B.W.D. YARDLEY, 40, 328–333, 2008.

1600 Hily, C., Potin, P., and Floc'h, J. Y.: Structure of subtidal algal assemblages on soft-bottom
1601 sediments: fauna/flora interactions and role of disturbances in the Bay of Brest, France, 85, 115–
1602 130, 1992.

1603 Höche, N., Peharda, M., Walliser, E. O., and Schöne, B. R.: Morphological variations of crossed-
1604 lamellar ultrastructures of *Glycymeris bimaculata* (Bivalvia) serve as a marine temperature proxy,
1605 237, 106658, 2020.

1606 Höche, N., Walliser, E. O., de Winter, N. J., Witbaard, R., and Schöne, B. R.: Temperature-
1607 induced microstructural changes in shells of laboratory-grown *Arctica islandica* (Bivalvia), 16,
1608 e0247968, 2021.

1609 Huyghe, D., de Rafelis, M., Ropert, M., Mouchi, V., Emmanuel, L., Renard, M., and Lartaud, F.:
1610 New insights into oyster high-resolution hinge growth patterns, 166, 48, 2019.

1611 Huyghe, D., Daëron, M., de Rafelis, M., Blamart, D., Sébilo, M., Paulet, Y.-M., and Lartaud, F.:
1612 Clumped isotopes in modern marine bivalves, *Geochimica et Cosmochimica Acta*,
1613 <https://doi.org/10.1016/j.gca.2021.09.019>, 2021.

1614 Iluz, D., Dishon, G., Capuzzo, E., Meeder, E., Astoreca, R., Montecino, V., Znachor, P., Ediger,
1615 D., and Marra, J.: Short-term variability in primary productivity during a wind-driven diatom bloom
1616 in the Gulf of Eilat (Aqaba), 56, 205–215, <https://doi.org/10.3354/ame01321>, 2009.

1617 Inoue, M., Nakamura, T., Tanaka, Y., Suzuki, A., Yokoyama, Y., Kawahata, H., Sakai, K., and
1618 Gussone, N.: A simple role of coral-algal symbiosis in coral calcification based on multiple
1619 geochemical tracers, *Geochimica et Cosmochimica Acta*, 235, 76–88,
1620 <https://doi.org/10.1016/j.gca.2018.05.016>, 2018.

1621 Ip, Y. K. and Chew, S. F.: Light-Dependent Phenomena and Related Molecular Mechanisms in
1622 Giant Clam-Dinoflagellate Associations: A Review, 8, 2021.

1623 Ip, Y. K., Loong, A. M., Hiong, K. C., Wong, W. P., Chew, S. F., Reddy, K., Sivaloganathan, B.,
1624 and Ballantyne, J. S.: Light induces an increase in the pH of and a decrease in the ammonia
1625 concentration in the extrapallial fluid of the giant clam *Tridacna squamosa*, 79, 656–664, 2006.

1626 Ip, Y. K., Koh, C. Z., Hiong, K. C., Choo, C. Y., Boo, M. V., Wong, W. P., Neo, M. L., and Chew,
1627 S. F.: Carbonic anhydrase 2-like in the giant clam, *Tridacna squamosa*: characterization,
1628 localization, response to light, and possible role in the transport of inorganic carbon from the host
1629 to its symbionts, 5, e13494, 2017.

1630 Ivany, L. C.: Reconstructing paleoseasonality from accretionary skeletal carbonates—challenges
1631 and opportunities, 18, 133–166, 2012.

1632 Ivany, L. C. and Judd, E. J.: Deciphering Temperature Seasonality in Earth's Ancient Oceans, 50,
1633 123–152, <https://doi.org/10.1146/annurev-earth-032320-095156>, 2022.

1634 Jablonski, D., Roy, K., Valentine, J. W., Price, R. M., and Anderson, P. S.: The Impact of the Pull
1635 of the Recent on the History of Marine Diversity, 300, 1133–1135,
1636 <https://doi.org/10.1126/science.1083246>, 2003.

1637 Jablonski, D., Huang, S., Roy, K., and Valentine, J. W.: Shaping the latitudinal diversity gradient:
1638 new perspectives from a synthesis of paleobiology and biogeography, 189, 1–12, 2017.

1639 Jochum, K. P., Nohl, U., Herwig, K., Lammel, E., Stoll, B., and Hofmann, A. W.: GeoReM: A New
1640 Geochemical Database for Reference Materials and Isotopic Standards, 29, 333–338,
1641 <https://doi.org/10.1111/j.1751-908X.2005.tb00904.x>, 2005.

1642 Jochum, K. P., Weis, U., Stoll, B., Kuzmin, D., Yang, Q., Raczek, I., Jacob, D. E., Stracke, A.,
1643 Birbaum, K., Frick, D. A., Günther, D., and Enzweiler, J.: Determination of Reference Values for
1644 NIST SRM 610–617 Glasses Following ISO Guidelines, 35, 397–429,
1645 <https://doi.org/10.1111/j.1751-908X.2011.00120.x>, 2011.

1646 Jones, D. S.: Sclerochronology: reading the record of the molluscan shell: annual growth
1647 increments in the shells of bivalve molluscs record marine climatic changes and reveal surprising
1648 longevity, 71, 384–391, 1983.

1649 Jones, D. S. and Quitmyer, I. R.: Marking Time with Bivalve Shells: Oxygen Isotopes and Season
1650 of Annual Increment Formation, *PALAIOS*, 11, 340–346, <https://doi.org/10.2307/3515244>, 1996.

1651 Judd, E. J., Wilkinson, B. H., and Ivany, L. C.: The life and time of clams: Derivation of intra-
1652 annual growth rates from high-resolution oxygen isotope profiles, *Palaeogeography,*
1653 *Palaeoclimatology, Palaeoecology*, <https://doi.org/10.1016/j.palaeo.2017.09.034>, 2017.

1654 Killam, D., Thomas, R., Al-Najjar, T., and Clapham, M.: Interspecific and Intrashell Stable Isotope
1655 Variation Among the Red Sea Giant Clams, 21, e2019GC008669,
1656 <https://doi.org/10.1029/2019GC008669>, 2020.

1657 Killam, D. E. and Clapham, M. E.: Identifying the ticks of bivalve shell clocks: Seasonal growth in
1658 relation to temperature and food supply, *PALAIOS*, 33, 228–236,
1659 <https://doi.org/10.2110/palo.2017.072>, 2018.

1660 Klein, R. T., Lohmann, K. C., and Thayer, C. W.: Bivalve skeletons record sea-surface
1661 temperature and $\delta^{18}\text{O}$ via Mg/Ca and $^{18}\text{O}/^{16}\text{O}$ ratios, 24, 415–418, 1996.

1662 Komagoe, T., Watanabe, T., Shirai, K., Yamazaki, A., and Uematu, M.: Geochemical and
1663 Microstructural Signals in Giant Clam *Tridacna maxima* Recorded Typhoon Events at Okinotori
1664 Island, Japan, 123, 1460–1474, <https://doi.org/10.1029/2017JG004082>, 2018.

1665 Kontoyannis, C. G. and Vagenas, N. V.: Calcium carbonate phase analysis using XRD and FT-
1666 Raman spectroscopy, *Analyst*, 125, 251–255, <https://doi.org/10.1039/A908609I>, 2000.

1667 Ku, H. H.: Notes on the use of propagation of error formulas, 70, 263–273, 1966.

1668 Lazareth, C. E., Vander Putten, E., André, L., and Dehairs, F.: High-resolution trace element
1669 profiles in shells of the mangrove bivalve *Isoognomon ephippium*: a record of environmental spatio-
1670 temporal variations?, 57, 1103–1114, 2003.

1671 Lazareth, C. E., Guzman, N., Poitrasson, F., Candaudap, F., and Ortlieb, L.: Nyctemeral
1672 variations of magnesium intake in the calcitic layer of a Chilean mollusk shell (*Concholepas*
1673 *concholepas*, Gastropoda), *Geochimica et Cosmochimica Acta*, 71, 5369–5383,
1674 <https://doi.org/10.1016/j.gca.2007.07.031>, 2007.

1675 LAZIER, A. V., SMITH, J. E., RISK, M. J., and SCHWARCZ, H. P.: The skeletal structure of
1676 *Desmophyllum cristagalli*: the use of deep-water corals in sclerochronology, 32, 119–130, 1999.

1677 Lin, I., Liu, W. T., Wu, C. C., Wong, G. T. F., Hu, C., Chen, Z., Liang, W. D., Yang, Y., and Liu,
1678 K.-K.: New evidence for enhanced ocean primary production triggered by tropical cyclone, 30,
1679 <https://doi.org/10.1029/2003GL017141>, 2003.

1680 Lorrain, A., Gillikin, D. P., Paulet, Y.-M., Chauvaud, L., Le Mercier, A., Navez, J., and André, L.:
1681 Strong kinetic effects on Sr/Ca ratios in the calcitic bivalve *Pecten maximus*, *Geology*, 33, 965–
1682 968, <https://doi.org/10.1130/G22048.1>, 2005.

1683 Lough, J. M.: Climate records from corals, 1, 318–331, <https://doi.org/10.1002/wcc.39>, 2010.

1684 Madkour, H. A.: Distribution and relationships of heavy metals in the giant clam (*Tridacna*
1685 *maxima*) and associated sediments from different sites in the Egyptian Red Sea Coast, توزيع
1686 وعلاقات العناصر الثقيلة في الكائن الصدفي الكبير (نرأى داكناً مكسيماً) والرواسب المصاحبة من مناطق مختلفة للساحل المصرى للبحر
1687 الاحمر, 2005.

1688 Mahé, K., Bellamy, E., Lartaud, F., and Rafélis, M. de: Calcein and manganese experiments for
1689 marking the shell of the common cockle (*Cerastoderma edule*): tidal rhythm validation of
1690 increments formation, *Aquat. Living Resour.*, 23, 239–245, <https://doi.org/10.1051/alr/2010025>,
1691 2010.

1692 Manasrah, R., Abu-Hilal, A., and Rasheed, M.: Physical and Chemical Properties of Seawater in
1693 the Gulf of Aqaba and Red Sea, in: *Oceanographic and Biological Aspects of the Red Sea*, edited
1694 by: Rasul, N. M. A. and Stewart, I. C. F., Springer International Publishing, Cham, 41–73,
1695 https://doi.org/10.1007/978-3-319-99417-8_3, 2019.

1696 Marin, F. and Luquet, G.: Molluscan shell proteins, *Comptes Rendus Palevol*, 3, 469–492,
1697 <https://doi.org/10.1016/j.crpv.2004.07.009>, 2004.

1698 Mat, A. M., Sarrazin, J., Markov, G. V., Apremont, V., Dubreuil, C., Eché, C., Fabioux, C., Klopp,
1699 C., Sarradin, P.-M., Tanguy, A., Huvet, A., and Matabos, M.: Biological rhythms in the deep-sea
1700 hydrothermal mussel *Bathymodiolus azoricus*, *Nat Commun*, 11, 3454,
1701 <https://doi.org/10.1038/s41467-020-17284-4>, 2020.

1702 Meibom, A., Stage, M., Wooden, J., Constantz, B. R., Dunbar, R. B., Owen, A., Grumet, N.,
1703 Bacon, C. R., and Chamberlain, C. P.: Monthly Strontium/Calcium oscillations in symbiotic coral
1704 aragonite: Biological effects limiting the precision of the paleotemperature proxy, 30,
1705 <https://doi.org/10.1029/2002GL016864>, 2003.

1706 Meyers, S. R.: Seeing red in cyclic stratigraphy: Spectral noise estimation for astrochronology,
1707 27, 2012.

1708 Meyers, S. R.: Astrochron: An R package for astrochronology, [http://cran.r-](http://cran.r-project.org/package=astrochron)
1709 [project.org/package=astrochron](http://cran.r-project.org/package=astrochron), 2014.

1710 Mohammed, T. A. A., Mohamed, M. H., Zamzamy, R. M., and Mahmoud, M. A. M.: Growth rates
1711 of the giant clam *Tridacna maxima* (Röding, 1798) reared in cages in the Egyptian Red Sea, *The*
1712 *Egyptian Journal of Aquatic Research*, 45, 67–73, <https://doi.org/10.1016/j.ejar.2019.02.003>,
1713 2019.

1714 Munro, J. L.: Estimation of the parameters of the von Bertalanffy growth equation from recapture
1715 data at variable time intervals, *ICES Journal of Marine Science*, 40, 199–200,
1716 <https://doi.org/10.1093/icesjms/40.2.199>, 1982.

1717 Nassar, M. Z., Mohamed, H. R., Khiray, H. M., and Rashedy, S. H.: Seasonal fluctuations of
1718 phytoplankton community and physico-chemical parameters of the north western part of the Red
1719 Sea, Egypt, The Egyptian Journal of Aquatic Research, 40, 395–403,
1720 <https://doi.org/10.1016/j.ejar.2014.11.002>, 2014.

1721 Onuma, N., Masuda, F., Hirano, M., and Wada, K.: Crystal structure control on trace element
1722 partition in molluscan shell formation, 13, 187–189, <https://doi.org/10.2343/geochemj.13.187>,
1723 1979.

1724 Pandolfi, J. M. and Kiessling, W.: Gaining insights from past reefs to inform understanding of coral
1725 reef response to global climate change, Current Opinion in Environmental Sustainability, 7, 52–
1726 58, <https://doi.org/10.1016/j.cosust.2013.11.020>, 2014.

1727 Pannella, G.: Tidal growth patterns in recent and fossil mollusc bivalve shells: a tool for the
1728 reconstruction of paleotides, 63, 539–543, 1976.

1729 Petersen, S. V., Tabor, C. R., Lohmann, K. C., Poulsen, C. J., Meyer, K. W., Carpenter, S. J.,
1730 Erickson, J. M., Matsunaga, K. K., Smith, S. Y., and Sheldon, N. D.: Temperature and salinity of
1731 the Late Cretaceous western interior seaway, 44, 903–906, 2016.

1732 Poitevin, P., Chauvaud, L., Pécheyran, C., Lazure, P., Jolivet, A., and Thébault, J.: Does trace
1733 element composition of bivalve shells record ultra-high frequency environmental variations?,
1734 Marine Environmental Research, 158, 104943, <https://doi.org/10.1016/j.marenvres.2020.104943>,
1735 2020.

1736 Polsenaere, P., Deflandre, B., Thouzeau, G., Rigaud, S., Cox, T., Amice, E., Bec, T. L., Bihannic,
1737 I., and Maire, O.: Comparison of benthic oxygen exchange measured by aquatic Eddy Covariance
1738 and Benthic Chambers in two contrasting coastal biotopes (Bay of Brest, France), Regional
1739 Studies in Marine Science, 43, 101668, <https://doi.org/10.1016/j.rsma.2021.101668>, 2021.

1740 Popov, S. V.: Formation of bivalve shells and their microstructure, 48, 1519–1531,
1741 <https://doi.org/10.1134/S003103011414010X>, 2014.

1742 R Core Team: R: A Language and Environment for Statistical Computing, R Foundation for
1743 Statistical Computing, Vienna, Austria, 2022.

1744 Richard, M.: Analyse de la composition élémentaire de *Pecten maximus* par HR-ICP-MS Element
1745 2: développements méthodologiques et interprétations écologiques., PhD Thesis, Université de
1746 Bretagne occidentale-Brest, 264 pp, 2009.

1747 Richardson, C. A., Crisp, D. J., Runham, N. W., and Gruffydd, L. D.: The use of tidal growth bands
1748 in the shell of *Cerastoderma edule* to measure seasonal growth
1749 rates under cool temperate and sub-arctic conditions, 60, 977–989,
1750 <https://doi.org/10.1017/S002531540004203X>, 1980.

1751 Richter, C., Rea-Quiaoit, H., Jantzen, C., Al-Zibdah, M., and Kochzius, M.: Collapse of a new
1752 living species of giant clam in the Red Sea, 18, 1349–1354, 2008.

1753 Rea-Quiaoit, H.: Ecology and culture of giant clams (Tridacnidae) in the Jordanian sector of the
1754 Gulf of Aqaba, Red Sea, http://elib.suub.uni-bremen.de/diss/docs/E-Diss1340_PHDROAQ.pdf,
1755 2005.

1756 Roberts, E. M., Bowers, D. G., and Davies, A. J.: Tidal modulation of seabed light and its
1757 implications for benthic algae, 63, 91–106, <https://doi.org/10.1002/lno.10616>, 2018.

1758 Robson, A. A., Chauvaud, L., Wilson, R. P., and Halsey, L. G.: Small actions, big costs: the
1759 behavioural energetics of a commercially important invertebrate, 9, 1486–1498,
1760 <https://doi.org/10.1098/rsif.2011.0713>, 2012.

1761 Rodland, D. L., Schöne, B. R., Holama, S., Nielsen, J. K., and Baier, S.: A clockwork mollusc:
1762 Ultradian rhythms in bivalve activity revealed by digital photography, *Journal of Experimental*
1763 *Marine Biology and Ecology*, 334, 316–323, <https://doi.org/10.1016/j.jembe.2006.02.012>, 2006.

1764 Sano, Y., Kobayashi, S., Shirai, K., Takahata, N., Matsumoto, K., Watanabe, T., Sowa, K., and
1765 Iwai, K.: Past daily light cycle recorded in the strontium/calcium ratios of giant clam shells, *Nat*
1766 *Commun*, 3, 761, <https://doi.org/10.1038/ncomms1763>, 2012.

1767 Schöne, B. R. and Giere, O.: Growth increments and stable isotope variation in shells of the deep-
1768 sea hydrothermal vent bivalve mollusk *Bathymodiolus brevior* from the North Fiji Basin, *Pacific*
1769 *Ocean*, 52, 1896–1910, 2005.

1770 Schöne, B. R. and Gillikin, D. P.: Unraveling environmental histories from skeletal diaries —
1771 *Advances in sclerochronology*, *Palaeogeography, Palaeoclimatology, Palaeoecology*, 373, 1–5,
1772 <https://doi.org/10.1016/j.palaeo.2012.11.026>, 2013.

1773 Schöne, B. R., Castro, A. D. F., Fiebig, J., Houk, S. D., Oschmann, W., and Kröncke, I.: Sea
1774 surface water temperatures over the period 1884–1983 reconstructed from oxygen isotope ratios
1775 of a bivalve mollusk shell (*Arctica islandica*, southern North Sea), 212, 215–232, 2004.

1776 Schöne, B. R., Fiebig, J., Pfeiffer, M., Gleß, R., Hickson, J., Johnson, A. L., Dreyer, W., and
1777 Oschmann, W.: Climate records from a bivalved *Methuselah* (*Arctica islandica*, Mollusca;
1778 Iceland), 228, 130–148, 2005a.

1779 Schöne, B. R., Houk, S. D., Castro, A. D. F., Fiebig, J., Oschmann, W., Kröncke, I., Dreyer, W.,
1780 and Gosselck, F.: Daily growth rates in shells of *Arctica islandica*: assessing sub-seasonal
1781 environmental controls on a long-lived bivalve mollusk, 20, 78–92, 2005b.

1782 Schöne, B. R., Dunca, E., Fiebig, J., and Pfeiffer, M.: Mutvei's solution: An ideal agent for
1783 resolving microgrowth structures of biogenic carbonates, *Palaeogeography, Palaeoclimatology,*
1784 *Palaeoecology*, 228, 149–166, <https://doi.org/10.1016/j.palaeo.2005.03.054>, 2005c.

1785 Schöne, B. R., Zhang, Z., Jacob, D., Gillikin, D. P., Tütken, T., Garbe-Schönberg, D.,
1786 McConnaughey, T., and Soldati, A.: Effect of organic matrices on the determination of the trace
1787 element chemistry (Mg, Sr, Mg/Ca, Sr/Ca) of aragonitic bivalve shells (*Arctica islandica*)—
1788 Comparison of ICP-OES and LA-ICP-MS data, 44, 23–37,
1789 <https://doi.org/10.2343/geochemj.1.0045>, 2010.

1790 Schwartzmann, C., Durrieu, G., Sow, M., Ciret, P., Lazareth, C. E., and Massabuau, J. C.: In situ
1791 giant clam growth rate behavior in relation to temperature: A one-year coupled study of high-
1792 frequency noninvasive valvometry and sclerochronology, 56, 1940–1951,
1793 <https://doi.org/10.4319/lo.2011.56.5.1940>, 2011.

1794 Service Hydrographique et Océanographique de la Marine, Géoportail:
1795 <https://www.geoportail.gouv.fr/>, last access: 28 June 2022.

1796 Sinclair, D. J., Kinsley, L. P. J., and McCulloch, M. T.: High resolution analysis of trace elements
1797 in corals by laser ablation ICP-MS, *Geochimica et Cosmochimica Acta*, 62, 1889–1901,
1798 [https://doi.org/10.1016/S0016-7037\(98\)00112-4](https://doi.org/10.1016/S0016-7037(98)00112-4), 1998.

1799 Soldati, A. L., Jacob, D. E., Glatzel, P., Swarbrick, J. C., and Geck, J.: Element substitution by
1800 living organisms: the case of manganese in mollusc shell aragonite, 6, 1–9, 2016.

1801 Soo, P. and Todd, P. A.: The behaviour of giant clams (Bivalvia: Cardiidae: Tridacninae), *Mar*
1802 *Biol*, 161, 2699–2717, <https://doi.org/10.1007/s00227-014-2545-0>, 2014.

1803 Surge, D., Lohmann, K. C., and Dettman, D. L.: Controls on isotopic chemistry of the American
1804 oyster, *Crassostrea virginica*: implications for growth patterns, *Palaeogeography,*
1805 *Palaeoclimatology, Palaeoecology*, 172, 283–296, [https://doi.org/10.1016/S0031-](https://doi.org/10.1016/S0031-0182(01)00303-0)
1806 [0182\(01\)00303-0](https://doi.org/10.1016/S0031-0182(01)00303-0), 2001.

1807 Takesue, R. K., Bacon, C. R., and Thompson, J. K.: Influences of organic matter and calcification
1808 rate on trace elements in aragonitic estuarine bivalve shells, *Geochimica et Cosmochimica Acta*,
1809 72, 5431–5445, <https://doi.org/10.1016/j.gca.2008.09.003>, 2008.

1810 Tanaka, K., Okaniwa, N., Miyaji, T., Murakami-Sugihara, N., Zhao, L., Tanabe, K., Schöne, B. R.,
1811 and Shirai, K.: Microscale magnesium distribution in shell of the Mediterranean mussel *Mytilus*
1812 *galloprovincialis*: An example of multiple factors controlling Mg/Ca in biogenic calcite, *Chemical*
1813 *Geology*, 511, 521–532, <https://doi.org/10.1016/j.chemgeo.2018.10.025>, 2019.

1814 Taylor, J. D. and Layman, M.: The mechanical properties of bivalve (Mollusca) shell structures,
1815 15, 73–87, 1972.

1816 Thébault, J., Chauvaud, L., L’Helguen, S., Clavier, J., Barats, A., Jacquet, Sé., PÉcheyran, C.,
1817 and Amouroux, D.: Barium and molybdenum records in bivalve shells: Geochemical proxies for
1818 phytoplankton dynamics in coastal environments?, 54, 1002–1014,
1819 <https://doi.org/10.4319/lo.2009.54.3.1002>, 2009.

1820 Thébault, J., Jolivet, A., Waeles, M., Tabouret, H., Sabarot, S., Pécheyran, C., Leynaert, A.,
1821 Jochum, K. P., Schöne, B. R., Fröhlich, L., Siebert, V., Amice, E., and Chauvaud, L.: Scallop
1822 shells as geochemical archives of phytoplankton-related ecological processes in a temperate
1823 coastal ecosystem, 67, 187–202, <https://doi.org/10.1002/lno.11985>, 2022.

1824 Thomson, D. J.: Spectrum estimation and harmonic analysis, 70, 1055–1096, 1982.

1825 Tierney, J. E., Poulsen, C. J., Montañez, I. P., Bhattacharya, T., Feng, R., Ford, H. L., Hönisch,
1826 B., Inglis, G. N., Petersen, S. V., Sagem, N., Tabor, C. R., Thirumalai, K., Zhu, J., Burls, N. J.,
1827 Foster, G. L., Goddérís, Y., Huber, B. T., Ivany, L. C., Turner, S. K., Lunt, D. J., McElwain, J. C.,
1828 Mills, B. J. W., Otto-Bliesner, B. L., Ridgwell, A., and Zhang, Y. G.: Past climates inform our future,
1829 370, <https://doi.org/10.1126/science.aay3701>, 2020.

1830 Tran, D., Nadau, A., Durrieu, G., Ciret, P., Parisot, J. P., and Massabuau, J. C.: Field
1831 Chronobiology of a Molluscan Bivalve: How the Moon and Sun Cycles Interact to Drive Oyster
1832 Activity Rhythms, 28, 307–317, <https://doi.org/10.3109/07420528.2011.565897>, 2011.

1833 Tran, D., Perrigault, M., Ciret, P., and Payton, L.: Bivalve mollusc circadian clock genes can run
1834 at tidal frequency, 287, 20192440, <https://doi.org/10.1098/rspb.2019.2440>, 2020.

1835 Vander Putten, E., Dehairs, F., Keppens, E., and Baeyens, W.: High resolution distribution of
1836 trace elements in the calcite shell layer of modern *Mytilus edulis*: environmental and biological
1837 controls, 64, 997–1011, 2000.

1838 Vermeij, G. J.: The evolution of molluscan photosymbioses: a critical appraisal, *Biological Journal*
1839 *of the Linnean Society*, 109, 497–511, <https://doi.org/10.1111/bij.12095>, 2013.

1840 Von Bertalanffy, L.: Quantitative laws in metabolism and growth, 32, 217–231, 1957.

1841 Warter, V. and Müller, W.: Daily growth and tidal rhythms in Miocene and modern giant clams
1842 revealed via ultra-high resolution LA-ICPMS analysis—A novel methodological approach towards
1843 improved sclerochemistry, 465, 362–375, 2017.

1844 WARTER, V., MÜLLER, W., WESSELINGH, F. P., TODD, J. A., and RENEMA, W.: LATE
1845 MIOCENE SEASONAL TO SUBDECADAL CLIMATE VARIABILITY IN THE INDO-WEST
1846 PACIFIC (EAST KALIMANTAN, INDONESIA) PRESERVED IN GIANT CLAMS, *PALAIOS*, 30,
1847 66–82, <https://doi.org/10.2110/paleo.2013.061>, 2015.

1848 Warter, V., Erez, J., and Müller, W.: Environmental and physiological controls on daily trace
1849 element incorporation in *Tridacna crocea* from combined laboratory culturing and ultra-high
1850 resolution LA-ICP-MS analysis, *Palaeogeography, Palaeoclimatology, Palaeoecology*, 496, 32–
1851 47, <https://doi.org/10.1016/j.palaeo.2017.12.038>, 2018.

1852 Wilson, S. A., Koenig, A. E., and Orklid, R.: Development of microanalytical reference material
1853 (MACS-3) for LA-ICP-MS analysis of carbonate samples, 72, A1025, 2008.

1854 de Winter, N. J.: ShellChron 0.4.0: a new tool for constructing chronologies in accretionary
1855 carbonate archives from stable oxygen isotope profiles, 15, 1247–1267,
1856 <https://doi.org/10.5194/gmd-15-1247-2022>, 2022.

1857 de Winter, N. J. and Claeys, P.: Micro X-ray fluorescence (μ XRF) line scanning on Cretaceous
1858 rudist bivalves: A new method for reproducible trace element profiles in bivalve calcite,
1859 *Sedimentology*, 64, 231–251, <https://doi.org/10.1111/sed.12299>, 2017.

1860 de Winter, N. J., Goderis, S., Dehairs, F., Jagt, J. W., Fraaije, R. H., Van Malderen, S. J.,
1861 Vanhaecke, F., and Claeys, P.: Tropical seasonality in the late Campanian (late Cretaceous):
1862 Comparison between multiproxy records from three bivalve taxa from Oman, 485, 740–760, 2017.

1863 de Winter, N. J., Vellekoop, J., Vorsselmans, R., Golreihan, A., Soete, J., Petersen, S. V., Meyer,
1864 K. W., Casadio, S., Speijer, R. P., and Claeys, P.: An assessment of latest Cretaceous
1865 *Pycnodonte vesicularis* (Lamarck, 1806) shells as records for palaeoseasonality: a multi-proxy
1866 investigation, 14, 725–749, 2018.

1867 de Winter, N. J., Goderis, S., Malderen, S. J. M. V., Sinnesael, M., Vansteenberge, S., Snoeck,
1868 G., Belza, J., Vanhaecke, F., and Claeys, P.: Subdaily-Scale Chemical Variability in a *Torreites*
1869 *Sanchezi* Rudist Shell: Implications for Rudist Paleobiology and the Cretaceous Day-Night Cycle,
1870 35, e2019PA003723, <https://doi.org/10.1029/2019PA003723>, 2020.

1871 de Winter, N. J., Müller, I. A., Kocken, I. J., Thibault, N., Ullmann, C. V., Farnsworth, A., Lunt, D.
1872 J., Claeys, P., and Ziegler, M.: Absolute seasonal temperature estimates from clumped isotopes
1873 in bivalve shells suggest warm and variable greenhouse climate, *Commun Earth Environ*, 2, 1–8,
1874 <https://doi.org/10.1038/s43247-021-00193-9>, 2021a.

1875 de Winter, N. J., Agterhuis, T., and Ziegler, M.: Optimizing sampling strategies in high-resolution
1876 paleoclimate records, 17, 1315–1340, <https://doi.org/10.5194/cp-17-1315-2021>, 2021b.

1877 Winter, N. J. de, Witbaard, R., Kocken, I. J., Müller, I. A., Guo, J., Goudsmit, B., and Ziegler, M.:
1878 Temperature dependence of clumped isotopes ($\Delta 47$) in aragonite,
1879 <https://doi.org/10.1002/essoar.10511492.1>, 31 May 2022.

1880 Wichern, N. M. A., de Winter, N. J., Johnson, A. L. A., Goolaerts, S., Wesselingh, F., Hamers, M.
1881 F. J., Kaskens, P., Claeys, P., Ziegler, M. The potential of high-resolution stable isotope records
1882 in the First sclerochronologic and isotopic analysis of bivalve *Angulus benedoni* shells to
1883 investigate Pliocene seasonality. *Climate of the Past*, In review, 2022

1884 Wisshak, M., Correa, M. L., Gofas, S., Salas, C., Taviani, M., Jakobsen, J., and Freiwald, A.: Shell
1885 architecture, element composition, and stable isotope signature of the giant deep-sea oyster
1886 *Neopycnodonte zibrowii* sp. n. from the NE Atlantic, 56, 374–407, 2009.

1887 Witbaard, R., Jenness, M. I., Van Der Borg, K., and Ganssen, G.: Verification of annual growth
1888 increments in *Arctica islandica* L. from the North Sea by means of oxygen and carbon isotopes,
1889 *Netherlands Journal of Sea Research*, 33, 91–101, [https://doi.org/10.1016/0077-7579\(94\)90054-](https://doi.org/10.1016/0077-7579(94)90054-X)
1890 [X](https://doi.org/10.1016/0077-7579(94)90054-X), 1994.

1891 Xing, Q., Zhang, L., Li, Y., Zhu, X., Li, Y., Guo, H., Bao, Z., and Wang, S.: Development of Novel
1892 Cardiac Indices and Assessment of Factors Affecting Cardiac Activity in a Bivalve Mollusc
1893 *Chlamys farreri*, 10, 2019.

1894 Yan, H., Shao, D., Wang, Y., and Sun, L.: Sr/Ca profile of long-lived *Tridacna gigas* bivalves from
1895 South China Sea: A new high-resolution SST proxy, *Geochimica et Cosmochimica Acta*, 112, 52–
1896 65, <https://doi.org/10.1016/j.gca.2013.03.007>, 2013.

1897 Yan, H., Liu, C., An, Z., Yang, W., Yang, Y., Huang, P., Qiu, S., Zhou, P., Zhao, N., Fei, H., Ma,
1898 X., Shi, G., Dodson, J., Hao, J., Yu, K., Wei, G., Yang, Y., Jin, Z., and Zhou, W.: Extreme weather
1899 events recorded by daily to hourly resolution biogeochemical proxies of marine giant clam shells,
1900 *PNAS*, 117, 7038–7043, <https://doi.org/10.1073/pnas.1916784117>, 2020.

1901 Yoshimura, T., Tamenori, Y., Kawahata, H., and Suzuki, A.: Fluctuations of sulfate, S-bearing
1902 amino acids and magnesium in a giant clam shell, 11, 3881–3886, [https://doi.org/10.5194/bg-11-](https://doi.org/10.5194/bg-11-3881-2014)
1903 [3881-2014](https://doi.org/10.5194/bg-11-3881-2014), 2014.

1904 Zhao, L., Schöne, B. R., and Mertz-Kraus, R.: Controls on strontium and barium incorporation into
1905 freshwater bivalve shells (*Corbicula fluminea*), *Palaeogeography, Palaeoclimatology,*
1906 *Palaeoecology*, 465, 386–394, <https://doi.org/10.1016/j.palaeo.2015.11.040>, 2017.